PHYSICAL REVIEW B **82**, 014421 (2010)

Extreme sensitivity of a frustrated quantum magnet: Cs_2CuCl_4

Oleg A. Starykh,[1] Hosho Katsura,[2] and Leon Balents[2]
[1]*Department of Physics and Astronomy, University of Utah, Salt Lake City, Utah 84112, USA*
[2]*Kavli Institute for Theoretical Physics, University of California, Santa Barbara, California 93106-9530, USA*
(Received 7 May 2010; published 20 July 2010)

We report a thorough theoretical study of the low temperature phase diagram of Cs_2CuCl_4, a spatially anisotropic spin $S=1/2$ triangular lattice antiferromagnet, in a magnetic field. Our results, obtained in a quasi-one-dimensional limit in which the system is regarded as a set of weakly coupled Heisenberg chains, are in excellent agreement with experiment. The analysis reveals some surprising physics. First, we find that when the magnetic field is oriented within the triangular layer, spins are actually most strongly correlated within planes *perpendicular* to the triangular layers. This is despite the fact that the interlayer exchange coupling in Cs_2CuCl_4 is about an order of magnitude smaller than the weakest (diagonal) exchange in the triangular planes themselves. Second, the phase diagram in such orientations is exquisitely sensitive to tiny interactions, heretofore neglected, of order a few percent or less of the largest exchange couplings. These interactions, which we describe in detail, induce entirely new phases, and a novel commensurate-incommensurate transition, the signatures of which are identified in NMR experiments. We discuss the differences between the behavior of Cs_2CuCl_4 and an ideal two-dimensional triangular model, and in particular, the occurrence of magnetization plateaux in the latter. These and other related results are presented here along with a thorough exposition of the theoretical methods, and a discussion of broader experimental consequences to Cs_2CuCl_4 and other materials.

DOI: 10.1103/PhysRevB.82.014421 PACS number(s): 75.10.Jm, 75.40.Cx, 75.50.Ee

I. INTRODUCTION

The spin-1/2 nearest-neighbor Heisenberg antiferromagnet on the two dimensional triangular (hexagonal) lattice is the simplest theoretical model for frustrated quantum magnetism.[1] Without additional perturbations, the model is believed to order at zero temperature into a three-sublattice coplanar ground state.[2–4] However, one may expect a strong sensitivity to additional perturbations to the isotropic triangular lattice Hamiltonian. The material Cs_2CuCl_4 provides an interesting example of a spatially *anisotropic* spin-1/2 triangular antiferromagnet.[5] For several years, neutron scattering,[6] magnetization, and specific heat measurements[7,8] on Cs_2CuCl_4 have intrigued the community with unexpected behavior. These experimental properties have been suggested by a variety of authors, including the experimentalists themselves, to indicate exotic physics such as a spin-liquid ground state, unconventional "spinon" excitations at higher energies, and quantum criticality. Theoretical work on this material has been intense.[9–15]

An advantage of Cs_2CuCl_4 is that the small exchange constants and high degree of magnetic isotropy allow for a fairly accurate determination of several of the largest Hamiltonian parameters, by comparison with the measured single magnon dispersion relation above an approximately fully polarized state. The approximate Hamiltonian, including a magnetic field, determined by the experimentalists in this way is

$$H=\frac{1}{2}\sum_{ij}\left[J_{ij}\boldsymbol{S}_i\cdot\boldsymbol{S}_j-\boldsymbol{D}_{ij}\cdot\boldsymbol{S}_i\times\boldsymbol{S}_j\right]-\boldsymbol{h}\cdot\sum_i\boldsymbol{S}_i. \qquad (1)$$

Here i, j are sites of a stack of triangular lattices (see Figs. 1 and 6). The principle exchange interactions determined in Ref. 16 are $J=0.374$ meV on nearest-neighbor bonds parallel to the b axis, significantly smaller $J'=0.128$ meV $\approx 0.34J$ on diagonal bonds in the b-c plane, and quite small $J''=0.045J$ along vertical bonds between adjacent triangular layers. A Dzyaloshinskii-Moriya (DM) coupling was also measured along the diagonal bonds, with $\boldsymbol{D}_{ij}=-\boldsymbol{D}_{ji}=\pm D\hat{a}$ where the sign in specific directions are as indicated in Fig. 6, and $D=0.020$ meV $=0.05J$.

The relative smallness of the couplings other than J suggests that one may perhaps fruitfully regard this Hamiltonian as one of Heisenberg spin chains along the b axis defined by J, which are weakly coupled together by the remaining interactions.[17,18] This point of view was validated in Refs. 12–15, where it was shown that much of the observed low energy ordering *and* the high energy inelastic neutron scattering data on Cs_2CuCl_4 can be calculated starting from known exact results for one-dimensional (1D) Heisenberg chains. Indeed, numerical approaches in Refs. 19–25 showed that, due to frustration, the diagonal interaction may be as

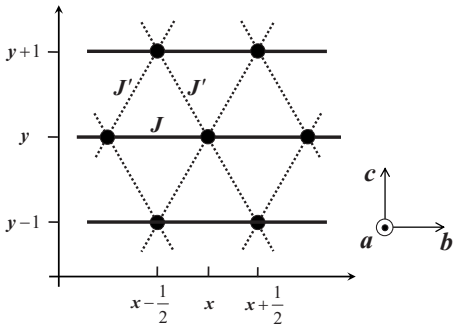

FIG. 1. Magnetic sites and exchange couplings in a 2D triangular layer in Cs_2CuCl_4: on-chain bonds J (thick lines $\parallel b$), frustrating diagonal bonds J' (dotted lines). Stacked layers are coupled by nearest-neighbor exchange J''. Crystallographic a, b, c axes are indicated.

large as $J'/J < 0.7$ while still retaining approximate quasi-one-dimensionality.

While this approach has been quite successful for Cs_2CuCl_4, most notably in directly confronting data *without any adjustable parameters*, there remain some puzzling features in the experiments. One of the most striking ones is the drastic difference in the low temperature phase diagrams of the material in magnetic fields aligned along the three different principle axes of the crystal. Though some aspects of these differences were explained in Ref. 14, based on the "standard" model in Eq. (1), other glaring discrepancies remain. In this paper, we resolve these outstanding differences between theory and experiment by correcting the standard model of Cs_2CuCl_4.

It is important to emphasize that the corrections to Eq. (1) *must* be small because the standard model does an excellent job in explaining a large volume of experimental data. The parameters in Eq. (1) were determined by high-field measurements of single-magnon spectra,[16] which leave little room for doubt of their correctness with relatively small error bars. Moreover, the same model, used at zero and intermediate fields, is quite successful in reproducing the full inelastic neutron spectrum, containing both continuum and magnon/triplon (sharp) contributions.[13,15] Nevertheless, in some field orientations, entirely different low-temperature phases are observed in experiment than are predicted by the standard model. Thus, we must somehow explain major *qualitative* differences in the ground states of Cs_2CuCl_4 in a field by very small corrections to H, of no more than a few percent.

A key message of this paper is that, indeed, the frustration and quasi-one-dimensionality of this problem can and do amplify tiny terms in the Hamiltonian to the point where they actually control the ground state. Sensitivity to small perturbations is of course an often-cited characteristic of frustrated systems. However, the extent to which this sensitivity can be fully characterized in the problem under consideration here is, to our mind, unprecedented. Using the methods of bosonization, the renormalization group, and chain mean-field theory (CMFT), we are able to distinctly identify the hierarchy of emergent low energy scales that control the very complex ordering behavior of the anisotropic triangular antiferromagnet, in a magnetic field and with a variety of very weak symmetry-breaking terms.

This paper contains many results, and a thorough presentation of the methods required to obtain them. To briefly summarize, we have determined the ground-state phase diagrams for the ideal two-dimensional (2D) anisotropic triangular antiferromagnetic (AF) Heisenberg model, and for the model appropriate to Cs_2CuCl_4, in all three distinct field orientations, over most of the range of applied magnetic fields. In the former, we find spin density wave (SDW) and cone states, and in the SDW, a family of quantized magnetization plateaux. In the latter, we find several phases, including an incommensurate cone state, an commensurate coplanar antiferromagnetic state, and a second incommensurate phase, descended from the antiferromagnetic one. The occurrence of these phases depends crucially on the field orientation and matches well with experiments on Cs_2CuCl_4. The associated phase diagrams in the temperature-magnetic field plane are shown schematically in Fig. 2. Details of each phase and its properties can be found in the appropriate section of the main text.

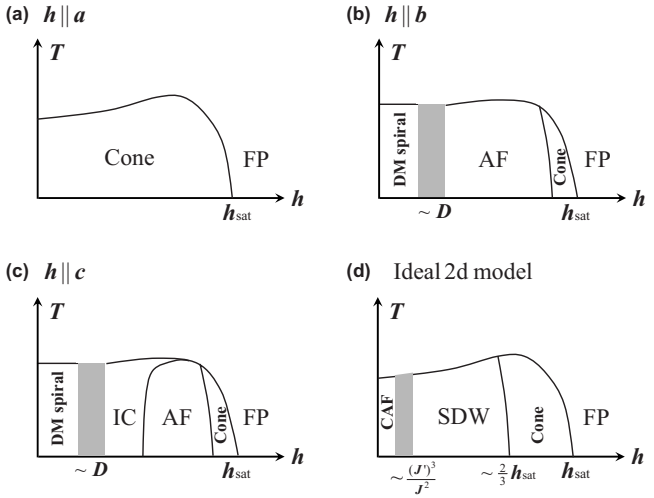

FIG. 2. Schematic phase diagrams in the temperature-magnetic field plane for fields along (a) the a axis, (b) the b axis, and (c) the c axis. (d) Schematic phase diagram for the ideal 2D (J-J') model. Here we use the abbreviations: FP=fully polarized state, AF =commensurate antiferromagnetic state, IC=incommensurate state, CAF=collinear antiferromagnetic state, and SDW=spin density wave state. The shaded areas denote the regions in which Dzyaloshinskii-Moriya and exchange nontrivially compete. For these regions, we do not have reliable theoretical predictions at this point.

One noteworthy highlight is that, remarkably, when the magnetic field is in the b-c plane, the spin correlations impugn the popular interpretation of Cs_2CuCl_4 as a two-dimensional "anisotropic triangular lattice" antiferromagnet. In fact, in this very wide regime, in the ground state, the spins are more correlated in the a-b planes, *perpendicular* to the triangular layers, than they are within those layers. Taking into account these correlations is crucial to obtaining the proper low temperature phase diagram. They lead to an enhanced sensitivity to some very weak second neighbor and effective "biquadratic" interactions, which are needed to stabilize the antiferromagnetic and incommensurate states mentioned above.

The remainder of the paper is organized as follows. In Sec. II, we present some necessary background, including the standard model Hamiltonian for Cs_2CuCl_4, the low energy properties of a single Heisenberg chain, the results of a space group analysis of allowed DM interactions in Cs_2CuCl_4, and a summary of the general scaling and CMFT approach to studying competing interactions. In Sec. III, we determine the ground-state behavior of the "ideal" model of an isolated spatially anisotropic triangular Heisenberg antiferromagnet, often presumed to apply to Cs_2CuCl_4. It clearly disagrees with experimental results for all three field orientations, as already pointed out in Ref. 14. In Sec. IV, we successfully apply the standard model to the case with a magnetic field applied perpendicular to the triangular plane, the DM interaction D playing a crucial role in reconciling the behavior with experiment. Next, in Sec. V, we study the case

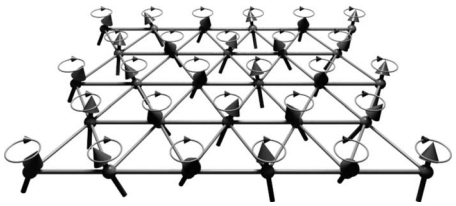

FIG. 3. A single triangular layer of the cone state, illustrated for a field along the a axis. Circles with arrows indicate the sense of precession of the spins, as one moves along the x axis. This is most easily seen intuitively by comparing every other spin, which compensates for the natural staggering due to the underlying Néel correlations of the 1D chains. Note that in the cone state, all spins precess in the same sense on all chains within a plane. For fields along a, however, this sense alternates between successive vertical layers, owing to the staggering of D. Within a single layer, cone states for fields along other axes are identical to this one after a global spin rotation.

of magnetic field along the b (chain) axis. The D term becomes rapidly negligible in this orientation, and we argue instead that the inter-plane coupling J'' becomes dominant. A subtle hierarchy of energy scales (see Fig. 9) is exposed, which leads to the establishment of competing antiferromagnetic and cone phases in this case. Then, in Sec. VI, we consider the field along the final principal axis, c, where an additional symmetry-allowed DM coupling plays a key role. It leads to the new incommensurate phase and an interesting commensurate-incommensurate phase transition. Having established all the ground state phases, we discuss some experimental consequences in Sec. VII. We give the explicit spin structures, describe the NMR line shapes, which provide a telling confirmation of the theoretical results, and establish the nature of the $T>0$ phase diagram. We conclude with some brief discussion in Sec. VIII. Several appendices present details of calculations underlying some of the results in the main text (Figs. 3–5).

II. BACKGROUND

A. Explicit Hamiltonian and coordinates

For the bulk of this paper, we will adopt a simple orthogonal coordinate system, with x along the crystallographic b direction, parallel to the chains, y along the c axis, perpendicular to the chains within the triangular plane, and z along the a axis, perpendicular to the triangular planes. Moreover, we will adopt a simplified geometry, which respects the topology and interactions between spins, but does not precisely reproduce the actual locations of Cu^{2+} ions. A description of the actual ion locations is given in Appendix B. In our simplified geometry, the spins form a set of regular triangular lattices stacked uniformly along the z axis, with spacing 1 between spins in the x and z directions, and spacing $\Delta y=1$ between chains in the triangular plane.

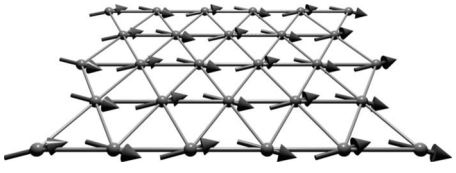

FIG. 4. A single layer of the AF state, illustrated for a field along the b axis. The spins lie in a plane spanned by the b axis and a second axis within the a-c plane but at a nonzero angle to both the a and c axes. The component of the spin normal to b is antiparallel on successive even (or odd) chains, so that the pattern has period $\Delta y=4$ along the c axis. This corresponds to a doubled crystallographic unit cell in this direction.

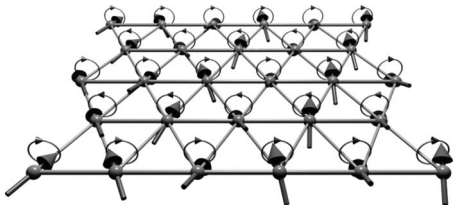

FIG. 5. A single layer of the IC state, illustrated for a field along the c axis. Circles with arrows indicate the sense of precession of the spins, as one moves along the x axis. This is most easily seen intuitively by comparing every other spin, which compensates for the natural staggering due to the underlying Néel correlations of the 1D chains. Note that in the IC state, by contrast to the cone state, spins on alternate chains in the plane precess in the opposite sense.

In this representation, the lattice Hamiltonian for the standard model is

$$H_{\rm sm}=\sum_{xyz}\{J\boldsymbol{S}_{x,y,z}\cdot\boldsymbol{S}_{x+1,y,z}-\boldsymbol{h}\cdot\boldsymbol{S}_{x,y,z}\}+H_1+H_2, \qquad (2)$$

with

$$H_1=\sum_{xyz}J'\boldsymbol{S}_{x,y,z}\cdot(\boldsymbol{S}_{x-1/2,y+1,z}+\boldsymbol{S}_{x+1/2,y+1,z}) \qquad (3)$$

and

$$H_2=\sum_{xyz}\{J''\boldsymbol{S}_{x,y,z}\cdot\boldsymbol{S}_{x,y,z+1}+D(-1)^z\hat{z}\cdot\boldsymbol{S}_{x,y,z}\times(\boldsymbol{S}_{x-1/2,y+1,z}-\boldsymbol{S}_{x+1/2,y+1,z})\}. \qquad (4)$$

B. Review of low energy properties of Heisenberg chains

We give a brief synopsis of known results on the low energy theory of the single Heisenberg chain in a field,

$$H_{1d}=J\sum_x \boldsymbol{S}(x)\cdot\boldsymbol{S}(x+1)-h\sum_x S^z(x). \qquad (5)$$

Here x are taken as integers, and we have taken the z axis in spin space along the field. In Eq. (5) the magnetization $M=\Sigma_x\frac{1}{N}S^z(x)=\langle S^z(x)\rangle$ is conserved (N is the number of spins), and so it is convenient to work at fixed M. The equilibrium relation between magnetization and field $M(h)$ is known from the Bethe ansatz solution (see Ref. 26).

For any M less than full saturation, $|M|<1/2$, the low energy theory can be described in Abelian bosonization by a single massless free scalar field θ and its "dual" ϕ (related to the canonical momentum conjugate to θ)

$$[\theta(x),\phi(x')] = -i\Theta(x-x'), \tag{6}$$

with $\Theta(x)$ as the Heaviside step function. The low-energy Hamiltonian is then

$$H_0 = \int dx \frac{v}{2}((\partial_x\phi)^2 + (\partial_x\theta)^2), \tag{7}$$

where the velocity v depends on M, see Fig. 9 of Ref. 27. At a given M, the fluctuations of the "longitudinal" spin component along the field axis are gapless at wave vectors $k_x = 0,\ \pi \pm 2\delta$, with $\delta = \pi M$. Similarly, the "transverse" spin fluctuations perpendicular to the field axis are gapless at $k_x = \pm 2\delta, \pi$. The lattice spin operator is decomposed thereby according to

$$S^z(x) \sim M + \mathcal{S}^z_0(x) + e^{i(\pi-2\delta)x}\mathcal{S}^z_{\pi-2\delta}(x) + e^{-i(\pi-2\delta)x}\mathcal{S}^z_{\pi+2\delta}(x),$$

$$S^+(x) \sim e^{-i2\delta x}\mathcal{S}^+_{2\delta}(x) + e^{i2\delta x}\mathcal{S}^+_{-2\delta}(x) + (-1)^x\mathcal{S}^+_{\pi}(x). \tag{8}$$

Here the scaling operators $\mathcal{S}^z_0, \mathcal{S}^z_{\pi\pm2\delta}$ describe longitudinal spin fluctuations, and $\mathcal{S}^\pm_{\pm2\delta}, \mathcal{S}^\pm_\pi$ transverse ones. These should be assumed to vary slowly with x (and time). Note that the operators $\mathcal{S}^\mu_k(\mu = z, \pm)$ do not mean the Fourier components of $S^\mu(x)$. They can be expressed in terms of bosonic fields as follows:

$$\mathcal{S}^z_0(x) = \beta^{-1}\partial_x\phi, \tag{9}$$

$$\mathcal{S}^z_{\pi-2\delta}(x) = -\frac{i}{2}A_1 e^{-2\pi i\phi/\beta}, \tag{10}$$

$$\mathcal{S}^+_{\pm2\delta}(x) = \pm\frac{i}{2}A_2 e^{i\beta\theta}e^{\pm i2\pi\phi/\beta}, \tag{11}$$

$$\mathcal{S}^+_{\pi}(x) = A_3 e^{i\beta\theta}. \tag{12}$$

The parameter β is obtained by solving the integral equations,[28–30] and the amplitudes A_1, A_2, and A_3 have been determined numerically in Ref. 31. We note that the above effective field theory describes the long-distance correlations of the spin chain and is a good approximation beyond some cutoff length a_0. For "generic" values of the magnetization, this is of the order of lattice spacing; however, it diverges near saturation ($|M| \to 1/2$), where it scales roughly as the distance between flipped spins (antiparallel to the field), $a_0 \sim (1/2 - |M|)^{-1}$.

The parameter $\beta = 2\pi R$ is related to the "compactification radius" R. At zero magnetization $M = h = 0$, the SU(2) invariant Heisenberg chain has $2\pi R^2 = 1$. In the field β and R decrease (see Fig. 12 of Appendix A) toward the limit $2\pi R^2 = 1/2$ as $|M| \to 1/2$. The scaling dimensions for general M are given in terms of R, and in the limits of zero and full polarization, are listed in Table I.

In addition to the scaling fields above, which appear in the expansion of spin operators, we will also make use of the spin current for the component of spin along the field axis. This has the form

TABLE I. Scaling dimensions of scaling fields associated with spin fluctuations in the one-dimensional Heisenberg chain at magnetization M. The third and fourth columns give the scaling dimensions in the limit of zero and full polarization, respectively.

Operator	Δ	$M=0$	$M \to 1/2$
$\mathcal{S}^z_0$	1	1	1
$\mathcal{S}^z_{\pi\pm2\delta}$	$1/4\pi R^2$	1/2	1
$\mathcal{S}^\pm_{\pm2\delta}$	$\pi R^2 + 1/4\pi R^2$	1	5/4
$\mathcal{S}^\pm_\pi$	πR^2	1/2	1/4

$$J^z(x) = \frac{-i}{2}[S^+(x)S^-(x+1) - S^-(x)S^+(x+1)] \sim \mathcal{J}^z(x). \tag{13}$$

Like the spin density $\mathcal{S}^z_0$, this has a simple bosonization formula,

$$\mathcal{J}^z = \frac{v}{\beta J}\partial_x\theta. \tag{14}$$

We note that at $M = 0$, $v/J = \pi/2$ takes a simple value, but at $M > 0$ the coefficient decreases continuously.

It may also be useful to connect with the limit of zero field $M = \delta = 0$, which is probably more familiar. Here the Hamiltonian has SU(2) symmetry. In this limit, the three operators $\mathrm{Re}[\mathcal{S}^+_\pi]$, $\mathrm{Im}[\mathcal{S}^+_\pi]$, and $\mathrm{Re}[\mathcal{S}^z_{\pi-2\delta}]$ become unified into the three components of the Néel field $\boldsymbol{N}$ (scaling dimension 1/2), while the other three operators, $\mathrm{Re}[\mathcal{S}^+_{2\delta}]$, $\mathrm{Im}[\mathcal{S}^+_{2\delta}]$, and $\mathcal{S}^z_0$, become the uniform magnetization operator $\boldsymbol{L} = \boldsymbol{J}_R + \boldsymbol{J}_L$, where $\boldsymbol{J}_{R/L}$ are the chiral spin currents (scaling dimension 1). The remaining operator, $\mathrm{Im}[\mathcal{S}^z_{\pi-2\delta}]$ becomes the staggered dimerization field ε (scaling dimension 1/2).

C. DM-ology

Here we present the DM terms which correct the standard model, as allowed by the space group symmetry of the lattice. They are derived in Appendix B. Since Cs_2CuCl_4 is an $S = 1/2$ system with a single unpaired electron in a nondegenerate orbital, we expect that spin-orbit effects to be perturbative. In this limit, the leading effect is to generate DM terms on the same bonds on which exchange interactions are present, and which are proportional to both the exchange coupling on that bond, and to the strength of spin orbit interactions. As a consequence, we need to consider DM terms only on bonds with reasonably strong exchange, that is, the intralayer triangular lattice bonds. These come in two types: the on-chain bonds and the diagonals. We denote the DM vectors on the former bonds by $\boldsymbol{D}$ and on the latter by $\boldsymbol{D}'$, in analogy to J and J' exchange couplings on the same bonds.

The space-group symmetry of the lattice determines the pattern of relative signs of the DM vectors on each of these bonds (see Appendix B). We find the following form:

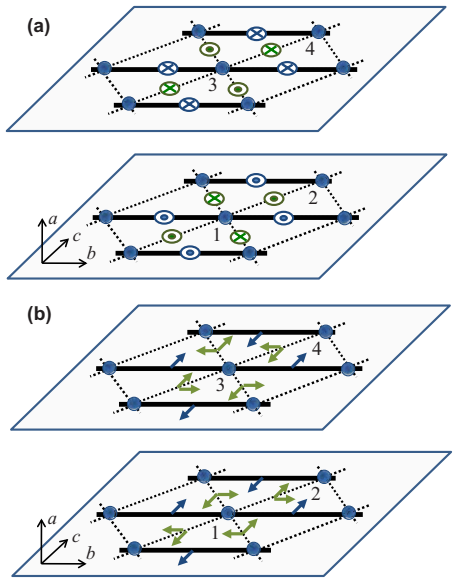

FIG. 6. (Color online) Distribution of the DM vectors. Sites 1, 2, 3, and 4 correspond to (x,y,z), $(x+\frac{1}{2},y+1,z)$, $(x,y,z+1)$, and $(x+\frac{1}{2},y+1,z+1)$, respectively. (a) The signs $\otimes$ and $\odot$ refer to the direction of the DM vectors along a axis. (b) The arrows indicate the direction of the DM vectors along b or c axis. We use the convention [see Eq. (15)] in which the first spin in the cross product $\boldsymbol{D}_{ij}\cdot\boldsymbol{S}_i\times\boldsymbol{S}_j$ is the one with smaller x for the on-chain bonds (i.e., it is on the left side of the bond), and it is the one with smaller y on the diagonal bonds (i.e., it is the lower of the two spins). Note that a different convention is used in Refs. 16 and 32.

$$H_D=\sum_{xyz}\{\boldsymbol{D}_{y,z}\cdot\boldsymbol{S}_{x,y,z}\times\boldsymbol{S}_{x+1,y,z}+\boldsymbol{D}^{+}_{y,z}\cdot\boldsymbol{S}_{x,y,z}\times\boldsymbol{S}_{x+1/2,y+1,z}+\boldsymbol{D}^{-}_{y,z}\cdot\boldsymbol{S}_{x,y,z}\times\boldsymbol{S}_{x-1/2,y+1,z}\},\tag{15}$$

where

$$\boldsymbol{D}_{y,z}=D_a(-1)^z\hat{a}+D_c(-1)^y\hat{c},\tag{16}$$

$$\boldsymbol{D}^{\pm}_{y,z}=\pm D'_a(-1)^z\hat{a}+D'_b(-1)^{y+z}\hat{b}\pm D'_c(-1)^{y+z}\hat{c},\tag{17}$$

and $D'_a\equiv D$ is the DM term in the standard model. The relative signs of the DM vectors are graphically shown in Fig. 6.

One sees that symmetry allows five distinct DM couplings: $D=D'_a$, D'_b, D'_c, D_a, and D_c. Of these, only D'_a and D_c will be invoked in the body of this paper. The remaining three can be safely neglected, as explained in Appendix F.

D. Competing interactions, scaling, and chain mean-field theory

We assume that *all* interchain couplings are weak. In this case, a scaling analysis based on a perturbative renormalization group (RG) treatment is appropriate. This proceeds in a standard way. One integrates out short-distance modes (i.e., small x or large k_x), progressively reducing the large momentum cutoff from its "bare" value Λ [of order the inverse lattice spacing, which we take in turn to be $O(1)$] to $\Lambda e^{-\ell}$, where $\ell\in[0,\infty]$ is the logarithmic RG scaling variable. Equivalently, the corresponding real space cutoff is $L=ae^{\ell}$, where a is a microscopic length [which we take to be $O(1)$]. As we integrate out modes, the couplings themselves are renormalized. For each given coupling constant γ_i, which appears in the Hamiltonian as $H=H_0+\cdots+\int dx\gamma_i\mathcal{O}_i$, we can define a *dimensionless* coupling $\breve{\gamma}_i=\gamma_i/(v\Lambda_\ell^2)$, which is measured relative to the typical magnitude of the terms in the free bosonic field theory. Equivalently, division by both a factor of $v\Lambda_\ell$ (the typical energy at this scale) and an additional factor of Λ_ℓ (a typical inverse length) are needed to render γ_i, which is an energy density, dimensionless. To linear order, each dimensionless coupling "flows" according to the RG equation

$$\partial_\ell\breve{\gamma}_i=(2-\Delta_i)\breve{\gamma}_i.\tag{18}$$

Note that the factor of 2 in this equation, which comes from the normalization by $1/\Lambda_\ell^2$, is equivalent to the space-time dimensionality of the $(1+1)$-dimensional field theory of the spin chains. In RG schemes in which space-time is rescaled to keep the cutoff fixed, this factor arises directly from that rescaling. We prefer to formulate the RG without rescaling in this paper so that all lengths, times, energies, etc., are explicit.

Many of the above operators may be *relevant* in the RG sense. This means that, with increasing ℓ, the dimensionless coupling constants *increase*, which implies $\Delta<2$ for that coupling. The RG is valid only so long as the *largest* of these dimensionless couplings remains small. Crudely, then, we may determine the length scale ξ at which interchain coupling becomes significant by the point $\ell=\ell^*$ *at which the first operator renormalizes to become of* $O(1)$, where $\xi=ae^{\ell^*}$. The length ξ defines a correlation length, below which the dynamics is approximately one dimensional.

If this first "diverging" operator is unique, one can often identify the nature of the associated instability of the decoupled chains. In many cases, this can be done by dropping the other operators and treating the remaining one by a type of mean-field theory. Sometimes it can be treated in a semiclassical fashion. None of these approaches are rigorous, but they are eminently reasonable and are likely to correctly predict the nature of the resulting state.

From this reasoning, we see that both the bare magnitude and the scaling dimension (relevance) of the different interactions are important in determining the low-energy state of the system. To be more concrete, consider two candidate operators, $\mathcal{O}_1$ and $\mathcal{O}_2$. Their renormalized coupling constants obey

$$\breve{\gamma}_i(\xi)=\frac{\gamma_i}{v}\xi^{2-\Delta_i}.\tag{19}$$

Here, since $\Lambda=\Lambda_{\ell=0}$ is $O(1)$, we replace $\breve{\gamma}_i(\ell=0)=\gamma_i(\ell=0)/v=\gamma_i/v$. Setting $\breve{\gamma}_i(\xi_i)=C$, an $O(1)$ constant, we obtain

$$\xi_i=\left(\frac{Cv}{\gamma_i}\right)^{1/(2-\Delta_i)}.\tag{20}$$

We expect that operator 1 (2) is dominant if ξ_1 (ξ_2) is the shorter length. Hence the boundary between the two regimes, in which one or the other operator dominates, occurs when $\xi_1=\xi_2$, or

$$\gamma_1^{2-\Delta_2} = (Cv)^{\Delta_1-\Delta_2}\gamma_2^{2-\Delta_1}. \quad (21)$$

Note that, although the scaling of this boundary is determined by this argument, the precise location is not due to the ambiguity of C. We can understand this conclusion also from the scaling of the ground state energy density, $\mathcal{E}_0$, which obeys

$$\mathcal{E}_0(\gamma_1,\gamma_2) = b^{-2}\mathcal{E}_0\left(\frac{\gamma_1}{v}b^{2-\Delta_1}, \frac{\gamma_2}{v}b^{2-\Delta_2}\right). \quad (22)$$

Choosing $b=(\frac{\gamma_1}{v})^{-1/(2-\Delta_1)}$, we obtain

$$\mathcal{E}_0(\gamma_1,\gamma_2) = \left(\frac{\gamma_1}{v}\right)^{2/(2-\Delta_1)} f(\gamma_2/(\gamma_1/v)^{(2-\Delta_2)/(2-\Delta_1)}), \quad (23)$$

where $f(\mathcal{X})$ is a universal scaling function. If there is a phase transition as γ_1 and γ_2 are varied, there must therefore be a nonanalyticity at $\mathcal{X}=\mathcal{X}^*$ in $f(\mathcal{X})$ for some $\mathcal{X}^*$. This gives an equivalent condition to Eq. (21). To precisely determine the phase boundary, we need to know $\mathcal{X}^*$ (or C), which means we need knowledge of $f(\mathcal{X})$. Such scaling functions are generally determined by the full RG flows out of the scale-invariant theory, and not just perturbative data.

To resolve this ambiguity, we turn to an approach which is equivalent to the former one at the *scaling* level, but which is more quantitative. A natural choice is the CMFT, in which interchain couplings are treated by a self-consistent Weiss-type decoupling, using the exact solutions of perturbed but decoupled individual chain problems.[33] The validity of this approach was tested in Ref. 34. Our CMFT approach is described in detail in Appendix D. In principle, it can be employed to determine a full mean-field phase diagram. Here, we will mostly use it in more limited ways, as convenient. To address the ambiguity discussed above, we use the CMFT to compute a putative ordering temperature, T_i, for each channel driven by an operator $\mathcal{O}_i$. The instability which sets in first upon lowering the temperature, i.e., with maximal T_i, is assumed to be dominant. Another application of CMFT will be to compute the magnitude of the ordering induced by a coupling γ_i at zero temperature. This will be useful in making quantitative estimates of more subtle smaller energy scales, as we will see below.

III. IDEAL 2D MODEL

In this section, we consider the behavior of the ideal 2D model, described by the standard model in Eqs. (1) and (3) with $J''=D=0$.

A. Continuum limit

For this case, the technology of the previous section can be straightforwardly applied. We begin with the naïve procedure of simply inserting the decompositions in Eq. (8) into the microscopic interchain lattice Hamiltonian in Eq. (3) (We will assess the need to go beyond this approximation later). Specifically, we have

$$S^z_{x,y,z} \sim M + \mathcal{S}^z_{y,z;0}(x) + e^{i(\pi-2\delta)x}\mathcal{S}^z_{y,z;\pi-2\delta}(x) + e^{-i(\pi-2\delta)x}\mathcal{S}^z_{y,z;\pi+2\delta}(x),$$

$$S^+_{x,y,z} \sim e^{-i2\delta x}\mathcal{S}^+_{y,z;2\delta}(x) + e^{i2\delta x}\mathcal{S}^+_{y,z;-2\delta}(x) + e^{i\pi x}\mathcal{S}^+_{y,z;\pi}(x). \quad (24)$$

It might appear that a slightly different formula should be applied for odd chains since in those cases in our convention the x coordinates are half-integer rather than integer. However, the differences can be removed by constant shifts of θ and ϕ for the odd chains, without any further changes. Hence we can uniformly apply Eq. (24) to all chains.

Having dropped the D term, the behavior of the model at zero temperature is independent of the direction of the field and is a function only of the magnetization M and the magnitude of J'. Inserting the decomposition of Eq. (8) into H_1 in Eq. (3), one need keep only terms which do not oscillate, the condition corresponding to momentum conservation. Using the slowly varying nature of the scaling operators in x (but *not* in y and/or z), one may take a continuum limit in x by gradient expansion to obtain the lowest nonvanishing terms of each type. One finds

$$H_1 \approx J'\sum_{y,z}\int dx\Big\{2M^2 + 2\mathcal{S}^z_{y,z;0}\mathcal{S}^z_{y+1,z;0} + 2\sin\delta[\mathcal{S}^z_{y,z;\pi-2\delta}\mathcal{S}^z_{y+1,z;\pi+2\delta} + \text{H.c.}] + \frac{1}{2}[-i\mathcal{S}^+_{y,z;\pi}\partial_x\mathcal{S}^-_{y+1,z;\pi} + \text{H.c.}] + \cos\delta[\mathcal{S}^+_{y,z;2\delta}\mathcal{S}^-_{y+1,z;2\delta} + \mathcal{S}^+_{y,z;-2\delta}\mathcal{S}^-_{y+1,z;-2\delta} + \text{H.c.}]\Big\} \quad (25)$$

Let us now assess the importance of each of the terms in Eq. (25). This is accomplished by ranking each of the terms in order of increasing scaling dimension, or equivalently, decreasing relevance in the RG sense. Formally, the most relevant term is the first (M^2) one, which is a c-number constant and hence of dimension zero. Though it is a "trivial" constant (at fixed magnetization) and hence does not affect the dynamics of the system, it is indeed the dominant correction to the ground state energy of the weakly coupled chains. Being positive, it implies an increase of this energy with increasing M, and hence a suppression of the $M(h)$ curve at fixed external field h. This is calculated in Ref. 14 and reproduced in Appendix A. The result agrees very well with experimental data on Cs_2CuCl_4.

Consulting Table I, one sees that of the remaining terms, the third and fourth terms are presumably most important. The third term involves $\mathcal{S}^z_{\pi\pm2\delta}$ operators, whose scaling dimensions approach the minimal value of $1/2$ at small magnetization. Because this term lacks any derivatives, it achieves nearly the smallest total scaling dimension ($\approx 2\times 1/2=1$) for small M. The fourth term contains a derivative (which adds 1 to its scaling dimension) but contains $\mathcal{S}^{\pm}_{\pi}$ operators, whose scaling dimensions decrease from $1/2$ toward $1/4$ near saturation. Thus the total scaling dimension of the fourth term decreases from $2\times 1/2+1=2$ at small M toward $2\times 1/4+1=1.5$ near saturation. This makes it less relevant than the third term at small M, but more relevant than it near saturation. The remaining (second and fifth) terms have

larger scaling dimensions for all values of the magnetization.

We therefore drop these less relevant terms, as well as the constant contribution to the energy to obtain $H_1 \to H_1'$, with

$$H_1' = \sum_{y,z} \int dx \{ \gamma_{\mathrm{SDW}} \mathcal{S}^z_{y,z;\pi-2\delta} \mathcal{S}^z_{y+1,z;\pi+2\delta} - i\gamma_{\mathrm{cone}} \mathcal{S}^+_{y,z;\pi} \partial_x \mathcal{S}^-_{y+1,z;\pi} + \mathrm{H.c.} \}, \quad (26)$$

with $\gamma_{\mathrm{SDW}}=2J' \sin\delta$ and $\gamma_{\mathrm{cone}}=J'/2$. Equivalently, using the bosonization formulas in Eq. (9), one can rewrite H_1' in sine-Gordon form,

$$H_1' = \sum_{y,z} \int dx \{ \tilde{\gamma}_{\mathrm{SDW}} \cos[2\pi(\phi_{y,z} - \phi_{y+1,z})/\beta] - \tilde{\gamma}_{\mathrm{cone}} (\partial_x \theta_{y,z} + \partial_x \theta_{y+1,z}) \cos[\beta(\theta_{y,z} - \theta_{y+1,z})] \}, \quad (27)$$

with $\tilde{\gamma}_{\mathrm{SDW}}=J'A_1^2 \sin\delta$ and $\tilde{\gamma}_{\mathrm{cone}}=J'A_3^2\beta/2$.

B. Phases of Eq. (27)

The names of these coupling constants have been chosen to reflect their probable consequences. For small magnetization, where γ_{SDW} is most strongly relevant, one expects collinear "spin density wave" (SDW) ordering of spins along the z (field) axis, with

$$\langle \mathcal{S}^z_{y,z;\pi\pm2\delta} \rangle = |\psi| (-1)^y e^{i\alpha_z}, \quad (28)$$

which minimizes the SDW interaction term. Here $\alpha_z \in [0, 2\pi]$ can be arbitrary for each z since the layers are decoupled. Near saturation, where γ_{cone} becomes more relevant, one expects a "spiraling" order of the components of the spins transverse to the field,

$$\langle \mathcal{S}^{\pm}_{y,z;\pi}(x) \rangle = |\psi| (\sigma_z)^y e^{i\sigma_z q_0 x} e^{i\Theta_z}, \quad (29)$$

with some $q_0 > 0$, and where $\sigma_z = \pm 1$ and Θ_z are independent for each z. Some incommensurate pitch q_0 is preferred by the derivative in Eq. (26) but is expected to be small as it is disfavored by the single chain Hamiltonian. Because of the nonzero magnetization along the z axis, the spins in this phase sweep out a "cone" as one moves along the b (chain) axis in real space.

Following the logic in Sec. II D, the dominant interaction, at each magnetization, is the one whose putative ordering temperature is largest. The estimated ordering temperatures for the SDW and cone states, calculated from CMFT, are shown in Fig. 7. One can see that the two curves cross at $M \approx 0.24$, which therefore separates a region of SDW state at lower magnetization from a cone state at higher magnetization.

This change from an SDW to a cone state is primarily due to the variation of scaling dimensions with magnetization. As M increases, the spin correlations are increasingly XY-like, i.e., enhanced transverse to the field and suppressed parallel to it. While the SDW term is obviously more relevant than the cone term near $M=0$ due to the derivative in the latter, the change in scaling dimensions eventually compensates. Equating the two scaling dimensions, one finds $R=R_c$, with $2\pi R_c^2 = (\sqrt{5}-1)/2 \approx 0.62$ (the golden ratio). This occurs at

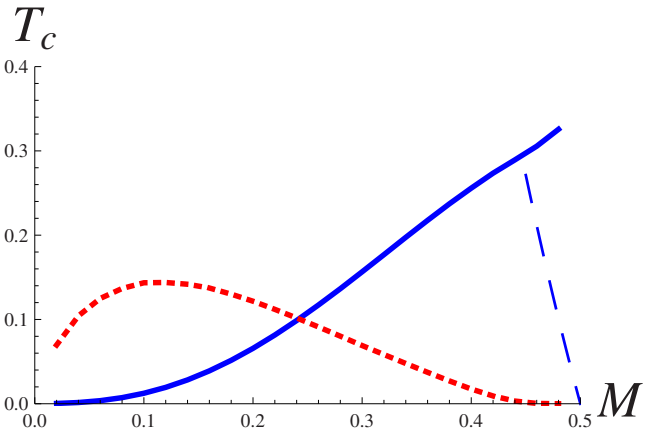

FIG. 7. (Color online) Putative ordering temperatures within chain mean field theory for SDW interaction, [T_{SDW}, dotted (red) line] and cone [T_{cone}, solid (blue) line] interactions, within the ideal two-dimensional model. Dashed blue line, emanating from $M=1/2$ point, represents $T_{\mathrm{cone}} \propto (1/2-M)$ [Eq. (31)] which describes the crossover between 1D behavior obtained by bosonization with CMFT, and 2D one, which takes over for $M \geqslant 0.45$. The larger ordering temperature is expected to be physical, while the putative lower temperature transition will be suppressed by the dominant competing order.

magnetization $M_c \approx 0.32$ (i.e., about 65% of the saturation value). This approximately recovers the more accurate estimate $M_c \approx 0.24$, obtained above. Similar estimate holds for the SDW-to-cone phase transition in a single zig-zag ladder.[35]

C. Critical temperature

Further details of the behavior of the critical temperatures in Fig. 7 can be understood physically. The SDW critical temperature increases from small values at small M, to a maximum around $M=0.1$, above which it again decreases. The initial rise is due to the partial relieve of frustration of the interchain J' coupling by increasing incommensurability of the longitudinal spin correlations. The ultimate decay of T_{SDW} is due simply to the suppression of longitudinal spin correlations as the chain becomes more XY-like. The same increasing XY-like behavior leads to the growth of T_{cone} with M.

The two endpoints, $M \to 0$ and $M \to 1/2$, require special consideration. Approaching zero field, the dominant SDW interaction vanishes. This case requires a subtle analysis of fluctuation-generated interactions, which was undertaken in Ref. 14. There it was observed that corrections to the naïve continuum limit are crucial to obtain the correct behavior, which is *neither* an SDW state nor a spiral, but rather a commensurate, collinear antiferromagnet (CAF). This CAF state replaces SDW as the ground state near the $M=0$ limit, see Fig. 2(d), which is the reason for $T_{\mathrm{SDW/cone}}$ curves in Fig. 7 (as well as in most other T_c vs M figures in the paper) start not at $M=0$ but at a finite $M=0.02$ value. We will not go into further detail on this point here but simply mention that another instance of fluctuation-generated couplings will be encountered later in Secs. V and VI.

The other limit, $M \to 1/2$, can be attacked differently. At $M=1/2$, one has full spin saturation, and the state is unique and trivial. Single spin-flip magnon excitations can be found exactly including the effects of J'. One may obtain in this limit a cone state as a magnon condensate, as in Refs. 36 and 37. In this formulation, it is clear that the critical temperature for the ordering must vanish as $M \to 1/2$. However, this is not observed in Fig. 7. This is due to a noncommuting order of limits. In the vicinity of saturation, scaling (see Sec. III D 6) in fact predicts that *all* physical quantities are functions of the combination

$$\Xi = \frac{J'/J}{\frac{1}{2} - M}, \tag{30}$$

when $\frac{1}{2} - M \ll 1$. The bosonization analysis carried out above is valid for $\Xi \ll 1$. However, for $\Xi \gg 1$ a different behavior obtains. Specifically, the critical temperature is expected to scale (up to logarithmic corrections) according to

$$T_{\text{cone}} = \left(\frac{1}{2} - M\right)^2 \mathcal{F}\left[\frac{J'/J}{\frac{1}{2} - M}\right], \tag{31}$$

where $\mathcal{F}[\Xi] \sim \Xi^2$ for $\Xi \ll 1$ and $\mathcal{F}[\Xi] \sim \Xi$ for $\Xi \gg 1$. One can see that this form indeed vanishes on approaching saturation. The maximum of T_{cone} should be obtained by differentiating, occurs when $\mathcal{F}(\Xi) = \Xi \mathcal{F}'(\Xi)$, which implies Ξ of $O(1)$. Hence the maximum T_{cone} occurs very close to saturation, where $\frac{1}{2} - M \sim J'/J$, and its presence is not captured in the bosonization result plotted in Fig. 7. Hence the temperature T_{cone} is overestimated, leading to an underestimate of the magnetization of the crossing point from Fig. 7. This effect is probably small, however, since this occurs relatively far from saturation.

D. SDW and magnetization plateaus

The above considerations treat only the most relevant terms in the effective Hamiltonian. This, however, neglects some important physics in the SDW phase. In particular, it misses *commensurability* effects, when the SDW period can become "locked" (i.e., fixed over a region of field and temperature) to a multiple of the lattice constant.

Microscopically, this effect arises from "umklapp" processes, which distinguish quasimomentum from true momentum, violating absolute conservation of the former. The x component of the quasimomentum is important here, and hence umklapp events carry momentum 2π. Since the SDW carries momentum $\pi \pm 2\delta$, a umklapp event occurs when a number k of SDW quanta are absorbed or emitted, adding to $\pm 2\pi$. This condition is rigorously derived below, where we outline symmetry considerations which fix the form of the allowed microscopic umklapp Hamiltonian completely.

1. Symmetry constraints

We start by analyzing how $\phi_y(x)$ transforms under discrete lattice symmetries.[38] For that, we rewrite Eq. (8) as

$$S_y^z(x) \sim M + \beta^{-1}\partial_x \phi_y(x) - A_1 \sin\left[\frac{2\pi\phi_y(x)}{\beta} - (\pi - 2\delta)x\right]. \tag{32}$$

It then follows that translation along the chain transforms $\phi_y(x)$ as

$$\phi_y(x) \to \phi_y(x+1) - \frac{\beta}{2\pi}(\pi - 2\delta), \tag{33}$$

while translation along the northeast diagonal ($y \to y+1, x \to x+1/2$) changes it to

$$\phi_y(x) \to \phi_{y+1}(x+1/2) - \frac{\beta}{4\pi}(\pi - 2\delta). \tag{34}$$

Spatial inversion ($x \to -x$) changes it as well,

$$\phi_y(x) \to \frac{\beta}{2} - \phi_y(-x). \tag{35}$$

In addition, $\phi_y(x)$ is defined modulo β so that

$$\phi_y(x) \to \phi_y(x) + \beta \tag{36}$$

must be respected also.

We now specify the general form for the kth order umklapp term,

$$H_{\text{umk}}^{(k)} = \sum_y \int dx t_k(y) \cos\left[\frac{2\pi k}{\beta}\phi_y(x) + \omega_k\right]. \tag{37}$$

where $t_k \sim O(J)$ is the bare amplitude and ω_k is yet undetermined phase. The periodicity requirement, Eq. (36), implies that k must be an *integer*. The translation in Eq. (33) changes the argument of cosine in Eq. (37) into $2\pi k\phi_y/\beta + \omega_k - k(\pi - 2\delta)$ which implies that

$$k(\pi - 2\delta) = 2\pi\nu. \tag{38}$$

Since $\delta = \pi M$, the above equation implies that allowed values of the magnetization are given by

$$M^{(k,\nu)} = \frac{1}{2}\left(1 - \frac{2\nu}{k}\right), \tag{39}$$

where ν and k are positive integers. This condition is equivalent to the magnetization quantization condition for a single spin chain.[39] However, we will see that ν and k are *not* arbitrary in the two-dimensional triangular lattice.

The remaining symmetries, translation along the diagonal of the triangular lattice, Eq. (34), and spatial inversion, Eq. (35), require that $t_k(y) = (-1)^{y\nu} t_k$ and $\omega_k = -\pi/2$ for *odd* k and $\omega_k = 0$ for *even* k. As a result, the most general form of the umklapp term, consistent with lattice symmetries and involving single chains and no spatial derivatives, reads

$$H_{\text{umk}}^{(k=\text{odd})} = \sum_y \int dx t_k (-1)^{y\nu} \sin\left[\frac{2\pi k}{\beta}\phi_y(x)\right], \tag{40}$$

$$H_{\text{umk}}^{(k=\text{even})} = \sum_y \int dx t_k (-1)^{y\nu} \cos\left[\frac{2\pi k}{\beta}\phi_y(x)\right]. \tag{41}$$

2. Energetic constraints

To proceed, we bring out the energetics associated with the underlying SDW order by making the shift

$$\phi_y(x) \to \phi_y(x) + (-1)^y \frac{\beta}{4} \tag{42}$$

so as to minimize the leading SDW term in Eq. (27) (see Appendix D 1). In terms of the transformed fields, the SDW ground state corresponds to an x- and y-independent configuration of $\phi_y(x)=\phi_0$. This shift modifies Eq. (40) as

$$H_{\text{umk}}^{(k=\text{odd})} = \sum_y \int dx t_k (-1)^{y(\nu+1)} \sin\left[\frac{\pi k}{2}\right] \cos\left[\frac{2\pi k}{\beta}\phi_y(x)\right]. \tag{43}$$

We immediately conclude that *odd-k* umklapp processes must have *odd* ν in order to be able to gain some energy—otherwise the sum oscillates with y and does not give an extensive contribution. Similarly, Eq. (41) becomes

$$H_{\text{umk}}^{(k=\text{even})} = \sum_y \int dx t_k (-1)^{y\nu} \cos\left[\frac{\pi k}{2}\right] \cos\left[\frac{2\pi k}{\beta}\phi_y(x)\right], \tag{44}$$

implying that now ν must be *even*.

This interesting result allows us to finally represent *all* allowed umklapp terms in a single compact equation

$$H_{\text{umk}}^{(k)} = \sum_y \int dx \tilde{t}_k \cos\left[\frac{2\pi k}{\beta}\phi_y(x)\right], \tag{45}$$

where $\tilde{t}_k = t_k(\cos[\frac{\pi k}{2}] + \sin[\frac{\pi k}{2}])$, and Eq. (45) must be supplemented by the important constraint

$$\nu = k \pmod 2, \tag{46}$$

i.e., ν *must have the same parity as* k.

3. Allowed plateaux

It is natural to consider the plateaux in order of increasing k—this will be directly related to the robustness of the plateau (see below). One finds that the first nontrivial possibility (different from the nonpolarized $M=0$ or the fully polarized $M=1/2$ limits), corresponds to $\nu=1$, $k=3$ when $M=1/6=\frac{1}{3}(\frac{1}{2})$. Assuming for concreteness $\tilde{t}_{k=3}>0$ we find that $\phi_0=\beta(2n+1)/6$ (with $n=0,1,2$) minimizes Eq. (45) [and, by construction, the SDW interaction in Eq. (27)]. Working backward through the chain of the transformations we find that Eq. (32) predicts [recall that $(\pi-2\delta)=2\pi/3$ here]

$$\langle S_y^z(x)\rangle_{M=1/6} = M + A_1(-1)^y \cos\left[\frac{2\pi x}{3} - \frac{\pi(2n+1)}{3}\right]. \tag{47}$$

This equation describes the famous[40] *up-up-down* (uud) spin configuration of the 1/3-magnetization plateau, i.e., with two-thirds of the sites having a larger spontaneous magnetic moment than the remaining third. It also correctly predicts relative arrangement of down spins on neighboring chains: the system gains energy by coupling every down spin with a pair of up spins on adjacent chains. The resulting pattern has down spins in the centers of hexagons formed by up spins. For the other sign, $\tilde{t}_{k=3}<0$, one finds instead of the uud configuration one in which two-thirds of the sites have a *smaller* spontaneous moment than the remaining third. This corresponds to the "quantum" magnetization plateau suggested in Ref. 41, where the magnetic unit cell is composed of a spin singlet on a pair of sites accompanied by an up-pointing spin.

Other possible plateaux include $M=3/10=\frac{3}{5}(\frac{1}{2})$ ($k=5$, $\nu=1$) and $M=5/14=\frac{5}{7}(\frac{1}{2})$ ($k=7$, $\nu=1$). Importantly, several of the smaller-k plateaux are excluded due to the "mismatch" between the parities of k and ν numbers. These include $k=4$, $\nu=1$ which leads to $M=1/4$ (one-half plateau) and $k=6$, $\nu=1$ which would result in $M=1/3$ (two-thirds plateau).

4. Effective two-dimensional sine-Gordon model

We now use the RG to derive an effective two-dimensional sine-Gordon model. Our starting point is given by the following Hamiltonian:

$$H_{\text{plateau}}^{(k)} = \sum_y \int dx \left\{ \frac{v}{2}(\partial_x \phi_y)^2 - \tilde{\gamma}_{\text{SDW}} \cos\left[\frac{2\pi}{\beta}(\phi_y - \phi_{y+1})\right] - \frac{v q(h)}{\beta}\partial_x \phi_y(x) + \tilde{t}_k \cos\left[\frac{2\pi k}{\beta}\phi\right]\right\}, \tag{48}$$

which incorporates the shift Eq. (42). Observe the appearance of the new, linear in spatial derivative term, which is added here[38] to describe variation of the magnetic field h near the optimal plateau value $h^{(k,\nu)}$. The optimal field is defined by the condition that the magnetization in the absence of the umklapp term, $M_0(h)$, is given by the plateau's value, $M_0(h^{(k,\nu)})=M^{(k,\nu)}$. Then $q(h)=2\pi k[M_0(h)-M^{(k,\nu)}]$.

We then iteratively integrate out high-energy modes, reducing the momentum cutoff from initial $\Lambda_0 \sim 1$ to $\Lambda_{\text{SDW}} = \Lambda_0 e^{-\ell_{\text{SDW}}}$, as described in Appendix E. The new, reduced cutoff Λ_{SDW} is determined by the condition that the renormalized SDW coupling, $\tilde{\gamma}_{\text{SDW}}(\Lambda_{\text{SDW}}/\Lambda_0)^{\Delta_{\text{SDW}}}$ becomes comparable to the contribution of the gradient term to the energy density at the same scale, $v\Lambda_{\text{SDW}}^2$. Here $\Delta_{\text{SDW}}=2/(4\pi R^2)$ is the scaling dimension of the SDW cosine in Eq. (48). This leads to the estimate $\Lambda_{\text{SDW}}/\Lambda_0 \sim (\frac{\tilde{\gamma}_{\text{SDW}}}{v\Lambda_0^2})^{1/(2-\Delta_{\text{SDW}})}$. At this scale, SDW coupling is of the order $v\Lambda^2 \sim (\tilde{\gamma}_{\text{SDW}}^2/v^{\Delta_{\text{SDW}}})^{1/(2-\Delta_{\text{SDW}})}$ and the SDW term should be minimized. Therefore, the argument of cosine is small and we can approximate

$$\cos\left[\frac{2\pi}{\beta}(\phi_y - \phi_{y+1})\right] \to 1 - \frac{1}{2}\left(\frac{2\pi}{\beta}\right)^2 [\partial_y \phi(x,y)]^2. \tag{49}$$

The umklapp term has a scaling dimension, $\Delta_k = (2\pi k/\beta)^2/(4\pi) = k^2/(4\pi R^2)$, which grows quadratically with the k and is thereby strongly suppressed by high-energy fluctuations,

$$\tilde{t}_k(\ell_{\rm SDW}) = \tilde{t}_k(0)\left(\frac{\Lambda_{\rm SDW}}{\Lambda_0}\right)^{k^2/(4\pi R^2)} \approx v\left(\frac{J'}{v}\right)^{k^2/(8\pi R^2-2)}. \tag{50}$$

At this stage it is convenient to define a rescaled field, $\varphi = 2\pi k\phi/\beta + \pi\Theta(\tilde{t}_k)$, which includes a shift to achieve a definite sign of the umklapp term [$\Theta(x)$ is the Heaviside step function]. This gives the *two-dimensional* sine-Gordon Hamiltonian of the kth plateau,

$$H^{(k)}_{\rm plateau} = \int dxdy\left\{\frac{u}{2}(\partial_x\varphi)^2 + \frac{c_y}{2}(\partial_y\varphi)^2 - \frac{vq(h)}{2\pi k}\partial_x\varphi_y(x) - |\tilde{t}_k|\cos[\varphi]\right\}. \tag{51}$$

Here $u = v(\beta/2\pi k)^2$, $c_y \sim k^{-2}(\tilde{\gamma}^2_{\rm SDW}/v^{\Delta_{\rm SDW}})^{1/(2-\Delta_{\rm SDW})}$.

5. Plateaux width

At $T=0$, the two-dimensional sine-Gordon Hamiltonian [Eq. (51)] can be analyzed classically.[42] We review this standard analysis as it is important both here and in Sec. VI C. The classical sine-Gordon model exhibits two phases: commensurate, describing the plateau, with $\langle\partial_x\varphi\rangle = 0$, and incommensurate, with $\langle\partial_x\varphi\rangle \neq 0$. The incommensurate state, which describes the SDW phase with field-dependent ordering momentum, is achieved for sufficiently strong $|q| \geqslant q_c$. The critical value q_c is determined by the condensation of *kinks*, when $E_{\rm kink}=0$. Here the kink represents the solution of Eq. (51) interpolating between two degenerate minima of cosine potential: $\varphi(x=-\infty,y)=0$ and $\varphi(x=+\infty,y)=2\pi$ for all y. One immediately observes that the linear derivative term in Eq. (51) contributes $-vq(h)/k$ to the kink's energy (per unit length in the y direction). The rest follows from standard steps,[42] which show that energy of the kink, relative to the energy of the uniform plateau state with, for example, $\varphi=0$, is given by

$$E_{\rm kink} = 8\sqrt{u|\tilde{t}_k|} - \frac{v|q|}{k}. \tag{52}$$

Thus

$$q_c = \frac{4\beta}{\pi}\sqrt{\frac{|\tilde{t}_k|}{v}} \sim \left(\frac{J'}{v}\right)^{k^2/(4(4\pi R^2-1))}. \tag{53}$$

Since in the relevant range of the magnetic field dM_0/dh is constant, the plateau width in field units, $\delta h_{(k,\nu)}$, is directly proportional to q_c.

Focusing on the 1/3-magnetization plateau we can estimate, with the help of Fig. 12, that $2\pi R^2 \approx 3/4$ at $M=1/6$. This leads to $\delta h_{(3,1)} \sim (J'/v)^{9/2}$. The next most robust plateau is at 3/5th of the saturation magnetization ($k=5$, $\nu=1$), for which $\delta h_{(5,1)} \sim (J'/v)^{25/2}$. The existence of this plateau is unclear since this magnetization is close to the boundary of the SDW state, and indeed, the calculation in Fig. 7 predicts that it falls outside the stability range of the SDW state. It is, however, *inside* the SDW phase as estimated from the pure scaling dimension criterion $2\pi R^2 > (\sqrt{5}-1)/2$. Thus this plateau still seems a reasonable candidate for observation in some anisotropic triangular materials.

Other plateaux, such as, for example, the one-half magnetization one ($M=1/4$), are much narrower due to the *equal parity requirement*, Eq. (46), which implies $k=8$, $\nu=2$. Then $\delta h_{(8,2)} \sim (J'/v)^{32}$, making it very hard to observe indeed. These arguments make it clear that the 1/3 plateau ($M=1/6$) is drastically more robust than others, and thereby it is expected to be much more commonly observed. We also reiterate that it should persist all the way down to the decoupled chains limit, $J'=0$.

It is interesting to compare our findings with those in Refs. 43 and 44 which studied magnetization plateaux in a single zigzag ladder, made of two spin chains (with exchange J) coupled in a triangular (zigzag) fashion by exchange J'. This geometry can also be viewed as a single chain with first and second-neighbor interactions $J_1=J'$ and $J_2=J$. In this one-dimensional system a robust 1/3-plateau is found to exist in the intermediate exchange region $0.487 \leqslant J/J' \leqslant 1.25$. In particular, it does not seem to extend far into the $J' \to 0$ limit, although a very narrow sleeve of the plateau phase cannot be reliably excluded by the current numerical studies. We note however that the much reduced extent of the long-range ordered plateau region, in comparison with the quasi-2D predictions above, simply reflects the reduced stability of the crystalline (more specifically SDW in this case) order in 1D systems (at $T=0$). In more technical terms, the magnetization plateau requires pinning of both the "center-of-mass" and relative combinations of $\phi_{1,2}$ fields in a two-chain system which, in turn, requires significant modification of the chain Luttinger parameter K from its bare value of 1/2, in notations of Ref. 44, by various marginal (density-density type) interchain terms. Such modifications generically require $J' \sim O(1)$, which is the reason for the absence of the plateau in the $J' \to 0$ limit in this case.

6. Critical behavior of the wave vector

Our description can be extended to the neighborhood of the plateau-SDW transition, where the ordering momentum $|q(h)| > q_c$ shows abrupt variation with magnetic field. Near the commensurate state, the incommensurate SDW phase can be understood as a *soliton lattice*, with a finite linear density n_s of solitons.[42,45] In the dilute limit $n_s w \ll 1$, where $w = \sqrt{u/|t_k|}$ is the width of the soliton, the solitons *repel* each other, with an exponentially decaying potential $Ue^{-x/w}$. The prefactor $U = 32\sqrt{u|t_k|}$ can be obtained by calculating the energy of two solitons separated by a distance x with the help of Eq. (51). As a result, the energy density of the dilute soliton lattice is given by

$$E_{\rm sol.lat.} = 2\pi v(q_c - q)n_s + n_s U e^{-1/(n_s w)}. \tag{54}$$

Here the last term represents the repulsion between the nearest solitons of the lattice. The optimal concentration n_s^*, for $q > q_c$, follows by minimizing Eq. (54) (with logarithmic accuracy),

$$n_s^* = \frac{1}{w \ln\left[\dfrac{U}{2\pi v(q-q_c)}\right]}. \tag{55}$$

This implies that the shift of the ordering momentum $\delta Q = 2\pi n_s^*$ from its commensurate value $Q_{k,\nu} = 2\pi\nu/k$ inside the plateau vanishes with an *infinite slope*, according to

$$\delta Q = \frac{-2\pi}{w \ln|(h-h^{(k,\nu)})/\delta h_{(k,\nu)}|}, \tag{56}$$

where the last expression is written with logarithmic accuracy.

IV. STANDARD MODEL: FIELD (INCLUDING ZERO) ALONG *a* AXIS

The predictions of the last section for the idealized model with $J''=D=0$ unfortunately do not agree with experiments on Cs_2CuCl_4. At zero magnetic field, the ground state is actually an incommensurate spiral, similar to that predicted at high fields in the previous section, rather than the collinear state produced by the fluctuation-generated interactions. Moreover, the zero field spiral ground state appears to continuously evolve on increasing fields along the *a* axis, with no intervening phase transition before reaching a fully polarized ferromagnetic state at the saturation field. The SDW state predicted in the previous section is entirely absent.

This behavior, however, is readily explained by the standard model *including* the D and J'' terms, as discussed in Ref. 14. To proceed, we again apply the decompositions, Eq. (24), to the these terms. Following the logic of the previous section, we keep only the most relevant contributions. This gives

$$\begin{aligned} H_2' = \sum_{y,z} \int dx \{ & -D(-1)^z (\mathcal{S}^+_{y,z;\pi}\mathcal{S}^-_{y+1,z;\pi} + \mathcal{S}^-_{y,z;\pi}\mathcal{S}^+_{y+1,z;\pi}) \\ & + \gamma''_z (\mathcal{S}^z_{y,z;\pi-2\delta}\mathcal{S}^z_{y,z+1;\pi+2\delta} + \mathcal{S}^z_{y,z;\pi+2\delta}\mathcal{S}^z_{y,z+1;\pi-2\delta}) \\ & + \gamma''_{\delta-z} (\mathcal{S}^z_{y,z;\pi-2\delta}\mathcal{S}^z_{y,z+1;\pi-2\delta} e^{-4i\delta x} \\ & + \mathcal{S}^z_{y,z;\pi+2\delta}\mathcal{S}^z_{y,z+1;\pi+2\delta} e^{4i\delta x}) \\ & + \gamma''_{\pm} (\mathcal{S}^+_{y,z;\pi}\mathcal{S}^-_{y,z+1;\pi} + \mathcal{S}^-_{y,z;\pi}\mathcal{S}^+_{y,z+1;\pi}) \}, \end{aligned} \tag{57}$$

with $\gamma''_z = \gamma''_{\delta-z} = 2\gamma''_{\pm} = J''$.

At zero field, we can simplify, using SU(2) symmetry and $\delta=0$,

$$\begin{aligned} H_2' = \sum_{y,z} \int dx \{ & -D(-1)^z (N^+_{y,z}N^-_{y+1,z} + N^-_{y,z}N^+_{y+1,z}) \\ & + J'' \boldsymbol{N}_{y,z} \cdot \boldsymbol{N}_{y,z+1} \}. \end{aligned} \tag{58}$$

A. Competition between D and J''

In Eq. (58) it is evident that both D and J'' induce strongly relevant perturbations, with scaling dimension 1. These are more relevant than any terms naïvely present in zero field (i.e., the two terms studied in the previous section), and much larger than the fluctuation-induced correction $[\sim (J')^4/J^3]$ with the same scaling dimension, which drives the formation of the collinear antiferromagnetic state[14] in their absence. They also become more relevant with increasing field. Hence we expect that these terms should control the actual ordering in Cs_2CuCl_4 for this field orientation.

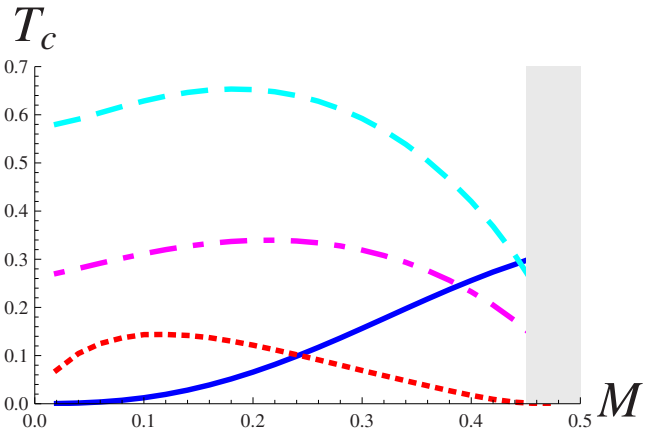

FIG. 8. (Color online) Same as Fig. 7, but with the chain mean field ordering temperature due to interlayer interactions [$T_{\rm il}$, dot-dashed (magenta) line] and DM interaction [$T_{\rm D}$, dashed (cyan) line] included. Note that the highest two temperatures are $T_{\rm D}$ and $T_{\rm il}$, with the former substantially larger. Thus for a magnetic field along the $\hat{a}$ axis, where the D term is present, it is expected to dominate the ordering except in the region close to saturation, $M \gtrsim 0.45$ or so. That later region, which is described by a 2d scaling, is represented by the shaded rectangle.

However, it is not so obvious which of the two is dominant. Indeed, they actually compete. This can be seen as follows. The D term is minimized (for $D>0$) by configurations in which

$$\langle N^+_{y,z} \rangle_D = (-1)^{yz} N e^{i\beta\vartheta_z}, \tag{59}$$

where the classical phase ϑ_z may depend on z. For such configurations, however, the J'' term oscillates in sign with y, and hence averages to zero. To instead minimize the J'' term, one requires configurations in which

$$\langle \boldsymbol{N}_{y,z} \rangle_{J''} = (-1)^z N \hat{\boldsymbol{n}}_y, \tag{60}$$

where the unit vector $\hat{\boldsymbol{n}}_y = (n^1_y, n^2_y, n^3_y)$ may depend on y. For all such configurations, the D term vanishes when averaged over z.

The balance of this competition is determined by the relative magnitudes of D and J''. We rely again on the chain mean field method, which indicates that the DM term dominates for the parameters of Cs_2CuCl_4—as shown by the fact that the associated mean-field ordering temperature in Fig. 8 is largest. This is essentially due to the fact that the DM interaction acts on twice as many bonds as does the interlayer exchange.

A physical distinction between the two candidate states, which may be compared to experiment, is in their vector chirality, which is concentrated on the diagonal bonds of the triangular lattice. Define

$$\chi^z_{y,z,\pm}(x) = \hat{z} \cdot \left\langle \boldsymbol{S}_{y,z}(x) \times \boldsymbol{S}_{y\pm1,z}\left(x+\frac{1}{2}\right)\right\rangle. \tag{61}$$

This quantity is nonzero in both phases. In the continuum limit, one obtains

$$\chi^z_{y,z,\pm} \sim \frac{1}{2}(N^+_{y,z}N^-_{y\pm1,z} + \text{H.c.}). \tag{62}$$

Let us compare this chirality for the states favored by D and J''. For the D term, one obtains $\chi^z_{y,z,\pm} \sim (-1)^z N^2$, which is constant in the triangular planes but alternates between layers. This staggering of chirality along the crystallographic a axis is observed experimentally in zero field. For the J'' term, one obtains instead $\chi^z_{\pm} \sim N^2(n^1_y n^1_{y+1} + n^2_y n^2_{y+1})$, which can vary within the triangular planes but is the same in every such layer. Thus experiment supports the D-induced order but not the J'' one, in agreement with the calculation described above.

Now consider nonzero field. In this case, returning to Eq. (57) with $\delta \neq 0$, we see that the third term is oscillatory and can be dropped. The second term is less relevant than the first and fourth, and thus is also subdominant. One is still left with a competition between the first and fourth terms, again controlled by the balance of DM and interlayer exchange. Since several terms that had formed part of the latter coupling for $h=0$ are now removed, we should expect that the DM will be relatively enhanced and continue to win the competition for all values of the field. This gives a natural explanation for the continuity of the ordered phase across the range of fields observed in experiments (with this field orientation). It is also interesting to note that the scaling dimension of the $\mathcal{S}^+_{y,z;\pi}$ operator decreases with increasing field, actually making the DM coupling more relevant. This is reflected in an increasing critical temperature for the ordered phase with increasing field, up to a maximum which occurs relatively close to saturation. Again, consulting Fig. 8, we see that indeed the D term dominates the ordering except very close to saturation ($M > 0.45$ or so). In that narrow field window, the larger bare value of the cone interaction $[O(J')]$ is sufficient to overcome its larger scaling dimension.

B. Incommensuration of the ordered state

Naïvely, it would appear from the above analysis that, in the region $M < 0.45$, a commensurate ordered state is induced by the D term. However, while the D term is indeed dominant in this regime, we still need to take into account the subsidiary effects of the J' interaction. It turns out that the cone coupling γ_{cone} does not actually compete with D so that it introduces a weak incommensuration in the ordered state.

To see this, we apply the expectation value in Eq. (59) to the cone interaction in Eq. (26) (using $\mathcal{S}^{\pm}_{y,z;\pi} = N^{\pm}_{y,z}$ in zero field), assuming ϑ_z is a slowly varying function of x,

$$H_1' \to -2\gamma_{\text{cone}}\beta N^2 \sum_{y,z} \int dx (-1)^z \partial_x \vartheta_z. \tag{63}$$

The (average) phase ϑ_z is obviously the classical analog of θ_z so that there is a gradient cost obtained from Eq. (7), which should be added to the above term to obtain

$$H_{\text{eff}} = \sum_{y,z} \int dx \left\{ \frac{v}{2}(\partial_x \vartheta_z)^2 - 2\gamma_{\text{cone}}\beta N^2 (-1)^z \partial_x \vartheta_z \right\}. \tag{64}$$

This is easily minimized with respect to ϑ_z,

$$\partial_x \vartheta_z = 2\frac{\gamma_{\text{cone}}}{v}\beta N^2 (-1)^z \equiv \frac{q_0}{\beta}(-1)^z. \tag{65}$$

Here q_0 is the induced incommensurability. For zero magnetization, we have $q_0 = (4J'/J)N^2$. However, Eq. (65) also applied to $M > 0$, if N is replaced by the magnitude of the expectation value of $\mathcal{S}^{\pm}_{y,z;\pi}$. In both cases, the result is that

$$\langle \mathcal{S}^+_{y,z;\pi} \rangle = (-1)^{yz} N e^{i(-1)^z q_0 x + i\Theta_z}, \tag{66}$$

where Θ_z is arbitrary for each layer since we have up to now neglected interlayer coupling. Let us compare to what is expected in the cone-dominated regime, $M > 0.45$. Here we should apply the ansatz in Eq. (29), which minimizes the cone interaction, to the D term in Eq. (57). One obtains

$$H_2' \to \sum_{y,z} \int dx (-D) |\psi|^2 (-1)^z \sigma_z, \tag{67}$$

which is minimized by taking $\sigma_z = \text{sgn}(D)(-1)^z$. Suppose that D is positive, which is always possible if we redefine z. Then Eq. (29) becomes

$$\langle \mathcal{S}^+_{y,z;\pi} \rangle = (-1)^{yz} |\psi| e^{i(-1)^z q_0 x + i\Theta_z}. \tag{68}$$

Comparing Eq. (66) and Eq. (68), we see the forms are identical. Thus, the regimes $M < 0.45$ and $M > 0.45$ are actually smoothly connected and distinguished only by which interaction controls the largest part of the ordering energy. This means that D and J' do not really compete. Indeed, in Appendix D 4, we show that in CMFT both interactions together increase the critical temperature of the cone state.

C. Interlayer correlations

The expression in Eq. (68) contains an undetermined phase, Θ_z, for each layer. One may look to J'', which has been neglected in obtaining the form in Eq. (68), to fix these phases. However, at the naïve level of first order perturbation theory, this is not the case. In particular, taking the expectation value of the J'' term in Eq. (58) or the corresponding $\gamma''_{\pm}$ term in Eq. (57), one finds a oscillating result, which vanishes upon summation over y. This indicates that the effects of J'' on the undetermined phases is second order in J''.

Such second order effects can be considered as a fluctuation-induced interaction, which can be derived in a similar way as in the calculation of Appendix E. One obtains

$$\Delta H = -J''_2 \sum_{y,z} \int dx \cos(\theta_{y,z} - \theta_{y,z+2}), \tag{69}$$

with *ferromagnetic* $J''_2 \sim (J'')^2/v > 0$. Taking its expectation value, this terms splits the large phase degeneracy, leaving only two undetermined values,

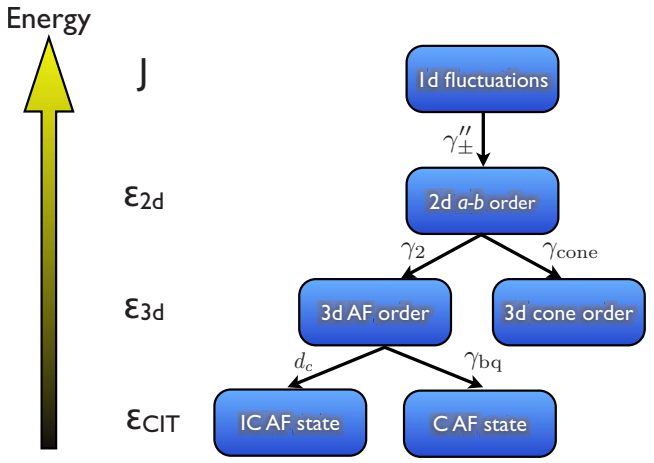

FIG. 9. (Color online) Cascade of energy scales operative for fields in the *b*-*c* plane. Symbols adjacent to the arrows indicate the interactions responsible for the associated (partial) ordering. The cascade can be quantified by different "condensation" energy densities, which give the lowering of the energy density due to the establishment of the associated partial order. At the highest energies, between J and $\varepsilon_{2d} \sim J''|\psi|^2$, the system exhibits one-dimensional fluctuations. Here $|\psi|$ is the amplitude of the order parameter, Eq. (75). Between ε_{2d} and ε_{3d}, the spins order within *a*-*b* planes, but the planes are not registered. Below $\varepsilon_{3d} \sim \max\{J_2|\psi|^2, \frac{(J')^2}{J}|\psi|^4\}$, full three-dimensional order develops, which may be of antiferromagnetic (AF) or cone type. In the former case, there may be yet another lower energy scale, $\varepsilon_{\mathrm{CIT}}$ (which is of the same order as ε_{3d}), below which the magnetic structure is completely determined. This may be commensurate or incommensurate, the latter occurring only for fields along the *c* axis and is driven by DM interactions.

$$\Theta_z = \begin{cases} \Theta_0 & \text{for } z \text{ even} \\ \Theta_1 & \text{for } z \text{ odd}. \end{cases} \tag{70}$$

Some bare microscopic second neighbor exchange might contribute to J''_2, but experiments indicate that the net result remains ferromagnetic, as there is no enlargement of the unit cell in the $a(z)$ direction.

For the standard model, the two remaining phase degeneracies are protected by symmetry. The *overall* U(1) phase, $\Theta_0+\Theta_1$ is of course expected to be arbitrary, owing to rotational symmetry of the Hamiltonian about the $a(z)$ axis. The *relative* phase, $\Theta_0-\Theta_1$, is protected by translation symmetry, $x \to x+1$, under which $\Theta_z \to \Theta_z+(-1)^z q_0$.

V. FIELD ALONG *b* AXIS

In this section and the next, we will discuss the physics determining the ordered ground states when the magnetic field is normal to the crystallographic *a* axis. These cases are much more complex than above because, as we will see, the ordering is determined by several distinct interactions which are important at different energy scales. The "cascade" of energy scales, which must be considered in turn, from largest to smallest, is indicated graphically in Fig. 9.

A. Irrelevance of *D* term

Having understood that the DM interaction D dominated the physics for fields along the *a* axis, we first consider its role in this field orientation. Remarkably, the change in orientation has a drastic effect. With a field in the *b*-*c* plane, the D term always involves one spin component parallel to the field and one perpendicular to it. Consulting the decomposition of spin operators in Eq. (24), we immediately see that the dominant fluctuations of these two spin components are always incommensurate. As a consequence, in the continuum limit all terms directly arising from D *oscillate* with a $e^{\pm 2i\delta x}$ factor. This makes them formally strongly irrelevant. More physically, upon coarse graining over length scales shorter than π/δ, these terms average to zero. Thus, provided that D does not scale to strong coupling under the RG before this scale is reached, they become negligible. This will be true everywhere except the low field limit. Specifically, since it has scaling dimension 1, the renormalized D term at this scale is of order $D(\pi/\delta)$. Demanding this be small compared to v, we obtain the criterion $\delta = \pi M \gtrsim D/J$ for it to be negligible.

Thus for most of the magnetic field range, we can drop the D term. This gives a simple reason why the experimental behavior in Cs_2CuCl_4 for this field orientation is completely different from that with field along the *a* axis. It is tempting to expect instead that the ideal 2D model discussed in Sec. III should apply. A comparison to experiments strongly suggests, however, that this is not the case, except perhaps at high fields. Unfortunately, no published low-temperature NMR or neutron data are available in this field orientation. However, magnetization and specific heat measurements[8] show a single phase occupying the region below the high field cone state and above the low field DM-dominated spiral. By comparison to the same measurements along the *c* axis, which are strikingly similar, it appears most likely that this intermediate phase represents a commensurate state. In the ideal 2D model, we would be forced to interpret it instead as an incommensurate SDW. This seems untenable, as such an SDW phase should also show a 1/3 magnetization plateau (see Sec. III D), of which there is no sign. Thus we conclude that the SDW phase has been superseded by another competing state. In the following, we find an explanation for this competing state as a commensurate AF phase.

B. Role of interlayer interactions

To explain this, we must take into account the one remaining interaction present in the standard but not ideal model—the exchange J'' between triangular planes. Like the (now absent) D term, it is strongly relevant, and unlike the D term, it is not averaged out in any field orientation. The appropriate continuum limit has already been given, the dominant piece being the last term of Eq. (57), reproduced here,

$$H'_2 = \gamma''_{\pm} \sum_{y,z} \int dx (\mathcal{S}^+_{y,z;\pi} \mathcal{S}^-_{y,z+1;\pi} + \mathcal{S}^-_{y,z;\pi} \mathcal{S}^+_{y,z+1;\pi}), \tag{71}$$

with $\gamma''_{\pm} = J''/2$. Written explicitly using bosonization, it becomes

$$H_2' = \tilde{\gamma}_\pm'' \sum_{y,z} \int dx \cos[\beta(\theta_{y,z} - \theta_{y,z+1})], \tag{72}$$

with $\tilde{\gamma}_\pm'' = 2A_3^2 \gamma_\pm''$. This coupling is more relevant than either the SDW or cone interaction, in the entire range of magnetization. We may therefore expect that it scales to strong coupling unambiguously before any competing interactions. To check this, we again consult the comparison of critical temperatures in Fig. 8. Neglecting the effects of the D term, as we have just discussed, we see that the interlayer interaction is clearly dominant for all magnetizations below about 80% of the saturation value. Above this magnetization, the larger bare value of the cone interaction, which is of order J' rather than J'', overcomes the difference in scaling dimensions and controls the physics. In this high magnetization regime, the physics is therefore very similar to that described in the previous sections, and an incommensurate cone state is expected.

In the remainder of this section, we focus on the main field regime, where $\gamma_\pm''$ is dominant. The latter obeys the RG equation [using the dimensionless coupling $\check{\gamma}_\pm'' = \gamma_\pm''/(v\Lambda_\ell^2)$ as discussed in Sec. III D]

$$\partial_\ell \check{\gamma}_\pm'' = (2 - 2\Delta_\pm)\check{\gamma}_\pm'', \tag{73}$$

where $\Delta_\pm = \pi R^2$ is the scaling dimension of the $\mathcal{S}_\pi^\pm$ fields. Integrating this to the scale $\ell = \ln(\xi'')$ such that $\check{\gamma}_\pm''(\ell) \sim v$ defines the length scale

$$\xi'' \sim (v/J'')^{1/(2-2\Delta_\pm)}. \tag{74}$$

For lengths shorter than ξ'', one-dimensional fluctuations are significant and approximately those of free chains. On longer length scales, we expect that $\gamma_\pm''$ drives ordering of the $\mathcal{S}_{y,z;\pi}^\pm$ fields. H_2' in Eq. (71) is minimized by configurations of the form

$$\langle \mathcal{S}_{y,z;\pi}^\pm \rangle = |\psi|(-1)^z e^{\pm i\beta\vartheta_y}, \tag{75}$$

where $|\psi|$ is a real number giving the magnitude of the spontaneous moment, and ϑ_y is a *classical* phase that can be chosen *independently* for each vertical a-b plane specified by y. Note that longitudinal order is strongly suppressed at this scale, $\langle \mathcal{S}_{y,z}^z \rangle = 0$, by the uncertainty principle (in bosonization this follows from the duality of the θ and φ fields). We expect by scaling that $|\psi| \sim (\xi'')^{-\Delta_\pm} \ll 1$, reflecting the suppressed magnitude of magnetic order by 1D fluctuations. Hence

$$|\psi| = \sigma(M)\left(\frac{J''}{v}\right)^{\Delta_\pm/(2-2\Delta_\pm)}, \tag{76}$$

where the prefactor $\sigma(M)$ is computed by CMFT in Appendix D 5. We estimate $|\psi| \approx 0.25$–0.3 over most of the field range. From this, we can estimate the lowering of the energy density due to the establishment of such two-dimensional order, simply by taking the expectation value of Eq. (71),

$$\varepsilon_{2d} \sim J''|\psi|^2. \tag{77}$$

An experimental measure of this energy density is the XY spin stiffness along the a axis, which is of the same order, $\rho_{s;a} \sim \varepsilon_{2d}$. Note that the spin stiffness along the b axis is much larger, of order $\rho_{s;b} \sim v$.

C. Exchange coupling of a-b planes

The arbitrary choice of ϑ_y for every y is a consequence of the fact that the dominant interaction, $\gamma_\pm''$, does not couple different a-b planes. Less relevant interactions can and do remove this arbitrariness, ultimately determining the precise nature of the ordered state.

To study this, we first include exchange interactions between chains within the b-c planes. In the standard model, this is only the J' coupling along the nearest-neighbor diagonals. However, it was argued in Ref. 14 that it is important to also take into account weak exchange J_2 between spins on *second-neighbor* chains separated by distance $\Delta y = 2$. While clearly $J_2 \ll J'$, it is important because it is unfrustrated, unlike the J' interaction.

In the continuum limit, these couplings lead to the Hamiltonian

$$H_3' = \sum_{y,z} \int dx \{ -i\gamma_{\text{cone}} \mathcal{S}_{y,z;\pi}^+ \partial_x \mathcal{S}_{y+1,z;\pi}^- + \text{H.c.} + \gamma_2 \mathcal{S}_{y,z;\pi}^+ \mathcal{S}_{y+2,z;\pi}^- + \text{H.c.} \}, \tag{78}$$

with $\gamma_2 = J_2/2$ (and $\gamma_{\text{cone}} = J'/2$ as given earlier).

Taking the expectation values using Eq. (75), the resulting renormalized Hamiltonian can then be treated classically and minimized to find the ground state. It is evident that the "twist" interaction γ_{cone} favors an incommensurate state with $k_x \neq \pi$. To describe this requires allowing for nonzero gradients $\partial_x \vartheta_y$. While such configurations are not ground states in the absence of γ_{cone}, they are low in energy because a small gradient comprises a soft (Goldstone) mode. The magnitude of the associated incommensurability is determined by a balance of γ_{cone} with the gradient terms in H_0, which of course favor commensurate order at $k_x = \pi$. We therefore include the latter and write the entire effective Hamiltonian explicitly in the ϑ_y variables, which we will allow to be x dependent but *independent* of z according to Eq. (75). The total energy becomes

$$E_b = L_z \sum_y \int dx \left\{ \frac{v}{2}(\partial_x \vartheta_y)^2 + g_2 \cos[\beta(\vartheta_y - \vartheta_{y+2})] - g_{\text{cone}}(\partial_x \vartheta_y + \partial_x \vartheta_{y+1}) \cos[\beta(\vartheta_y - \vartheta_{y+1})] \right\}, \tag{79}$$

with $g_2 = 2\gamma_2|\psi|^2$ and $g_{\text{cone}} = \gamma_{\text{cone}}|\psi|^2\beta$.

Now we can see that, for $g_2 > 0$, which is expected from antiferromagnetic superexchange, the two interactions strongly compete. In this case, the minima of the g_2 term are states with

$$\vartheta_y = \frac{\pi y}{2\beta} + \frac{\Theta_{\text{mod}(y,2)}}{\beta}. \tag{80}$$

Here Θ_0 and Θ_1 define the overall phase on the even and odd chains, respectively. Inserting this into the twist term, one finds a vanishing result due to cancellations when the sum

over y is carried out, even if Θ_0 and Θ_1 are allowed to have gradients. Hence this solution has energy density equal to $-g_2$. This is a commensurate AF state. Conversely, the solutions which minimize the twist term have $\vartheta_y = \kappa x$, for which the g_2 term is *maximized* rather than minimized. Here $\kappa = 2g_{\rm cone}/v$ is determined by minimizing the full energy, leading to the energy density $-2g_{\rm cone}^2/v + g_2$. This is the incommensurate cone state. Comparing the energies of the two states, one finds that the AF state obtains for $g_2 > g_{\rm cone}^2/v$. This requires a minimum value of second neighbor exchange for the commensurate state, $J_2 > J_2^*$, where

$$J_2^* = \frac{\beta^2|\psi|^2}{4}\frac{(J')^2}{v}. \tag{81}$$

For Cs_2CuCl_4, J_2^* is very small, and is in fact only a few percent ($\leqslant 5\%$) of J for the relevant field range. Moreover, we argue below that the above value of J_2^* is actually an overestimate, as it neglects a fluctuation-generated interaction which is of the same order. Thus, an exceedingly tiny second neighbor coupling J_2, likely undetectable directly, qualitatively changes the ground state. In general, reexpressing the minimum energy density in terms of bare variables, we have

$$\varepsilon_{3d} \sim -\max\left\{J_2|\psi|^2, \frac{\beta^2|\psi|^4}{4}\frac{(J')^2}{v}\right\}. \tag{82}$$

This energy scale determines the spin stiffness along the c axis, $\rho_{s;c} \sim \varepsilon_{3d}$.

D. Locking of even and odd *a-b* layers

When J_2 is dominant in establishing three-dimensional AF order, it is ineffective in coupling the even and odd layers. As a consequence, there remains an artificial degeneracy of solutions, specifically, one may make opposite rotations of the phases Θ_1 and Θ_2. This rotation is not a true symmetry of the microscopic theory. However, the simplest possible coupling of phases in neighboring chains, of the form $\cos\beta(\vartheta_y - \vartheta_{y+1})$, *is* prohibited by reflection symmetry, see Eqs. (B14) and (B17). Instead, the leading possible coupling between neighboring chains is of the form

$$H_{\rm bq} = +g_{\rm bq}\sum_{y,z}\int dx \cos[2\beta(\vartheta_{y,z} - \vartheta_{y+1,z})]. \tag{83}$$

Here we have already assumed Eq. (75) and taken the average of the fluctuation-generated interaction, see Appendix E for details. For classical XY spins with phase $\beta\vartheta$, this interaction would correspond to a biquadratic coupling $(\boldsymbol{S}_i \cdot \boldsymbol{S}_j)^2$, between spins on neighboring chains. Such fluctuation-generated biquadratic interactions are indeed familiar from the theory of frustrated magnets, and are a manifestation of "order by disorder."[46,47] In that context, it is well-known that fluctuations generally favor collinear states, which requires $g_{\rm bq} > 0$. This is indeed confirmed by the microscopic calculation in Appendix E, which leads to the estimate

$$g_{\rm bq} \sim \frac{(J')^2}{v}|\psi|^4. \tag{84}$$

In the AF phase, we may use the solutions for $\theta_{y,z}$ determined above and hence rewrite Eq. (83) as

$$E_{\rm bq} = -g_{\rm bq}L_xL_yL_z\cos[2(\Theta_0 - \Theta_1)]. \tag{85}$$

Clearly states with $\Theta_0 = \Theta_1 + n\pi$ are preferred, which implies commensurate, collinear, AF order. The condensation energy density associated with the selection of the collinear order is thus $\varepsilon_{\rm CIT} \sim g_{\rm bq}$ (the reason for the choice of this subscript will become clear in the next section). Physically, this energy scale determines the gap of the antisymmetric pseudo-Goldstone mode corresponding to $\Theta_0 - \Theta_1$, which is of order

$$\Delta_{\rm as} \sim \sqrt{v\varepsilon_{\rm CIT}} \sim J'|\psi|^2. \tag{86}$$

This can potentially be measured as an emergent low energy (but gapped) mode in neutron scattering.

Comparing Eq. (82) with Eqs. (84) and (85), we observe that the energy gain due to $g_{\rm bq}$ term is of the same order as the energy gain of the incommensurate cone state. This is not a coincidence as the both effects have their common origin in the interchain exchange J'. This suggests that, even in the absence of any microscopic J_2 exchange, a collinear state could be energetically preferred to the cone state. However, the RG approach used to obtain Eq. (84) is not accurate in determining the $O(1)$ numerical prefactor, which is essential for making such a comparison quantitatively. Thus we at present can only speculate that this might be the case. Even if not, these considerations imply that the interaction J_2 needed to induce the AF state is even lower than the estimate in Eq. (81).

VI. FIELD ALONG *c* AXIS

Experimentally, this field orientation shows the most complex phase diagram. In addition to the commensurate "AF" phase seen for fields along the b axis, a broad region of incommensurate phase is also clearly observed in NMR measurements[48] (and defined by earlier magnetization measurements[8]). Within the model used up to now, the difference in phase diagrams for fields along the b and c axes is inexplicable: the Hamiltonian has a symmetry under spin rotations within the b-c plane.

A. DM interaction on chain bonds

Therefore additional spin-rotational symmetry breaking interactions *must* be included to explain this discrepancy. We therefore turn to the general set of allowed DM interactions in Sec. II C for our consideration. As we saw in the previous section, DM terms whose DM vector is orthogonal to the applied field average out rapidly in the presence of an applied field. Hence we need consider only components of the DM vectors along the c axis. There are two independent such terms: D_c and D_c'. Given that DM terms are generally proportional to the corresponding exchange, we expect D_c to be the largest of the two, and we focus on its effects (in Appendix F 3 we explain in detail why D_c' can be neglected). It introduces the perturbation

$$H_c \sim D_c \sum_{y,z} (-1)^y \int dx \mathcal{J}^z_{y,z}(x) \sim d_c \sum_{y,z} (-1)^y \int dx \partial_x \theta_{y,z}, \tag{87}$$

where $d_c = vD_c/(\beta J)$.

Notably, H_c is linear in the boson fields, and hence, in the absence of any other interactions, the term d_c can be taken into account exactly. Moreover, it is actually a pure boundary term, whose effect on the energy depends solely on the *winding numbers*, $[\theta_{y,z}(\infty) - \theta_{y,z}(-\infty)]/(2\pi\beta)$, and vanishes in the zero winding number sector. However, H_c favors sectors with nonvanishing winding numbers (proportional to L_x, in fact).

B. D_c does not compete with J, J', and J''

To understand the degree of competition of H_c with the other interactions, it is instructive to consider the shifted variables

$$\tilde{\theta}_{y,z}(x) = \theta_{y,z}(x) + (-1)^y \frac{d_c}{v} x. \tag{88}$$

With this shift, d_c is "eliminated" from the free Hamiltonian, up to a constant: $H_0[\theta] + H_c[\theta] = H_0[\tilde{\theta}] + \text{const}$. Physically, this change of variables corresponds to a shift of the dominant wave vector of correlations from $k_x = \pi$ to $k_x = \pi \pm \beta d_c/v = \pi \pm D_c/J$. Significantly, the dominant $\gamma''_{\pm}$ coupling is invariant under the shift: $H'_2[\theta] = H'_2[\tilde{\theta}]$. Thus J'' and D_c do not compete. The same is true for the γ_2 (J_2) interaction. Thus, in the region where the AF phase appears for the case of field along the b axis since the J'' and J_2 couplings dominate, we expect the energetics is unchanged at the three highest energy scales in Fig. 9.

C. Commensurate-incommensurate transition

Differences do appear, however, once the cone and biquadratic interactions are considered, as these are *not* invariant under the shift in Eq. (88). We focus on the putative AF region, for which we may assume the decomposition in Eq. (80). Allowing for small gradients in $\Theta_{\pm}(x,y,z) = \Theta_0(x,y,z) \pm \Theta_1(x,y,z)$, we obtain the continuum Hamiltonian $H = H_+ + H_-$, with

$$H_+ = \int d^3\boldsymbol{r} \left\{ \sum_{\mu} \frac{c_\mu}{2} (\partial_\mu \Theta_+)^2 \right\}, \tag{89}$$

$$H_- = \int d^3\boldsymbol{r} \left\{ \sum_{\mu} \frac{c_\mu}{2} (\partial_\mu \Theta_-)^2 + \frac{d_c}{2\beta} \partial_x \Theta_- - g_{\text{bq}} \cos(2\Theta_-) \right\}, \tag{90}$$

where $c_x = v/4\beta^2$, $c_y = g_2$, and $c_z = \tilde{\gamma}''_{\pm}/4$.

Here the cone interaction has dropped out, and the low energy Hamiltonian has decomposed into two decoupled parts. The first, H_+, is simply the Hamiltonian of a free massless boson. It describes the Goldstone mode Θ_+ associated with spin rotations about the field axis. The second part, H_-, is the familiar sine-Gordon model, discussed earlier in Sec. III D 4. In this case it is in three dimensions, but this has no significant consequences. As in Sec. III D 4, the sine-Gordon model describes a commensurate phase (here, the AF state) and an incommensurate (IC) one, separated by a *commensurate-incommensurate transition* (CIT).

The results for the CIT can be taken over directly from Sec. III D, with the mapping $\Theta_- \to \varphi/2$. Here, it is d_c which plays the role of the tuning parameter, favoring the IC phase, for $|d_c| > d_c^*$, where

$$d_c^* = \frac{4\sqrt{v g_{\text{bq}}}}{\pi}. \tag{91}$$

On entering the IC phase, the system forms a soliton lattice, with a corresponding incommensurate wave vector q_0 (measured relative to the AF state). Note that the IC phase found here is thus a smooth deformation of the AF state, which makes it quite distinct from the cone state, which is also incommensurate. The incommensurate wave vector grows rapidly after the CIT, which can be seen by translating Eq. (56) to the current case,

$$q_0 = \frac{\langle \partial_x \Theta_- \rangle}{2} \sim \frac{\pi}{4\beta} \sqrt{\frac{g_{bq}}{v}} \frac{1}{\ln[(|d_c| - d_c^*)/d_c^*]}, \tag{92}$$

where the brackets $\langle \partial_x \Theta_- \rangle$ indicates the spatial average. Once the above logarithm is not large, the solitons are strongly overlapping, and Eq. (92) is no longer valid. Instead, one may simply minimize the energy neglecting g_{bq}, which gives

$$q_0 = \frac{\beta d_c}{v} = \frac{D_c}{J}. \tag{93}$$

To summarize, q_0 varies from its maximal value given in Eq. (93) at the low field end of the IC phase and *decreases* with increasing field, vanishing asymptotically according to Eq. (92) at the CIT to the AF phase. Because the variation in Eq. (92) is so rapid, very likely q_0 appears approximately constant in most of the IC phase, dropping precipitously to zero in a narrow region near the CIT.

VII. EXPERIMENTAL CONSEQUENCES

In this section, we consider a few key experimental consequences of the analysis of the previous sections. First, we give explicit expressions for the spin structures in the various phases predicted there, which should be useful for comparison to neutron scattering measurements. Next, we derive the nuclear magnetic resonance (NMR) line shapes in each of these phases, using these expressions, and compare to experiments by Takigawa and collaborators. Finally, we describe the phase diagrams in the magnetic field–temperature plane for the different field orientations.

A. Explicit spin structures

Here we reconstruct explicit formulae and plots of the spin ordering patterns in the various phases discussed earlier.

1. Cone state

First consider the incommensurate ordered "cone" state, described in Sec. IV B, which occurs for any field along the

a axis. This is described by Eq. (66). Using Eq. (24), we can express the microscopic spin operator's expectation value

$$\begin{aligned}\langle S^x_{xyz}\rangle_{\text{cone}} &= (\langle S^+_{xyz}\rangle e^{i\pi x} + \text{c.c.})/2 \\ &= (-1)^{yz} N \cos[(\pi + (-1)^z q_0)x + \Theta_z] \\ &= (-1)^{yz} N \cos[(\pi + q_0)x \\ &\quad + ((-1)^z - 1)\pi x + (-1)^z \Theta_z]. \end{aligned} \tag{94}$$

To further simplify, we note that the x coordinate takes integer values for even y and half-integer values for odd y. As a consequence, $((-1)^z-1)\pi x$ is an integer multiple of 2π *unless* y is odd *and* z is odd. This allows this factor inside the cosine to be removed in favor of an overall $(-1)^{yz}$ factor in front of it, which cancels the one already present. Therefore one finds, finally

$$\langle S^x_{xyz}\rangle_{\text{cone}} = N \cos[(\pi + q_0)x + \tilde{\Theta}_z], \tag{95}$$

where $\tilde{\Theta}_z = (-1)^z \Theta_z$. Similar manipulations for the y component of the spins give

$$\langle S^y_{xyz}\rangle_{\text{cone}} = (-1)^z N \sin[(\pi + q_0)x + \tilde{\Theta}_z]. \tag{96}$$

and of course, one has

$$\langle S^z_{xyz}\rangle_{\text{cone}} = M. \tag{97}$$

2. Antiferromagnetic phase

Here we simply apply Eq. (80) and use $\Theta_0 = \Theta$, $\Theta_1 = \Theta + \pi n$ (with $n = 0, 1$) as preferred in the commensurate AF phase by Eq. (85). This gives

$$\langle S^x_{xyz}\rangle_{\text{AF}} = (-1)^z |\psi| \cos[\pi x + \sigma \pi y/2 + \Theta], \tag{98}$$

$$\langle S^y_{xyz}\rangle_{\text{AF}} = (-1)^z |\psi| \sin[\pi x + \sigma \pi y/2 + \Theta], \tag{99}$$

where the $\sigma = \pm 1 = (-1)^n$. These equations describe a state in which the x-y components of the spins are *collinear*. This may not be obvious but is true because the combination $\pi x + \sigma \pi y/2$ is always an integer multiple of π, owing to the fact that x is integer (half-integer) for even (odd) y. Combined with the constant uniform magnetization, Eq. (97), these equations describe a *coplanar* spin state, distinct from the three-dimensional cone configuration. We note, however, that small perturbations due to the various DM interactions will probably disrupt this ideal coplanarity. The commensurate nature of the ordering is, however, robust.

3. Incommensurate phase for fields along the c axis

Here we consider the incommensurate phase which is discussed in Sec. VI. For simplicity, we will ignore the narrow but subtle region in the vicinity of the CIT, where a nontrivial soliton lattice should be taken into account. The basic symmetry of this phase is well described by the "smooth" regime (corresponding to strongly overlapping solitons), where we simply treat the incommensuration as linear shift of the phase fields, i.e., we take $\tilde{\theta}_{y,z}$ in Eq. (88) as constant. The preceding formula now are modified to

$$\langle S^x_{xyz}\rangle_{\text{IC}} = (-1)^z |\psi| \cos[(\pi + (-1)^y q_0)x + \pi y/2 + \Theta_y], \tag{100}$$

$$\langle S^y_{xyz}\rangle_{\text{IC}} = (-1)^z |\psi| \sin[(\pi + (-1)^y q_0)x + \pi y/2 + \Theta_y], \tag{101}$$

where $q_0 = \beta d_c / v$—see Eq. (93)—and Θ_y is a phase taking two distinct arbitrary values for even and odd y.

B. NMR line shape

Recent NMR experiments by Takigawa and collaborators[48] have revealed numerous phases and transitions in Cs_2CuCl_4 in magnetic fields. Here we wish to address the signatures of the phases predicted in this paper in the NMR lineshape. The basic approach is to consider the Hamiltonian of a given nuclear spin $\mathbf{I}_i$ to be the sum of two effective fields

$$H_a = (\mathbf{h}^{\text{ext}}_i + \mathbf{h}^{\text{hf}}_a) \cdot \mathbf{I}_i, \tag{102}$$

where $\mathbf{h}^{\text{ext}}_i$ is the effective field on the nucleus i due to the external field $\mathbf{H}$, factoring in any anisotropies of the nuclear g tensor (which are believed to be small[49]). The remaining "hyperfine field" $\mathbf{h}^{\text{hf}}_i$ represents transferred hyperfine interactions with nearby electronic spins. The NMR resonance frequency of this particular nucleus is simply proportional to the magnitude of the total effective field. The simplest approximation, which we take here, is to assume in addition that $|\mathbf{h}^{\text{hf}}_i| \ll |\mathbf{h}^{\text{ext}}_i|$. This is certainly so in intermediate and high-field regions, which we focus on. For lower fields, of the order of 1–2 T, this may not be such a good approximation.[49] But even in this case the off-diagonal contribution [see Eq. (105) below], which is central to our consideration, should be smaller than the diagonal one and a modified expansion in off-diagonal components of $\mathbf{h}^{\text{hf}}_i$ should be possible. With these assumptions in mind, and disregarding the g-factor anisotropy (so that $\mathbf{h}^{\text{ext}}_i \propto \mathbf{H}$), we can approximate the shift due to the hyperfine interaction by

$$\Delta \nu_i \propto \mathbf{h}^{\text{hf}}_i \cdot \mathbf{h}^{\text{ext}}_i / |\mathbf{h}^{\text{ext}}_i| = \mathbf{h}^{\text{hf}}_i \cdot \hat{\mathbf{H}}, \tag{103}$$

where $\hat{\mathbf{H}} = \mathbf{H}/|\mathbf{H}|$. In Cs_2CuCl_4, there are two inequivalent Cs sites measured in the Cs NMR measurements. We focus on the Cs(A) site, which is located slightly above or below the center of a triangle of Cu spins.[50] The NMR response of the[49] Cs(B) site, which is coupled to Cu spins in the two planes adjacent to it, is more difficult to analyze at present, but we do expect the qualitative conclusions derived below to remain valid for this situation as well. In the Cs(A) case, the hyperfine field of nucleus i located between spins j at the sites of this triangle should be given by the sum of three transferred contributions,

$$\mathbf{h}^{\text{hf}}_i = \sum_{j \text{ nn } i} \mathbf{K}_{ij} \langle \mathbf{S}_j \rangle, \tag{104}$$

where $\mathbf{K}_{ij}$ is a tensor describing the anisotropic transferred hyperfine exchange from the Cu spin at site j to the nucleus i (see Fig. 10). According to recent measurements,[50] in these

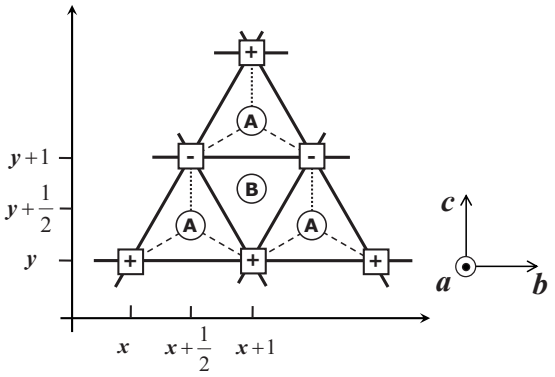

FIG. 10. Scheme of the transferred hyperfine interaction for Cs(A). The signs +/− refer to the relative signs of the off-diagonal entry κ_{ij} in Eq. (105). κ_{ij} takes equal value for two sites of a triangle as shown by the dashed lines while that for the other site can be different as shown by the dotted line.

tensors, the only significant off-diagonal entry is $[\mathbf{K}_{ij}]^{ac}=[\mathbf{K}_{ij}]^{ca}=\kappa_{ij}$, and moreover, κ_{ij} takes equal values for the two sites j of the triangle which are on the same chain.

For magnetic fields along a and c, this off-diagonal transferred exchange is crucial in determining the NMR line shape. Let us see how this occurs. In either of these cases, we define, as usual the z axis of spin along the field axis. Let us then take the x axis of spin along the other of the two, i.e., for $\hat{\mathbf{H}}=\hat{a}$, take $S^x=S^c$, and conversely, if $\hat{\mathbf{H}}=\hat{c}$, then $S^x=S^a$. From Eq. (103), the NMR shift is entirely determined by the z component of the hyperfine field. This, in turn, is given by

$$[\mathbf{h}_i^{\mathrm{hf}}]^z=\sum_{j\ \mathrm{nn}\ i}([\mathbf{K}_{ij}]^{zz}\langle S_j^z\rangle+\kappa_{ij}\langle S_j^x\rangle). \tag{105}$$

In all of the phases predicted for Cs_2CuCl_4, the component of the spins parallel to the field is constant, and equal to the average magnetization M (this is *not* true in the SDW phase, which is expected in the ideal 2D case of Sec. III). Therefore the first term in Eq. (105) gives a constant contribution to the shift, which is the same for all Cs(A) nuclei. Thus

$$\Delta\nu_i\propto\mathrm{const}+\sum_{j\ \mathrm{nn}\ i}\kappa_{ij}\langle S_j^x\rangle. \tag{106}$$

Using the experimentally determined form of the hyperfine couplings, and dropping the constant, one has

$$\Delta\nu_{x+1/2,y+1/2,z}=(-1)^y(\kappa_1[\langle S_{x,y,z}^x\rangle+\langle S_{x+1,y,z}^x\rangle]+\kappa_2\langle S_{x+1/2,y+1,z}^x\rangle). \tag{107}$$

Here we have absorbed the proportionality constant in the shift into the definitions of κ_1 and κ_2. We are now in a position to evaluate the NMR line shape for the different magnetic phases.

1. Cone state

In the cone state, we can use Eq. (95) to evaluate Eq. (107). One obtains

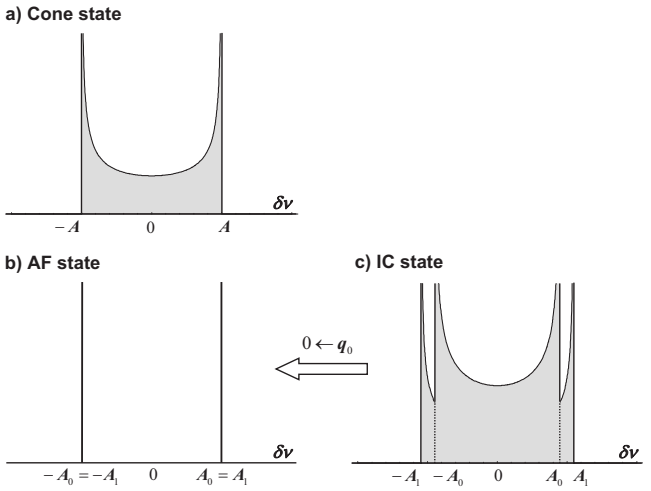

FIG. 11. Schematic NMR spectra in (a) the cone state, (b) the AF state, and (c) the IC state. On approaching the commensurate AF phase from the IC phase, i.e., $q_0\to 0$ limit, four peaks merge pairwise as indicated by the arrow.

$$\Delta\nu_{x+1/2,y+1/2,z}=(-1)^yN\left[\kappa_2-2\kappa_1\sin\frac{q_0}{2}\right]\times\cos[(\pi+q_0)(x+1/2)+\tilde{\Theta}_z]. \tag{108}$$

Now the NMR line shape reflects the *distribution* of shifts, $p(\Delta\nu)$, over all the Cs(A) sites. We may consider this as a sum of distributions of the shifts for the nuclei associated with each pair of chains, i.e., ranging over x for fixed y and z. Because q_0 is incommensurate, the argument of the cosine above is distributed *uniformly* over the full angular interval from 0 to 2π. Thus the cosine itself is distributed between −1 and +1, and we obtain a distribution for the shift, for fixed y and z with support between $\pm N|\kappa_2-2\kappa_1\sin\frac{q_0}{2}|$,

$$p(\Delta\nu)=\frac{1}{\pi}\frac{1}{\sqrt{A^2-(\Delta\nu)^2}}\Theta[A-|\Delta\nu|], \tag{109}$$

with

$$A=N\left|\kappa_2-2\kappa_1\sin\frac{q_0}{2}\right|. \tag{110}$$

We see that the distribution is in fact independent of y and z so that the full distribution over all Cs(A) sites is identical to that for a single pair of chains. It has two peaks, at the edges of the distribution, $\delta\nu=\pm A$ as shown in Fig. 11(a).

2. AF state

Applying Eq. (98) to Eq. (107), we obtain

$$\Delta\nu_{x+1/2,y+1/2,z}=\sigma(-1)^{y+z}|\psi|\kappa_2\cos[\pi(x+\sigma y/2)+\Theta]=\pm\kappa|\psi|\cos\Theta. \tag{111}$$

One expects therefore two sharp peaks in the Cs(A) NMR spectrum, separated by $2\kappa_2\psi|\cos\Theta|$ [see Fig. 11(b)]. Note that $\cos\Theta$ is generically nonzero, as argued by symmetry in Appendix C 2.

3. IC state

Here we apply Eq. (100) to Eq. (107). We find that the NMR shift can be written as

$$\Delta\nu_{x+1/2,y+1/2,z} = A_y \cos(q_0 x + \phi_y), \tag{112}$$

where

$$|A_y| = |\psi|\left[4\kappa_1^2 \sin^2\frac{q_0}{2} + \kappa_2^2 - (-1)^y 4\kappa_1\kappa_2 \sin\frac{q_0}{2}\sin(\Theta_0+\Theta_1)\right]^{1/2}, \tag{113}$$

and

$$\tan\phi_y = \begin{cases} \dfrac{\kappa_1(\sin(q_0+\Theta_0)-\sin\Theta_0)+\kappa_2\sin\left(\dfrac{q_0}{2}-\Theta_1\right)}{\kappa_1(\cos(q_0+\Theta_0)-\cos\Theta_0)+\kappa_2\cos\left(\dfrac{q_0}{2}-\Theta_1\right)} & y \text{ even} \\ \dfrac{\kappa_1(\sin(q_0-\Theta_1)+\sin\Theta_1)+\kappa_2\sin\left(\dfrac{q_0}{2}+\Theta_0\right)}{\kappa_1(\cos(q_0-\Theta_1)-\cos\Theta_1)+\kappa_2\cos\left(\dfrac{q_0}{2}+\Theta_0\right)} & y \text{ odd}. \end{cases} \tag{114}$$

For each y, we expect from Eq. (112) a continuum line shape of the form of Eq. (109), owing to the incommensurate wave vector q_0. However, in general, A_y takes two distinct values for even and odd y [owing to the $(-1)^y$ factor in Eq. (113)]. Note that the prefactor of this term is nonvanishing since $\sin(\Theta_0+\Theta_1)$ is generally nonzero, as argued in Appendix C 3. Hence the full Cs(A) line shape is expected to be the sum of both distributions and hence has *four peaks*, at $\Delta\nu = \pm A_0, \pm A_1$ as schematically shown in Fig. 11(c). Notably, these peaks merge pairwise as $q_0 \to 0$, i.e., on approaching the commensurate AF phase from the IC state. Precisely such a merging of the peaks has been seen in the NMR experiments by Takigawa and collaborators.[48]

C. Phase diagrams

In Secs. IV–VI, we have determined (most of) the zero temperature phases for the three major field orientations. Here we discuss the extension of these results to $T>0$.

1. Field along the a axis

This is the simplest case. At zero temperature, the cone state extends across the entire field range from zero up to saturation. We have seen that it is predominantly controlled by the DM interaction $D=D'_a$, perturbed somewhat by the interchain exchange J'. We therefore expect a single phase boundary, $T_{\text{cone}}(H)$. One estimate for this curve is obtained from CMFT and is shown in Fig. 19 (plotted versus magnetization M rather than field). One observes that T_{cone} at first increases with the applied field for small fields and then reaches a maximum, followed by a decrease to zero at the saturation field.

These trends can be understood simply as follows. With increasing magnetization, the spins become more XY-like, which decreases the scaling dimension $\Delta_{\pm}$. As a consequence, the DM interaction becomes more relevant with increasing field, enhancing the critical temperature. However, on approaching saturation, the magnitude of the transverse components of the spins, which constitute the cone order, decrease to zero, and hence suppress the ordering temperature to zero.

As these trends are correctly captured by CMFT, we may perhaps trust the result for the phase boundary. However, we note that the *nature* of the phase transition is somewhat subtle and probably not properly described by this approximation. Neglecting J'', which has a very weak effect upon the cone state [see Eq. (69)], the system is effectively two-dimensional, and as a consequence exhibits strong effects of thermal fluctuations. Since the DM terms (e.g., D_c) with DM-vectors perpendicular to a are also negligible here, the Hamiltonian has approximate XY spin rotation symmetry. As a consequence, the cone phase is approximately a *quasi-long-range-ordered state* at $T>0$, and its thermal transition should be of Kosterlitz-Thouless (KT) type. Obviously the CMFT approximation does not describe the KT universality class and instead predicts mean-field critical behavior.

It is interesting to verify that, nevertheless, the magnitude of T_c obtained from CMFT agrees with an analysis based on KT theory. For simplicity, we will focus on the DM-dominated field range and neglect entirely J' and J'' for simplicity. In this case, the system decouples into 2D triangular x-y planes, consisting of chains connected by the DM interaction only. Taking the expectation value using Eq. (59) in Eq. (58), one obtains the energy

$$H_{2d} = \sum_{y,z} \int dx \left\{ \frac{v}{2} (\partial_x \vartheta_{y,z})^2 - 2D|N|^2 \cos \beta (\vartheta_{y,z} - \vartheta_{y+1,z}) \right\}. \tag{115}$$

In the ordered phase, one may expand the cosine and take the continuum limit (in y) for fields $\vartheta_{y,z}$ that are slowly varying in y,

$$H_{2d} = \sum_{z} \int dxdy \left\{ \frac{v}{2} (\partial_x \vartheta_z)^2 + D|N|^2 \beta^2 (\partial_y \vartheta_z)^2 \right\}. \tag{116}$$

Now, according to KT theory, the critical temperature is proportional to the geometric mean of the two stiffnesses, i.e., $T_{KT} \sim \sqrt{vD}|N|$. We are neglecting all $O(1)$ prefactors here, as we are only interested in the scaling behavior. Now from scaling, or from the CMFT calculations in Appendix D 5, one has $|N| \sim (D/v)^{\Delta_\pm/(2-2\Delta_\pm)}$, from which one obtains finally $T_{KT} \sim v(D/v)^{1/(2-2\Delta_\pm)}$. Precisely the same scaling is found directly from the CMFT treatment at $T>0$ in the Appendix D 4. [Please note that the described calculation corresponds to setting $J'=0$ the coupling $\hat{\Gamma}^a_{\text{cone}}$, see Eq. (D27). That implies $q_0=0$ which, via second equation in Eq. (D23), leads to the scaling $T_c \sim v(D/v)^{1/(2-2\Delta_\pm)}$.] It may appear surprising that the two approaches, which describe the transition so differently, agree in this respect. The reason for the agreement is that the *scale* of T_c is entirely determined by the scaling properties of the weakly perturbed one-dimensional chains. Any approximation which respects this scaling (and both the CMFT and the KT analysis do) will obtain the same order of magnitude answer. Differences would appear in the prefactor, which, however, is beyond the scope of the rough KT analysis carried out here.

2. Field along b axis

The situation in a field along b is considerably more complicated. The analysis in Sec. V implies *at least* four phases at $T=0$: the zero field phase "spiral" phase, dominated by D, the AF phase, the high-field cone phase, and the saturated phase. Due to the difficulty of treating the competition between the D term and magnetic field when the two are comparable, the intervening range between the AF and zero field phases has not been fully clarified here. Thermodynamic measurements[8] appear to show a single transition between the spiral and AF states and therefore the absence of any intermediate states.

For the "high field" phases (i.e., in the region where the D term is negligible), we can attempt to apply CMFT to determine the uppermost phase boundaries, describing the transitions from the ordered to paramagnetic states. The key observation is that *both ordered phases* (AF and cone) are driven by the same J'' interaction. The two states are only distinguished by the competing effects of the weaker (at least in the renormalized sense) J' and J_2 interactions. Thus the upper phase boundary should be approximately continuous across this field range up to saturation, and not very sensitive to the precise nature (AF or cone) of the ordered phase it demarcates. This boundary should be similar in shape to the $T_{\text{cone}}(H)$ discussed above, as it arises from a term of the same scaling dimension as D in that case, and suffers the same reduction on approaching saturation.

The high-field region requires one further phase boundary, between the AF and cone states. This should be approximately vertical but is expected to bend "to the left," as the cone state has higher entropy than the AF one and is thus favored with increasing temperature. This reasoning is based on higher order effects of other DM interactions that we have neglected up to now (mentioned in passing in Sec. VII A 2): these subdominant terms are expected to break the U(1) rotational symmetry of the AF state and gap out its Goldstone modes, while preserving the commensurability of the AF structure. The cone state, being incommensurate, is expected to not be affected by these small perturbations and preserve its gapless excitations. As a result, we expect the entropy of the cone state to be greater than that of the AF one and result in the mentioned bending of the AF-cone boundary to the left. The transition between the two states is first order and observables such as the ordering wave vector jump at the critical field.

3. Field along c axis

In this, most complex field orientation, all the phases predicted for the field along b must appear, *and* in addition the IC state, taking up some territory between the AF and spiral phases. Experiments seem to show[5,8,48] even beyond these five states, one or two additional ones in the regime when the D term is comparable to the Zeeman energy. At present we have little to say about these states. The observed linear relation between the ordering momentum of the intermediate "S" state (in the notation of Ref. 5) is suggestive of an SDW phase, but at the present we do not have a good understanding of how the competition between the DM and the Zeeman terms may bring out the SDW order discussed in Sec. III B.

In the high-field region, we expect, by similar arguments to the previous section, a rather continuous boundary between the IC, AF, and cone states and the paramagnetic phase. The AF-cone boundary should appear very similar to that for this field orientation as well. The new feature introduced here is the IC-AF boundary, which is the location of the CIT. Like the cone phase, the IC phase is expected to have more entropy than the AF state, and hence be stabilized by increasing temperature. Experimentally, this boundary bends quite sharply "to the right," in marked contrast to the nearly vertical AF-cone transition line.

To understand this, consider the expression for the CIT location, Eq. (91). It can be rewritten, using the expressions for g_{bq}, Eq. (84), and for d_c [given in the text following Eq. (87)], as

$$|\psi|^2 \sim \frac{vD_c}{\beta JJ'}, \tag{117}$$

where we drop all $O(1)$ factors. A simple treatment, which takes into account some of the one-dimensional fluctuations, but not the high-dimensional ones, is to simply apply Eq. (91), but replacing $|\psi|^2$ with its reduced value *at* $T=T_{\text{CIT}}$. In general, this is difficult to actually calculate analytically, e.g.,

with CMFT, but the detailed form is not important to our argument. Scaling implies that it can be written as

$$|\psi|^2(T) = |\psi_0|^2 \mathcal{F}(T/T_c), \tag{118}$$

where T_c is the critical temperature at which ψ vanishes, and the scaling function $\mathcal{F}$ is smooth and obeys $\mathcal{F}(0)=1$ and $\mathcal{F}(1)=0$. For illustrative purposes, we can take the simple approximation $\mathcal{F}(t)=1-t^2$. Using this form, one finds

$$\frac{T_{\mathrm{CIT}}}{T_c} = \sqrt{1 - \frac{vD_c}{\beta JJ'|\psi_0|^2}}. \tag{119}$$

By construction, the right-hand side vanishes at the zero temperature CIT, where $T_{\mathrm{CIT}}=0$. Both ψ_0 and β are rather weak functions of magnetic field. However, the velocity v varies considerably (on the scale of J) with field, indeed vanishing as saturation is approached. Hence, the right-hand-side increases rather quickly with field, leading to rapid variation of T_{CIT} with an approximate square-root form, consistent with experiments.

It is interesting to note that, in experiment,[8,48] the AF-IC and AF-cone boundaries are observed to approach each other very closely with increasing temperature, leading to an extremely narrow range of transition directly from the paramagnet to the AF phase. This suggests some physical mechanism which "avoids" this transition. In fact, one can argue that, according to Landau theory, a *continuous* AF-paramagnetic transition is *forbidden* for this field orientation. To do so, consider the Landau expansion of the free energy F in the "order parameters" $\psi_{y,z}(x) \equiv \langle \mathcal{S}^-_{y,z}(x) \rangle$. Such an expansion, in powers of $\psi_{y,z}$, is valid near any putative continuous transition. We presume $\psi_{y,z}(x)$ to be a slowly varying function of x. The Landau expansion has the form $F=F_2+F_4+\cdots$, where

$$\begin{aligned} F_2 = \sum_{y,z} \int dx \Big\{ & \frac{\bar{v}}{2} |\partial_x \psi_{y,z}|^2 \\ & - i\bar{\gamma}_c (\psi^*_{y,z} \partial_x \psi_{y+1,z} + \text{c.c.}) - i\bar{d}_c (-1)^y \psi^*_{y,z} \partial_x \psi_{y,z} \\ & + \bar{\gamma}_2 (\psi^*_{y,z} \psi_{y+2,z} + \text{H.c.}) + \bar{\gamma}''_{\pm} (\psi^*_{y,z} \psi_{y,z+1} + \text{H.c.}) + r|\psi_{y,z}|^2 \Big\} \end{aligned} \tag{120}$$

contains quadratic terms in the order parameter, and

$$F_4 = \sum_{y,z} \int dx \{ u|\psi_{y,z}|^4 + \bar{\gamma}_{\mathrm{bq}} [(\psi^*_{y,z} \psi_{y+1,z})^2 + \text{H.c.}] \} \tag{121}$$

is quartic. In Eqs. (120) and (121), the couplings with overlines on them are analogous to the corresponding couplings in the bosonized Hamiltonian, as can be seen if one assumes $\psi_{y,z} = |\psi| e^{i\vartheta_{y,z}}$. They are, however, from the present point of view, phenomenological coefficients which are at best proportional to those microscopic couplings.

Let us consider possible continuous transitions from the paramagnetic state. In this case, we may assume $|\psi_{y,z}|$ is arbitrarily small, and thus F_4 is a small perturbation to F_2. The transition occurs on decreasing r from large positive values, at the point at which the smallest eigenvalue of the quadratic form in F_2 vanishes. Fourier transforming into the two-site unit cell, $\psi_{y,z}(x) = \int d^3k/(2\pi)^3 \psi_{a,k} e^{ik_x x + ik_y y + ik_z z}$, with $a=0$ for y even and $a=1$ for y odd, one obtains

$$F_2 = \int \frac{d^3k}{(2\pi)^3} \psi^*_{a,k} \mathcal{F}_{ab}(k) \psi_{b,k}, \tag{122}$$

where the matrix $\mathcal{F}(k)$ can be decomposed into the identity matrix, $\boldsymbol{I}$, and the Pauli matrices, $\boldsymbol{\sigma}_\mu$, according to

$$\mathcal{F}(k) = \mathcal{F}_0 \boldsymbol{I} + \mathcal{F}_x \boldsymbol{\sigma}_x + \mathcal{F}_z \boldsymbol{\sigma}_z, \tag{123}$$

with

$$\begin{aligned} \mathcal{F}_0 &= \frac{\bar{v}}{2} k_x^2 + 2\bar{\gamma}''_{\pm} \cos k_z + 2\bar{\gamma}_2 \cos 2k_y + r, \\ \mathcal{F}_x &= 2\bar{\gamma}_c k_x \cos k_y, \\ \mathcal{F}_z &= \bar{d}_c k_x. \end{aligned} \tag{124}$$

One immediately concludes that the minimum eigenvalue of $\mathcal{F}$ is

$$\mathcal{F}_{\mathrm{min}} = \mathcal{F}_0 - \sqrt{\mathcal{F}_x^2 + \mathcal{F}_z^2} = \mathcal{F}_0(k) - |k_x| \sqrt{4\bar{\gamma}_c^2 \cos^2 k_y + \bar{d}_c^2}. \tag{125}$$

This, in turn, should be minimized over k. Minimization over k_x and k_z is simple: the minimum occurs at

$$|k_x| = \sqrt{4\bar{\gamma}_c^2 \cos^2 k_y + \bar{d}_c^2}/\bar{v} \tag{126}$$

and $k_z=\pi$. Then

$$\begin{aligned} \mathcal{F}_{\mathrm{min}}(k_y) &= r - 2\bar{\gamma}''_{\pm} - \frac{\bar{d}_c^2}{2\bar{v}} - \frac{2\bar{\gamma}_c^2 \cos^2 k_y}{\bar{v}} + 2\bar{\gamma}_2 \cos 2k_y \\ &= r - 2\bar{\gamma}''_{\pm} - \frac{\bar{d}_c^2 + 2\bar{\gamma}_c^2}{2\bar{v}} + \left(2\bar{\gamma}_2 - \frac{\bar{\gamma}_c^2}{\bar{v}} \right) \cos 2k_y. \end{aligned} \tag{127}$$

From here we immediately see that the minimum free energy is obtained for $k_y=0$ when $\bar{\gamma}_c^2/\bar{v} > 2\bar{\gamma}_2$ and for $k_y=\pi/2$ otherwise. In either case, we see from Eq. (126) that $k_x \neq 0$. The two cases therefore correspond to the cone and IC states, respectively. Notably, the commensurate AF state is *absent*. This is easily understood since it is stabilized by the biquadratic coupling g_{bq}, which in Landau theory corresponds to the *quartic* interaction $\bar{\gamma}_{\mathrm{bq}}$. Since this becomes parametrically small relative to the quadratic terms as $|\psi| \to 0$, it cannot stabilize a commensurate phase in this limit. Thus we conclude that *if* there is a continuous transition from the paramagnet to an ordered state for this field orientation, it can only be to the cone or IC phases, and *not* to the AF state. Conversely, if there is a direct transition between the paramagnet and AF states, it must be first order. This latter scenario appears to be the case in experiment.[8,48] We note that for fields along the b axis, where $d_c=0$, a direct continuous transition to the AF state is possible, since in that case $k_y=\pi/2$ and k_x vanishes from Eq. (126).

D. Cs_2CuBr_4

It is instructive to compare the case of Cs_2CuCl_4 extensively reviewed here with that of its isostructural equivalent Cs_2CuBr_4. The latter material is more two dimensional, with $J'/J \approx 0.75$ as estimated in Ref. 51 by comparing the observed momentum of magnetic Bragg reflections, $\mathbf{q}_0 = (0, 0.575, 0)$, with the result of the series expansion calculations in Ref. 52. This estimate should be taken with some caution, as the theory neglects DM coupling, which is clearly present in experiment (as witnessed by the distinct differences between the behavior in a field along a and perpendicular to it). Reference 51 argued that the interplane coupling in Cs_2CuBr_4 is weaker than in Cs_2CuCl_4 since the ratio of the saturation field to the Néel temperature is approximately 1.5 times larger in Cs_2CuBr_4 than in Cs_2CuCl_4, and usually the Néel temperature in quasi-2D systems is expected to be determined by interplane coupling. In principle, this need not be the case when DM interactions are strong, but we believe the conclusion is probably correct. Thus, compared to Cs_2CuCl_4, we surmise that J'/J is increased and J''/J is decreased. This behavior is in agreement with the estimate based on the band-structure calculation of material's microscopic parameters in Ref. 53.

We believe that reduced three-dimensional coupling is the primary reason for the observed cascade of phase transitions in Cs_2CuBr_4 subject to magnetic field in b-c plane.[51,54–57] Particularly striking is the observation of a robust $M = \frac{1}{3}M_{\mathrm{sat}}$ magnetization plateau as well as a hint of possible second plateau, at or near 2/3 of the saturation magnetization.

In the quasi-one-dimensional approach adopted here, as discussed in Section III D, the existence of the SDW state is a necessary condition for the plateau. Given that interplane exchange J'' strongly favors cone state over the SDW one, we understand that Cs_2CuBr_4 with its small interplane coupling is indeed a good candidate for the magnetization plateau. One must remember that this argument is based on one-dimensional reasoning, the validity of which in Cs_2CuBr_4 ($J'/J = 0.75$) is questionable. However, the final outcome of this—that the magnetization plateau is stable in the full range of $J'/J \leqslant 1$ ratio—is completely consistent with two recent studies[25,58] which approached the problem as a spatially deformed two-dimensional one.

It is worth noting that abrupt variation of the SDW ordering momentum Q on approaching the plateau value, described by Eq. (56), can be clearly seen in Fig. 9 of Ref. 51. While this strong feature was interpreted there as an indication of a first order transition, our theory would predict very similar behavior from a continuous two-dimensional C-IC transition.

It is interesting to contrast the physical scenario emerging from the quasi-one-dimensional approach to what is expected based on semiclassical physics and the more isotropic regime.[58] Notably, the phases immediately bordering the 1/3 magnetization plateau in the latter case *are not* collinear SDW states. Instead, Ref. 58 finds commensurate planar or noncoplanar incommensurate distorted umbrella states. These states are connected to the uud plateau state by continuous phase transitions which however can be driven first order by residual DM interactions,[58] which generally allow for cubic terms in free energy expansion. NMR measurements[55] find that the states below and above the plateau are incommensurate, but cannot distinguish SDW from distorted umbrella states. These experiments and others[56] also find some hysteresis at the plateau edges, which suggests first order transitions there. As we have discussed, one expects second order transitions in the SDW case, so this probably suggests that SDW state does not occur in Cs_2CuBr_4. This is also supported by the neutron scattering experiments,[54] which observe a smooth evolution of the scattering intensity from zero field up to the plateau edge.

Despite the evident absence of SDW physics in Cs_2CuBr_4, it is still interesting to consider the predictions of our theory for the plateaux themselves. Apart from the persistence of the 1/3 plateau to small J'/J, the most striking outcome of our theory is probably that the second "strongest" candidate plateau is *not* at 2/3 of saturation but at 3/5 of it. This feature should be taken as another definite prediction of our work.

VIII. DISCUSSION

A. Resume

In this paper, we have presented a fairly thorough analysis of the low temperature phases of Cs_2CuCl_4, obtained from a quasi-one-dimensional approach. The results explain most of the specific heat, magnetization, NMR, and neutron data available. Several aspects are particularly remarkable. First, contrary to the popular view of this material as an "anisotropic triangular lattice antiferromagnet," for magnetic fields within the XY plane, the strongest two-dimensional ground-state correlations are within the a-b planes, *perpendicular* to the nominal triangular (b-c) layers. Second, in establishing the phase diagram, we have argued for the critical importance of *four* different very weak interactions (D, J'', D_c, and J_2), only two of which have been generally recognized (D and J'') in prior work. It is remarkable that interactions of a magnitude of only a few percent of the largest exchange can induce entirely new phases. Finally, we have discovered an heretofore unnoticed commensurate-incommensurate transition in this material, and located its telltale signature in NMR experiments.

B. Relation to previous work

The subject of quantum antiferromagnetism on the triangular lattice is long and storied. Here, we will review various aspects of the problem discussed in the literature which relate to this paper. Some of the earliest work[18,59] applied the random phase approximation (RPA) using bosonization results for one-dimensional Heisenberg chains to study the susceptibility in the paramagnetic phase and estimate critical temperatures. Indeed, the RPA is equivalent to the CMFT used here, as far as predictions of the critical temperature are concerned, provided the same interactions are taken into account. At a more general level, this early work correctly emphasized the importance of the one-dimensional regime. However, the analysis here (and in Ref. 14) is much more

complete in a number of significant ways. It treats the ordered phases below T_c, takes full account of anisotropic DM couplings, and includes fluctuation-generated interactions which are ignored within RPA. These effects rather dramatically alter the phase diagram of Cs_2CuCl_4 from the expectations of Refs. 18 and 59.

Much of the theoretical work motivated by Cs_2CuCl_4 focused on the inelastic neutron structure factor, addressing experiments[6] which observed very broad line shapes and extracted dispersion relations for putative "magnon" peaks. Several groups applied spin-wave theory[60–63] to study the ground state (staggered) magnetization and the structure factor, including higher order corrections in $1/S$. The low-energy dispersion of the zero field magnon peak is reasonably well reproduced by this approach, while higher energy portions are not. To fit them, requires "renormalizing" the exchange couplings by hand, in a manner inconsistent with other measurements (e.g., at high fields). Moreover, the large continuum scattering is not obtained in this approach. Another series of works study the excitation spectrum of "magnons" using series expansions.[64–67] In our opinion, because the ground state *is* ordered, and the series are constructed from such a starting point, they are fairly reliable in determining the energies of magnon-type excitations of the system. (Although they do miss important finite lifetime effects which can be quite large in noncollinear spin configurations.[68]) Indeed, the results compare well to the dispersion of the peaks of intensity in experiment.[64] This method provides a useful computational tool, especially helpful in estimating exchange couplings. However, it does not elucidate the *mechanism* of magnetic ordering or provide a full description of *all* the excitations. Thus it is much less useful if the ground state is not known (as in much of the nonzero field experiments), and it does not address the dominant continuum portion of the experimental spectra. Several theories approached the excitation spectrum from more exotic perspectives,[10,11,69–71] postulating proximity to quantum spin liquid phases and/or quantum critical points. We believe there is little support for such proximate exotic phases from experiments on Cs_2CuCl_4. Instead, the most compelling explanation for the neutron experiments comes from a theory[12,13,15] in which the excited states are constructed from superposition of a small number of elementary "spinon" excitations of the individual Heisenberg chains. This approach quantitatively and qualitatively explains the main features of experiment, with no adjustable parameters. Its success is a strong argument in favor of the quasi-one-dimensional approach adopted here.

Several works address the ground states of spatially anisotropic triangular antiferromagnets, and Cs_2CuCl_4 in particular. In zero magnetic field, the ideal problem (discussed here in Sec. III) has been heavily studied.[14,19,22,24,52,72,73] Many approaches find simply that, in the quasi-1D limit, the correlations between chains are extremely weak, and either regard this small J'/J region as a "spin liquid" or are inconclusive as to the actual ground state.[19,24,52] The most recent series expansion calculations of Ref. 22 favor a spiral state but do not make a definitive conclusion. The approach described here, applied to this case in Ref. 14, predicts definitively a collinear ground state, arising from a rather subtle fourth-order fluctuation effect. Very recently, a numerical coupled cluster method[73] also obtained this state. Unfortunately, because of the very weak fourth-order nature of the stabilization of this phase, we expect this to be a somewhat academic result. The DM interactions in Cs_2CuCl_4 (and likely in many other anisotropic triangular systems) completely overwhelm the fluctuation effect and result in a spiral state, as described in Sec. III.

In a nonzero applied field, there has been less effort.[14,32,37,69] Spin wave theory, applied to the "standard" model of Cs_2CuCl_4, has considerable success in reproducing many of the features of the ground state phase diagram.[32,37] It does not, however, explain the broad regions of AF and IC phases appearing for fields in the b-c plane. An explanation of the region corresponding to the AF phase found here was given in Ref. 37, based on a dilute spin-flip approximation. However, the state obtained there differs from our AF state. It is a noncoplanar commensurate state, with the spin components transverse to the field lying in orthogonal directions on neighboring chains. Such a state would obtain for *negative* biquadratic coupling [$g_{bq}<0$ in Eq. (83)], and would probably have distinct signatures in NMR measurements. In our opinion, the sign $g_{bq}>0$, found here, is rather more natural, and more consistent with the usual expectation that fluctuations ("order by disorder") favor more collinear states.[47] The IC phase and CIT discussed here are entirely new and could not possibly have been obtained in previous works, all of which assume rotational symmetry of the exchange interactions in the b-c plane. As a general point, it is not too surprising that spin-wave based approximations can capture most of the phases in an applied field. This is because we have found that these have "classical" order parameters (nonzero $\langle \mathcal{S}^{\pm}_{y,z}(x)\rangle$) and are thus adiabatically connected to mean-field states. Such approaches may, however, have large quantitative errors, and furthermore, may miss states where fluctuation-induced interactions are important (such as the AF state). The problems with spin-wave theory are most extreme actually in the ideal model, which we have found displays a wide range of SDW state, which is entirely nonclassical and difficult to obtain from spin waves. The SDW state is very naturally related to magnetization plateaus, which have been widely discussed, mostly in the spatially isotropic regime. This is discussed in detail in Sec. VII D.

C. Open questions and parting remarks

Our study has resolved most of the main questions regarding the phase diagram of Cs_2CuCl_4. However, there are still some smaller details which remain to be understood. We have not addressed the regime of magnetic fields h of order D, for fields in the triangular plane. There, the ground state should involve a nontrivial balance between D and interchain exchanges. Evidently, this gives rise to additional phases for fields along the c axis. There is also a discrepancy between the measured incommensurability (q_0) in the high-field cone state for this field orientation[32] and theoretical expectations. To check whether this discrepancy might be explained by the additional DM interactions considered in this paper, we evaluated in Appendix G the single-magnon spectrum in the

TABLE II. List of notations.

Hydrodynamic rep.	Bosonized rep.	Scaling dimension
$\gamma_{\mathrm{SDW}}(\mathcal{S}^z_{y,z;\pi-2\delta}\mathcal{S}^z_{y+1,z;\pi+2\delta}+\mathrm{H.c.})$ $\gamma_{\mathrm{SDW}}=2J'\sin\delta$	$\tilde{\gamma}_{\mathrm{SDW}}\cos[\frac{2\pi}{\beta}(\phi_{y,z}-\phi_{y+1,z})]$ $\tilde{\gamma}_{\mathrm{SDW}}=J'A_1^2\sin\delta$	$\frac{1}{2\pi R^2}$
$-i\gamma_{\mathrm{cone}}\mathcal{S}^+_{y,z;\pi}\partial_x\mathcal{S}^-_{y+1,z;\pi}+\mathrm{H.c.}$ $\gamma_{\mathrm{cone}}=J'/2$	$-\tilde{\gamma}_{\mathrm{cone}}(\partial_x\theta_{y,z}+\partial_x\theta_{y+1,z})\cos[\beta(\theta_{y,z}-\theta_{y+1,z})]$ $\tilde{\gamma}_{\mathrm{cone}}=J'A_3^2\beta/2$	$2\pi R^2+1$
$\gamma''_{\pm}(\mathcal{S}^+_{y,z;\pi}\mathcal{S}^-_{y,z+1;\pi}+\mathrm{H.c.})$ $\gamma''_{\pm}=J''/2$	$\tilde{\gamma}''_{\pm}\cos[\beta(\theta_{y,z}-\theta_{y,z+1})]$ $\tilde{\gamma}''_{\pm}=A_3^2J''$	$2\pi R^2$
$\gamma_2\mathcal{S}^+_{y,z;\pi}\mathcal{S}^-_{y+2,z;\pi}+\mathrm{H.c.}$ $\gamma_2=J_2/2$	$\tilde{\gamma}_2\cos[\beta(\theta_{y,z}-\theta_{y+2,z})]$ $\tilde{\gamma}_2=A_3^2J_2$	$2\pi R^2$
Biquadratic fluctuation—generated coupling	$-\tilde{\gamma}_{\mathrm{bq}}\cos[2\beta(\theta_{y,z}-\theta_{y+1,z})]$ $g_{\mathrm{bq}}=\tilde{\gamma}_{\mathrm{bq}}(\ell'')\sim(J')^2\lvert\psi\rvert^4/v$	$8\pi R^2$
$D_c(-1)^y\mathcal{J}^z_{y,z}$	$d_c(-1)^y\partial_x\theta_{y,z}$ $d_c=vD_c/(\beta J)$	1

fully polarized state, including these interactions. We have not found any set of parameters which appear consistent with the measured incommensurability, which is *reduced* compared to the expected one. Indeed, the theoretical result in Eq. (G20) shows that DM interactions only *increase* the incommensurability, making the problem worse. This might be a point that warrants more extensive experimental investigation.

While we have focused on the application of our methods to Cs_2CuCl_4 (and to a lesser extent, Cs_2CuBr_4), the analysis can be applied to other quasi-1D materials. Indeed, it appears that the commensurate AF state described here has been observed[74] in the another triangular lattice material, Cs_2CoCl_4, in Ref. 75. This material is a spin-1/2 *XY*-like antiferromagnet forming a spatially anisotropic triangular lattice. In contrast with the naïve expectation of incommensurate spiral order along the chains, experiment[75] finds commensurate antiferromagnetic ordering in the absence of an applied magnetic field. This finding matches nicely our description here, as in Cs_2CoCl_4 pronounced easy-plane anisotropy (the estimate[75] is $J^z/J^{x,y}=0.25$, where J^a represents in-chain exchange between S^a components of the nearest spins) plays a role quite similar to the external magnetic field: it enhances *XY* spin correlations at the expense of *Z* ones (which, however, remain commensurate with the lattice). In fact, the behavior of the compactification radius as function of *XY* anisotropy[27] is not very different from that in a magnetic field, discussed in Appendix A: $2\pi R^2=1-\arccos[J^z/J^{x,y}]/\pi$. Thus the results of Sec. V provide a natural theoretical explanation of the observed commensurate AF phase in Cs_2CoCl_4.

To facilitate further application of our methods such as this one, we have described them here in sufficient detail that they could be readily applied to other problems. We hope that the level of detail exposed here serves to amplify the tremendous power of the quasi-one-dimensional approach, which allows real quantitative contact between the microscopic spin Hamiltonian and universal long-wavelength physics, while including at the same time strong fluctuations and frustration.

ACKNOWLEDGMENTS

We thank J. Alicea, A. Chubukov, R. Coldea, V. Mitrovic, O. Motrunich, M. Takigawa, and Y. Takano for stimulating discussions. Much of this work was carried out using resources provided by the KITP through NSF Grant No. PHY05-51164. O.A.S. is supported by the National Science Foundation through Grant No. DMR-0808842. L.B. was supported by the Packard Foundation, and the National Science Foundation through Grant No. DMR-0804564. H.K. is partly supported by the JSPS.

APPENDIX A: NOTATIONS AND PARAMETERS

Throughout the paper the following conventions are used: coupling constants of quantum Hamiltonians written in terms of spin densities $\mathcal{S}^{z,\pm}$ are denoted as γ. When these terms are expressed in terms of bosonic fields ϕ and θ, the corresponding couplings change into $\tilde{\gamma}$. Coupling constants of various interaction terms of the effective two- and three-dimensional Hamiltonians, expressed in terms of the *classical* phase ϑ, are denoted as g.

Table II contains a list of notations in which several perturbations are summarized along with their scaling dimensions. The scaling dimensions are functions of $2\pi R^2$. The parameter $2\pi R^2$ as a function of the magnetization M is obtained by solving the Bethe ansatz integral equations.[28–30] Figures 12 and 13 shows the numerical data obtained from $\beta=2\pi R$ in Ref. 76. Near the saturation magnetization, $M\sim 1/2$, one can solve the integral equation analytically and obtain

$$2\pi R^2=\frac{3}{4}-\frac{M}{2}. \tag{A1}$$

In the opposite limit of zero magnetization, $M\sim 0$, $2\pi R^2$ is well fitted by the following function:

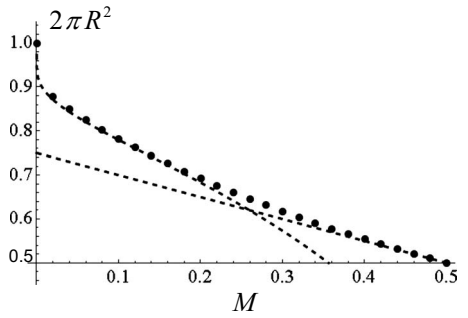

FIG. 12. Parameter $2\pi R^2$ as a function of the magnetization M. Numerical solutions in Ref. 76 shown by the dots are compared with asymptotic solutions [Eqs. (A1) and (A2)].

$$2\pi R^2 = 1 - \frac{1}{2\ln(M_0/M)}, \tag{A2}$$

where $M_0=\sqrt{8/(\pi e)}$. An abrupt, inverse-log, deviation from the SU(2) value is due to the marginally irrelevant current-current interaction typical for the spin-1/2 Heisenberg chain.[27]

The relation between the magnetization M and the magnetic field h has been discussed previously in Ref. 14 and we briefly describe the result here. As discussed below (25), the interchain interaction J' increases the energy of the system of coupled chains by $2J'M^2$ which results in suppression of the *two-dimensional* $M(h)$ curve with respect to the one-dimensional $M_1(h)$ curve for a single spin chain, at fixed external field h. Using the relation $h=-\frac{\partial E}{\partial M}$, we observe that the field h naturally decomposes into a sum of "one-dimensional" field $h_1=-\frac{\partial E_1}{\partial M}$ for a single magnetized chain with energy $E_1(M)$ and the inter-chain contribution $-4J'M$. As a result, we arrive at a self-consistent equation where magnetization $M(h)$ of the system of coupled chains is approximated by that of the single chain, but evaluated at a shifted field $h-4J'M$,

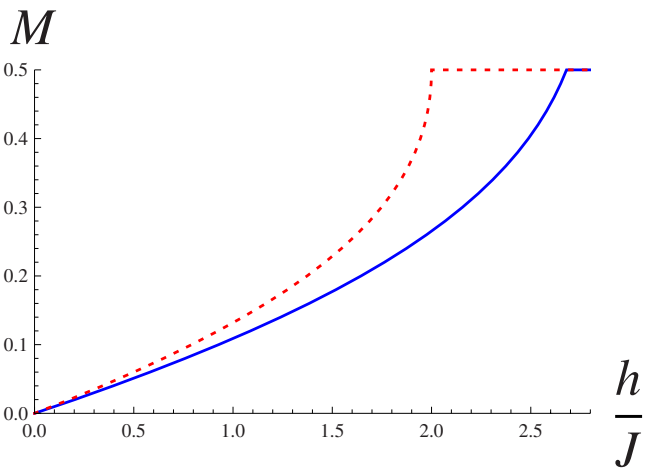

FIG. 13. (Color online) Magnetization M versus magnetic field h. Dashed (red) curve shows magnetization of a single Heisenberg chain, based on the data in Ref. 76. Solid (blue) line shows mean-field result (A3).

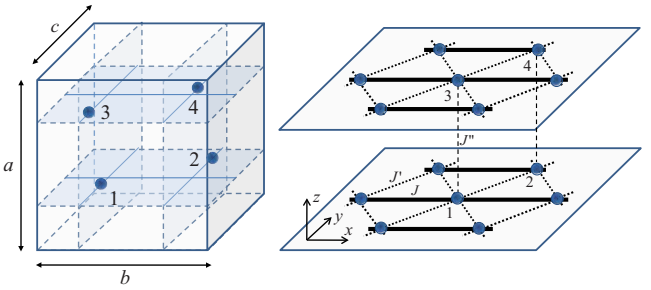

FIG. 14. (Color online) Left: four independent Cu spins (labeled by 1, 2, 3, and 4) in the unit cell of Cs_2CuCl_4. The spins 1(2) and 3(4) lie in the same a-c plane. Right: layered-triangular lattice formed by magnetic sites. Thick, dotted, and broken lines indicate J, J', and J'' exchange couplings, respectively.

$$M(h) = M_1(h - 4J'M). \tag{A3}$$

This equation is easily solved numerically using data of Ref. 76 and results in $M(h)$ curve going below $M_1(h)$ for all h. An essentially identical result is obtained if one uses the interpolating formula $M_1(h)=\pi^{-1}\arcsin[1/(1-\pi/2+\pi/h)]$, suggested in Ref. 8 (see Fig. 13). This approximation predicts saturation field $h_{sat}=2J+2J'$ which is very close to the exact 2D result $h_{sat}^{exact}=2J+2J'+(J')^2/(2J)$. It is also worth noting that while M_1 approaches saturation with an infinite slope, $\partial M_1/\partial h\sim(2-h)^{-1/2}$, the two-dimensional curve is characterized by the finite slope $1/(4J')$ so that $M(h\approx h_{sat})=1/2+(h-h_{sat})/(4J')$.

APPENDIX B: SYMMETRY ANALYSIS

Here we consider the full symmetries of Cs_2CuCl_4, and some of their consequences. Most importantly, we derive the possible DM vectors of the on-chain and diagonal bonds. The direction of the DM vectors are constrained by the space group symmetry in the crystal. In the ideal triangular lattice, the DM vectors must be perpendicular to the plane and hence is parallel to the a axis. However, this is not true in the real crystal due to the lower symmetry.

1. Crystal structure and symmetry generators

Cs_2CuCl_4 has an orthorhombic crystal structure with space group $Pnma$.[77] The lattice parameters are $a=9.65$ Å, $b=7.48$ Å, and $c=12.35$ Å at 0.3 K. The unit cell contains four independent Cu^{2+} ions as shown in Fig. 14. The locations of the ions are given by $\boldsymbol{R}+\boldsymbol{\delta}_\alpha$ ($\alpha=1$, 2, 3, and 4), where

$$\boldsymbol{R} = l\hat{a} + m\hat{b} + n\hat{c} \tag{B1}$$

denotes the location of the unit cell and

$$\boldsymbol{\delta}_1 = z_0\hat{a} + \frac{1}{4}\hat{b} + y_0\hat{c},$$

$$\boldsymbol{\delta}_2 = \left(\frac{1}{2} - z_0\right)\hat{a} + \frac{3}{4}\hat{b} + \left(\frac{1}{2} + y_0\right)\hat{c},$$

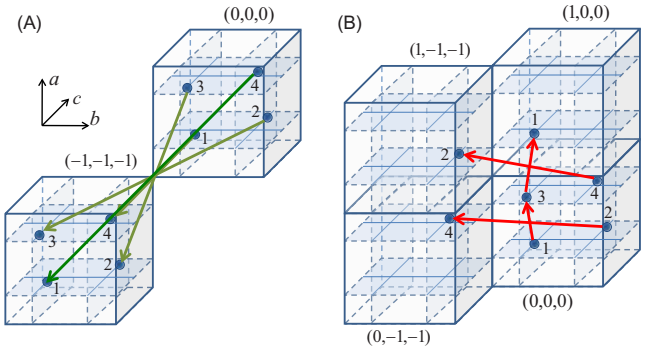

FIG. 15. (Color online) Symmetry operations A and B. The locations of unit cells are indicated by (l,m,n).

$$\boldsymbol{\delta}_3 = \left(\frac{1}{2} + z_0\right)\hat{a} + \frac{1}{4}\hat{b} + \left(\frac{1}{2} - y_0\right)\hat{c},$$

$$\boldsymbol{\delta}_4 = (1 - z_0)\hat{a} + \frac{3}{4}\hat{b} + (1 - y_0)\hat{c},$$

with $z_0=0.23$ and $y_0=0.42$. In the simplified notation used in Eq. (3), the spins 1, 2, 3, and 4 correspond to $\boldsymbol{S}_{x,y,z}$, $\boldsymbol{S}_{x+1/2,y+1,z}$, $\boldsymbol{S}_{x,y,z+1}$, and $\boldsymbol{S}_{x+1/2,y+1,z+1}$, respectively. Note that m in Eq. (B1) is the coordinate along the chains, i.e., x. For fixed l, 1 and 2 spins constitute one triangular layer while 3 and 4 another layer. On the other hand, 1 and 3 spins lie in the same a-c plane which is a mirror plane through the midpoints of the on-chain bonds (see Fig. 14). The same thing holds for 2 and 4 spins. Therefore, according to Moriya's rule, the DM vector on the chain bonds must lie in the a-c plane.[78] In contrast to this, there is no symmetry constraint on the DM vectors on diagonal bonds.

We shall next determine the pattern of relative signs of the DM vectors, which requires a more elaborate argument of symmetry. The *Pnma* space group has three kinds of symmetry operations, A and B, and reflection apart from Bravais lattice translations. We consider the transformation property of spins under A and B. Let us denote by $\boldsymbol{S}_\alpha(l,m,n)$ the spin at the position $\boldsymbol{R}+\boldsymbol{\delta}_\alpha$. The spins are transformed under A as follows:

$$A:\begin{cases} S_1^\mu(l,m,n) \leftrightarrow S_4^\mu(-l-1,-m-1,-n-1) \\ S_2^\mu(l,m,n) \leftrightarrow S_3^\mu(-l-1,-m-1,-n-1), \end{cases} \tag{B2}$$

where $\mu=a,b,c$. Since A is the inversion operation as shown in Fig. 15, the spins do not change sign. The symmetry operation B, graphically shown in Fig. 15, corresponds to a π rotation about an axis parallel to a. Under it, two of three components of the spin change sign. Therefore, one obtains

$$B:\begin{cases} S_1^\mu(l,m,n) \leftrightarrow \gamma_\mu S_3^\mu(l,-m,-n) \\ S_2^\mu(l,m,n) \leftrightarrow \gamma_\mu S_4^\mu(l,-m-1,-n-1), \end{cases} \tag{B3}$$

where $\gamma_b=\gamma_c=-1$ and $\gamma_a=1$.

2. DM vectors

We can determine the relative signs of the DM vectors using Eqs. (B2) and (B3). Let us first consider components of the DM interactions on the on-chain bonds,

$$\sum_{\alpha=1}^{4} (D_{\alpha,a}\hat{a} + D_{\alpha,c}\hat{c}) \cdot \boldsymbol{S}_\alpha(l,m,n)\boldsymbol{S}_\alpha(l,m+1,n). \tag{B4}$$

Applying A and translations, we find

$$D_{1,a} = -D_{4,a}, \quad D_{2,a} = -D_{3,a}, \tag{B5}$$

$$D_{1,c} = -D_{4,c}, \quad D_{2,c} = -D_{4,c}, \tag{B6}$$

while applying B and translations, we find

$$D_{1,a} = -D_{3,a}, \quad D_{1,c} = D_{3,c}. \tag{B7}$$

These six relations determine the relative signs of D_a and D_c as in Eq. (16). Let us apply the same technique to analyze the DM vectors on the diagonal bonds. Since each site lies in the mirror plane, we can assume the coupling of the following form:

$$\begin{aligned} &\boldsymbol{D}_{12}^{+} \cdot \boldsymbol{S}_1(l,m,n) \times \boldsymbol{S}_2(l,m,n) + \boldsymbol{D}_{12}^{-} \cdot \boldsymbol{S}_1(l,m,n) \\ &\quad \times \boldsymbol{S}_2(l,m-1,n) + \boldsymbol{D}_{21}^{+} \cdot \boldsymbol{S}_2(l,m,n) \\ &\quad \times \boldsymbol{S}_1(l,m+1,n+1) + \boldsymbol{D}_{21}^{-} \cdot \boldsymbol{S}_2(l,m,n) \\ &\quad \times \boldsymbol{S}_1(l,m,n+1) + (1 \to 3, 2 \to 4), \end{aligned} \tag{B8}$$

with

$$\boldsymbol{D}_{\alpha\beta}^{\pm} = \pm (D'_{\alpha\beta,a})\hat{a} + (D'_{\alpha\beta,b})\hat{b} \pm D'_{\alpha\beta,c}\hat{c}. \tag{B9}$$

Here we have used the fact that S_α^a and S_α^c change signs while S_α^b does not under reflection through a mirror plane. Applying A and translations, we find

$$\boldsymbol{D}_{12}^{\pm} = -\boldsymbol{D}_{34}^{\pm}, \quad \boldsymbol{D}_{21}^{\pm} = -\boldsymbol{D}_{43}^{\pm}. \tag{B10}$$

On the other hand, applying B with translations, we obtain

$$D'_{12,a} = -D'_{43,a}, \quad D'_{12,b} = D'_{43,b}, \quad D'_{12,c} = D'_{43,c}. \tag{B11}$$

Using Eqs. (B10) and (B11), one can show that relative signs are given by Eq. (17), which is shown in Fig. 6.

3. Symmetry with in-plane magnetic field

To fully determine the spin structures, it is sometimes useful to have a more detailed understanding of the residual symmetry in a field. The uniform applied field obviously preserves the translational symmetry of the lattice but breaks time reversal symmetry. Its effects upon the point group operations are less obvious. In general, the *Pnma* space group contains seven nontrivial (and one trivial) point operations, which are not all independent (see Table III). Of these seven operations, three preserve any one component of the magnetization, and of these 3, two are independent. Therefore the point group symmetry in the presence of the magnetic field is generated by just two operations, which have Ising character. The first operation is simply the inversion transformation A, from Eq. (B2) in Appendix B 1. In the notation of the main text, this operation reads

$$A:\mathbf{S}_{x,y,z} \to \mathbf{S}_{(1/2)-x,1-y,1-z}. \tag{B12}$$

TABLE III. Point group operations in the *Pnma* space group.

No.	x_a'	x_b'	x_c'	$\mathcal{S}^{a'}$	$\mathcal{S}^{b'}$	$\mathcal{S}^{c'}$
0	x_a	x_b	x_c	$\mathcal{S}^a$	$\mathcal{S}^b$	$\mathcal{S}^c$
1 (A)	$-x_a$	$-x_b$	$-x_c$	$\mathcal{S}^a$	$\mathcal{S}^b$	$\mathcal{S}^c$
2	$\frac{1}{2}-x_a$	$-x_b$	$\frac{1}{2}+x_c$	$-\mathcal{S}^a$	$-\mathcal{S}^b$	$\mathcal{S}^c$
3 (D)	$\frac{1}{2}+x_a$	x_b	$\frac{1}{2}-x_c$	$-\mathcal{S}^a$	$-\mathcal{S}^b$	$\mathcal{S}^c$
4	$-x_a$	$\frac{1}{2}+x_b$	$-x_c$	$-\mathcal{S}^a$	$\mathcal{S}^b$	$-\mathcal{S}^c$
5 (C)	x_a	$\frac{1}{2}-x_b$	x_c	$-\mathcal{S}^a$	$\mathcal{S}^b$	$-\mathcal{S}^c$
6 (B)	$\frac{1}{2}+x_a$	$\frac{1}{2}-x_b$	$\frac{1}{2}-x_c$	$\mathcal{S}^a$	$-\mathcal{S}^b$	$-\mathcal{S}^c$
7	$\frac{1}{2}-x_a$	$\frac{1}{2}+x_b$	$\frac{1}{2}+x_c$	$\mathcal{S}^a$	$-\mathcal{S}^b$	$-\mathcal{S}^c$

Clearly, this operation preserves *all* components of the uniform magnetization and hence is a symmetry for an arbitrary applied magnetic field.

For a magnetic field along a, the B operation given in the previous subsection, Eq. (B3), can be chosen as the other symmetry generator. It can be written as

$$B: S^{\mu}_{x,y,z} \to \upsilon_{\mu} S^{\mu}_{-x,-y,z+1}, \tag{B13}$$

with $\upsilon_a=1$, $\upsilon_b=\upsilon_c=-1$.

However, operation B does not keep either the b or the c-axis magnetization invariant. The second independent operation should be chosen differently for these field orientations. For a magnetic field along b, it can be taken as a reflection in an a-c plane,

$$C: S^{\mu}_{x,y,z} \to \zeta_{\mu} S^{\mu}_{-x,y,z}, \tag{B14}$$

where $\zeta_a=\zeta_c=-1$ and $\zeta_b=1$.

For a field along c, it can be taken as a reflection in an a-b plane,

$$D: S^{\mu}_{x,y,z} \to \eta_{\mu} S^{\mu}_{x,-y,z}, \tag{B15}$$

where $\eta_a=\eta_b=-1$ and $\eta_c=1$.

Using the bosonization formulas, Eq. (24), one can deduce the transformation of the boson field $\theta_{y,z}(x)$ under these symmetries. One finds, for the inversion operation,

$$A: \theta_{y,z}(x) \to \theta_{1-y,1-z}\left(\frac{1}{2}-x\right)+\frac{\pi}{2\beta}(-1)^y. \tag{B16}$$

For the field along b, the reflection gives

$$C: \theta_{y,z}(x) \to \theta_{y,z}(-x)-\frac{\pi}{2\beta}[1-(-1)^y]. \tag{B17}$$

For the field along c, the corresponding reflection instead gives

$$D: \theta_{y,z}(x) \to \theta_{-y,z}+\frac{\pi}{\beta}. \tag{B18}$$

APPENDIX C: BREAKING OF U(1) SPIN ROTATION SYMMETRY

In the discussion of Secs. V and VI, the *overall* phase angle of the spins in the plane perpendicular to the magnetic field remained arbitrary. This reflects the U(1) symmetry of spin rotations about the field axis, which is present in the effective Hamiltonian having dropped DM terms with DM-vectors perpendicular to the field. While we expect this to be an excellent approximation, it is not exact, and the weak effects which we have neglected should remove this artificial invariance. This is appropriate for a crystalline system with only discrete symmetries. In this appendix, we use symmetry analysis to determine how this symmetry breaking occurs, for different field orientations. We will not attempt to determine the microscopic origin of these effects here, which might be, for instance, symmetric exchange anisotropy, or fluctuation-generated interactions. Instead, we ask what terms might arise in the energy as a function of the remaining parameters describing the orientation of the spins in the plane perpendicular to the field. To do so, we must consider the *reduced* symmetries of the system in the presence of the magnetic field.

1. Cone state

In Sec. IV, we obtained a cone state for arbitrary magnetic fields (below saturation) along the a axis. Considering the standard model, this incommensurate state has both a U(1) spin-rotational degeneracy and a pseudo U(1) phason degeneracy. The latter degeneracy is protected by translational invariance, but the U(1) rotational symmetry is an artifact, violated, for instance, by the D_c term and other DM interactions with DM vectors along b or c. To study the breaking of the U(1) spin rotational symmetry, it is useful to consider the combinations $\Theta_{\pm}=\Theta_0\pm\Theta_1$. The Θ_- field describes the phason mode. We focus instead of Θ_+.

Apart from translation invariance, the residual symmetries in the field along a are A and B. Under these operations, we find

$$A: \Theta_+ \to -\Theta_+ + 2\pi, \tag{C1}$$

$$B{:}\Theta_+ \to -\Theta_+. \tag{C2}$$

One sees from this that the effective potential should be an even, 2π-periodic function of Θ_+. *There are no further symmetry restrictions on this potential.* In the simplest situation, e.g., $V_{\text{eff}}(\Theta_+)=V\cos\Theta_+$, this potential has a unique minimum ($\Theta_+=0$ or π, depending on the sign of V). Thus one expects the artificial U(1) rotational symmetry about the a axis to be completely lifted, and the only degeneracy of the cone state to be that associated with the phason mode.

2. AF state

The breaking of the spin-rotation symmetry about the field axis is crucial for determining the precise nature of the spin structure in the AF phase. Since this phase is commensurate, and the Hamiltonian has only discrete symmetries, we expect only a discrete ground state degeneracy. This will fix the angles of the spin projections into the plane transverse to the magnetic field. We want to construct an effective potential which depends upon the parameters of the AF state, Θ and σ.

a. Field along the *b* axis

For a field along the b axis, the remaining symmetries are the inversion and reflection operations, denoted A and C, given in Eqs. (B12) and (B15), in Appendix B 3. Using the formula in the appendix, and Eq. (80), we find that under these operations,

$$A{:}\sigma \to \sigma, \quad \Theta \to \Theta + \frac{\pi}{2}(1+\sigma), \tag{C3}$$

$$C{:}\sigma \to -\sigma, \quad \Theta \to \Theta. \tag{C4}$$

In addition to these symmetries, under translations by one unit along x, one has

$$T{:}\sigma \to \sigma, \quad \Theta \to \Theta + \pi. \tag{C5}$$

From this, we may construct the simplest energy function which depends on Θ and σ, in the spirit of Landau theory. From C, Eq. (C4), we see that it must be independent of σ. From A and T, Eqs. (C3) and (C5), it must be periodic in Θ with period π. Importantly, *there are no other symmetry restrictions*. Hence the most general energy is of the form

$$V(\Theta) = \sum_{n=1}^{\infty} a_n \cos(2n\Theta - \alpha_n). \tag{C6}$$

Generically, since there are no restrictions on α_n, such a potential $V(\Theta)$ has two inequivalent minima (e.g., if we take the simplest form with $a_n=0$ for $n>1$, located at $\Theta=\alpha_1/2$, $\alpha_1/2+\pi$) located at points of no particular symmetry. This means that the transverse (to the magnetic field) components of spins do not lie parallel to *either* the a or c axes. In total, one therefore expects four ground states, with $(\sigma,\Theta)=(\pm 1,\Theta_0),(\pm 1,\Theta_0+\pi)$. Physically, the four states are obtained from one another by the arbitrary choice of global sign for the transverse components of the spins on the even and odd chains, separately.

b. Field along the *c* axis

In this field orientation, the good symmetry operations are A, T and D, given in Eqs. (B12) and (B15) of Appendix B. A and T continue to act as in Eqs. (C3) and (C5), while D leads instead to

$$D{:}\sigma \to -\sigma, \quad \Theta \to \Theta + \pi. \tag{C7}$$

Combining the D and T operations, one sees that the energy must be independent of σ, and then using A or D, one obtains again the effective potential for Θ in form of Eq. (C6). Thus, the ground state degeneracy (fourfold) is the same as in the AF state for fields along b, and the transverse components of the spins do not point along the a or b axes.

3. Incommensurate phase

Here we must reconsider the valid symmetry operations—A, T, and D—when acting upon the spin structure in Eq. (100). This structure is parametrized by two angles, Θ_0 and Θ_1, which describe the spins in the even and odd chains, respectively. Equivalently, we can choose the combinations $\Theta_\pm=\Theta_0\pm\Theta_1$. We find

$$A{:}\Theta_+ \to \Theta_+ + 2\pi, \quad \Theta_- \to -\Theta_- - q_0, \tag{C8}$$

$$D{:}\Theta_+ \to \Theta_+ + \pi, \quad \Theta_- \to \Theta_- + \pi, \tag{C9}$$

$$T{:}\Theta_+ \to \Theta_+ + 2\pi, \quad \Theta_- \to \Theta_- + 2q_0. \tag{C10}$$

Note that the transformations of the Θ_- field under A and T involve shifts by multiples of the incommensurate wave vector q_0. Under multiple actions of such shifts, any value of Θ_- can be approached arbitrarily closely (due to the 2π periodicity). Thus there is *no* potential which can pin the values of Θ_-. This is the reason for the gapless "phason" mode in the IC phase.

By contrast, the effective Hamiltonian can certainly depend upon Θ_+, reflecting the lack of rotational invariance about the c axis. In general, due to the action of D (which is most constraining), the effective potential must be a π-periodic function of Θ_+. There are, however, no other constraints. Since shifts of either Θ_0 or Θ_1 by 2π have no physical significance, Θ_+ is itself defined only up to 2π. This implies that there should be two discrete sets of IC solutions, described by $\Theta_+=\Theta_0$, $\Theta_0+\pi$, and Θ_0 should generically take an incommensurate value with no special symmetry.

APPENDIX D: CHAIN MEAN-FIELD THEORY

1. SDW order

We start by applying CMFT to the ideal 2D model Eq. (27) and consider first SDW order at finite temperature. Thus we write

$$H_{1,\mathrm{SDW}} = \sum_{y,z} \int dx \tilde{\gamma}_{\mathrm{SDW}} \cos[2\pi(\phi_{y,z} - \phi_{y+1,z})/\beta]. \tag{D1}$$

It is convenient to shift ϕ fields slightly, $\phi_{y,z} \to \phi_{y,z} + (-1)^y \beta/4$, so as to change the sign of the interaction in the equation above. In terms of the shifted fields the minimum corresponds to a uniform configuration $\phi_{y,z} = \phi_0(z)$ for each z since the layers are decoupled. It is clear that the interchain interaction can next be written as $\boldsymbol{\sigma}_{y,z} \cdot \boldsymbol{\sigma}_{y+1,z}$, where $\boldsymbol{\sigma}_{y,z} = (\cos[2\pi\phi_{y,z}/\beta], \sin[2\pi\phi_{y,z}/\beta])$ is the SDW order parameter vector describing chain (y,z). Chain mean-field consists in a self-consistent assumption that SDW order spontaneously develops at some critical temperature T_{SDW}, below which the SDW order parameter acquires a finite value along some arbitrary direction in the SDW plane. For concreteness we choose this direction to be along the x axis, $\langle \boldsymbol{\sigma}_{y,z} \rangle = (\tilde{\psi}, 0)$. This choice corresponds to $\alpha_z = 0$ in Eq. (28). With these approximations we have

$$H_{1,\mathrm{SDW}} \to H^{\mathrm{mf}}_{1,\mathrm{SDW}} = -2\tilde{\psi}\tilde{\gamma}_{\mathrm{SDW}} \sum_{y,z} \int dx \cos\left[\frac{2\pi}{\beta}\phi_{y,z}\right], \tag{D2}$$

where the factor of 2 arises from the coordination number of chain y in the layer z. The self-consistent condition reads

$$\tilde{\psi} = \left\langle \cos\left[\frac{2\pi}{\beta}\phi_{y,z}\right] \right\rangle_{\mathrm{SDW}}, \tag{D3}$$

where angular brackets denote finite-temperature average with the sine-Gordon Hamiltonian $H^{\mathrm{mf}}_{\mathrm{SDW}}$ of the single chain,

$$H^{\mathrm{mf}}_{\mathrm{SDW}} = \int dx \frac{v}{2}((\partial_x \theta_{y,z})^2 + (\partial_x \phi_{y,z})^2) + H^{\mathrm{mf}}_{1,\mathrm{SDW}}. \tag{D4}$$

The right-hand side of Eq. (D3) is evaluated perturbatively in powers of vanishing $\tilde{\psi}$ and the leading order result is

$$\tilde{\psi} = 2\tilde{\psi}\tilde{\gamma}_{\mathrm{SDW}} \chi_{\Delta_{\mathrm{SDW}}}(q = 0, \omega_n = 0; T). \tag{D5}$$

Here we defined the momentum and frequency dependent *susceptibility*, $\chi_\Delta(q, \omega_n; T)$, of the vertex operator $\mathcal{O}_\Delta = \cos(\sqrt{4\pi\Delta}\phi)$ [or $\mathcal{O}_\Delta = \cos(\sqrt{4\pi\Delta}\theta)$, which gives identical results] at temperature T, in the canonical free boson theory, Eq. (7),

$$\chi_\Delta(q = 0, \omega_n = 0; T) = \int_{-\infty}^{\infty} dx \int_0^{1/T} d\tau e^{iqx + i\omega_n \tau} \times \langle \mathcal{O}_\Delta(x,\tau)\mathcal{O}_\Delta(0,0)\rangle_0. \tag{D6}$$

The subscript 0 reminds us that this is evaluated in the free theory. This susceptibility, in various limits, plays a central role in the determination of critical temperatures within CMFT. It is evaluated at the end of this appendix, Appendix D 7. Here, we need the SDW susceptibility, for which $\Delta_{\mathrm{SDW}} = 1/4\pi R^2$. At the critical temperature Eq. (D5) acquires a nontrivial solution, $\tilde{\psi} \neq 0$, resulting in the implicit equation for T_{SDW},

$$1 = 2\tilde{\gamma}_{\mathrm{SDW}} \chi_{\Delta_{\mathrm{SDW}}}(q = 0, \omega_n = 0; T_{\mathrm{SDW}}). \tag{D7}$$

Using Eq. (D55) from Appendix D 7 a, we obtain

$$\left(\frac{2\pi T_{\mathrm{SDW}}}{v}\right)^{2-2\Delta_{\mathrm{SDW}}} = \lambda_{\mathrm{SDW}} \frac{\Gamma(1-\Delta_{\mathrm{SDW}})\Gamma^2(\Delta_{\mathrm{SDW}}/2)}{\Gamma(\Delta_{\mathrm{SDW}})\Gamma^2(1-\Delta_{\mathrm{SDW}}/2)} \times [1 + \lambda_{\mathrm{SDW}}\Gamma(\Delta_{\mathrm{SDW}} - 1/2)/(\sqrt{\pi}\Gamma(\Delta_{\mathrm{SDW}})(1-\Delta_{\mathrm{SDW}}))]^{-1}, \tag{D8}$$

where $\lambda_{\mathrm{SDW}} = \pi\tilde{\gamma}_{\mathrm{SDW}}/v = \pi A_1^2 \sin(\delta) J'/v$. This result, T_{SDW} as a function of magnetization M, is plotted in Fig. 7.

2. Cone order

Here we consider the cone (twist) ordering instability of the ideal 2d model Eq. (27). The cone Hamiltonian is given by

$$H_{1,\mathrm{cone}} = -\tilde{\gamma}_{\mathrm{cone}} \sum_{y,z} \int dx (\partial_x \theta_{y,z} + \partial_x \theta_{y+1,z}) \times \cos[\beta(\theta_{y,z} - \theta_{y+1,z})], \tag{D9}$$

where $\tilde{\gamma}_{\mathrm{cone}} = J' A_3^2 \beta/2$. The spatial derivatives in Eq. (D9) require a generalization of the procedure described in Appendix D 1. We begin by shifting the θ fields by a position-dependent phase corresponding to a wave vector shift q_0, the magnitude of which is to be determined later self-consistently. Thus

$$\theta_{y,z}(x) = q_0 x/\beta + \tilde{\theta}_{y,z}(x). \tag{D10}$$

This shift transforms Eq. (D9) into

$$\tilde{H}_{1,\mathrm{cone}} \approx -2\frac{q_0 \tilde{\gamma}_{\mathrm{cone}}}{\beta} \sum_{y,z} \int dx \cos[\beta(\tilde{\theta}_{y,z} - \tilde{\theta}_{y+1,z})], \tag{D11}$$

where we have neglected as subleading $\partial_x \tilde{\theta}$ terms. The transformed Hamiltonian [Eq. (D11)] is now of the form Eq. (D1) and can be manipulated similarly. However, the shift Eq. (D10) has modified the free boson Hamiltonian Eq. (7) into

$$\tilde{H}_0 = \sum_{y,z} \int dx \frac{v}{2}((\partial_x \tilde{\theta}_{y,z} + q_0/\beta)^2 + (\partial_x \phi_{y,z})^2). \tag{D12}$$

Introducing the order parameter

$$\tilde{\psi} = \langle \cos[\beta\tilde{\theta}_{y,z}] \rangle_{\mathrm{cone}}, \tag{D13}$$

where the average is over the Hamiltonian

$$H^{\mathrm{mf}}_{\mathrm{cone}} = \tilde{H}_0 - 2\tilde{\psi}\hat{\gamma}_{\mathrm{cone}} \sum_{y,z} \int dx \cos[\beta\tilde{\theta}_{y,z}], \tag{D14}$$

and $\hat{\gamma}_{\mathrm{cone}} = 2q_0\tilde{\gamma}_{\mathrm{cone}}/\beta = q_0 J' A_3^2$. As before, expanding the expectation value in Eq. (D13) to leading order in $\hat{\gamma}$, and assuming $\tilde{\psi} \neq 0$, gives the condition for the critical temperature

$$1 = 2\hat{\gamma}_{\mathrm{cone}} \tilde{\chi}_{\Delta_+}(q = 0, 0; T_c), \tag{D15}$$

where *tilde* on the susceptibility indicates that it is to be calculated using the free but *shifted* Hamiltonian Eq. (D12). However we can now undo the shift Eq. (D10) and transform back to the original θ fields. As a result, one obtains the identity

$$\tilde{\chi}_{\Delta_\pm}(q=0,0;T_c)=\chi_{\Delta_\pm}(q_0,0;T_c). \tag{D16}$$

Then Eq. (D15) becomes

$$1=2\hat{\gamma}_{\rm cone}\chi_{\Delta_\pm}(q_0,0;T_c). \tag{D17}$$

This wave-vector-dependent static susceptibility is well known and given in Eq. (D51). Using it, Eq. (D17) can be solved by maximizing the right-hand side with respect to q_0 at given T, and then finding the maximum $T_c=T_{\rm cone}$ (this is equivalent to choosing the wave vector q_0 for which T_c is maximum). Expressing all quantities in terms of dimensionless variables, $r=vq_0/(4\pi T_{\rm cone})$ and $s=2\pi T_{\rm cone}/v$, we obtain a system of two equations

$$4\,{\rm Im}\,\Psi\left(\frac{\Delta_\pm}{2}+ir\right)=\frac{2\pi\sinh[2\pi r]}{\cosh[2\pi r]-\cos[\pi\Delta_\pm]}+\frac{1}{r},$$

$$s^{1-2\Delta_\pm}=\frac{2\tilde{\gamma}_{\rm cone}}{\pi\beta v}\frac{\Gamma(1-\Delta_\pm)}{\Gamma(\Delta_\pm)}r\left|\Gamma\left(\frac{\Delta_\pm}{2}+ir\right)\right|^4 \times(\cosh[2\pi r]-\cos[\pi\Delta_\pm]). \tag{D18}$$

The resulting $T_{\rm cone}$ is plotted in Fig. 7.

It is worth mentioning here that the outlined calculation can be done by keeping track of lattice as well, so that spatial derivatives in Eq. (D9) become lattice differences. Following this route (see for example Ref. 18) one again arrives at Eq. (D17) but with the coupling constant given by $\hat{\gamma}_{\rm cone,lattice}=2J'A_3^2\sin[q_0/2]$. This difference, $q_0\to 2\sin[q_0/2]$, does not affect the outcome as in the regime where CMFT is applicable the ordering vector remains small, $q_0\sim J'/J\ll 1$, see Appendix D 6 for more discussion.

3. Interlayer interaction J''

Here we consider the fate of SDW and cone orders in the presence of interlayer coupling J''. As discussed in Sec. IV, the interlayer interaction is a strongly relevant perturbation which should be accounted for in CMFT.

a. SDW order

Consider the SDW channel first. Equation (D1) should now be complimented by

$$H'_{2,\rm SDW}=J''\sum_{y,z}\int dx(\mathcal{S}^z_{y,z;\pi-2\delta}\mathcal{S}^z_{y,z+1;\pi+2\delta}+\mathcal{S}^z_{y,z;\pi+2\delta}\mathcal{S}^z_{y,z+1;\pi-2\delta}). \tag{D19}$$

This is simply a rewriting of the γ''_z term in Eq. (57). Its bosonized form is

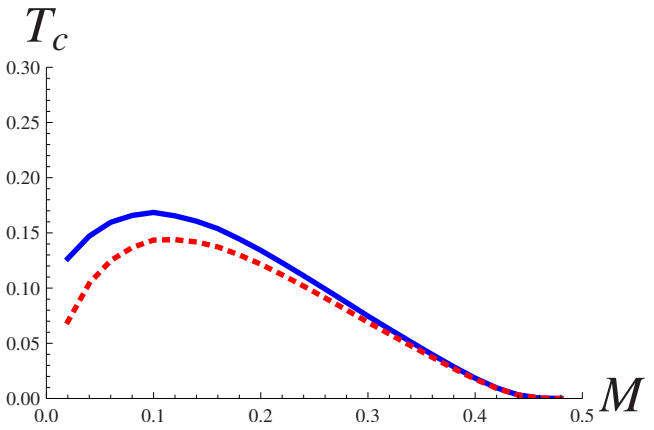

FIG. 16. (Color online) SDW ordering temperature $T_{\rm SDW}$ [dotted (red) line] of the ideal 2D model, as obtained from Eq. (D7). Solid (blue) line: the same but with interlayer J'' accounted for, see Eq. (D21).

$$H'_{2,\rm SDW}=\frac{1}{2}A_1^2J''\sum_{y,z}\int dx\cos[2\pi(\phi_{y,z}-\phi_{y,z+1})/\beta]. \tag{D20}$$

The total SDW Hamiltonian is obtained by adding Eqs. (D1) and (D20). Both terms can be made negative by a shift $\phi_{y,z}\to\phi_{y,z}+((-1)^y+(-1)^z)\beta/4$. Following the same steps as in Appendix D 1, we find that T_c is determined by an equation of the same form as Eq. (D7), but with the replacement

$$\tilde{\gamma}_{\rm SDW}\to\tilde{\Gamma}_{\rm SDW}=\tilde{\gamma}_{\rm SDW}+A_1^2J''/2=A_1^2(J'\sin\delta+J''/2). \tag{D21}$$

Figure 16 shows that $T_{\rm SDW}$ is mildly enhanced by J'' at low magnetization M.

b. Transverse/cone order

Interlayer exchange J'' strongly enhances the transverse (to the field) order (underlying the cone, AF, and IC states) for magnetic fields along the b and c axes, for which the DM interaction D is ineffective. In this case, we need to account for the $\gamma''_\pm$ ($\tilde{\gamma}''_\pm$) term represented in Eq. (71), which is bosonized in Eq. (72). To bring the latter into canonical form for CMFT, we change its sign by a simple shift $\theta_{y,z}\to\theta_{y,z}+\pi z/\beta$, which does not affect any of the manipulations in Appendix D 2. Transforming next to $\tilde{\theta}_{y,z}$ as in Eq. (D10), we arrive at the modification of Eq. (D17) where $\hat{\gamma}_{\rm cone}$ is replaced by $\hat{\Gamma}^{b\text{-}c}_{\rm cone}$,

$$\hat{\gamma}_{\rm cone}\to\hat{\Gamma}^{b\text{-}c}_{\rm cone}=A_3^2(J'q_0+J''). \tag{D22}$$

As in Appendix D 2, we obtain two equations for q_0 and T by maximizing the right-hand side of the modified Eq. (D17) with respect to q_0, and using the equation itself. The result reads, in terms of dimensionless pair (r,s) introduced in Eqs. (D18),

$$4\,{\rm Im}\,\Psi\left(\frac{\Delta_\pm}{2}+ir\right)=\frac{2\pi\sinh[2\pi r]}{\cosh[2\pi r]-\cos[\pi\Delta_\pm]}+\frac{2J's}{2J'sr+J''},$$

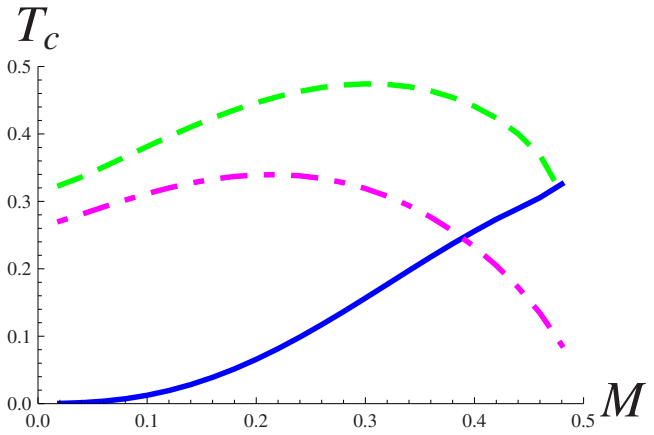

FIG. 17. (Color online) Critical temperature of cone ordering as obtained in the ideal 2D model, Eq. (D9), [solid (blue) line] and in the 3D model [dashed (green) line] as given by Eq. (D23). The dot-dashed (magenta) curve represents the critical temperature for T_{il} of the interlayer-driven order, relevant for the AF and IC phases, which we obtain by setting $J'=0$ in Eq. (D22).

$$\frac{s^{2-2\Delta_\pm}}{2J'sr+J''}=\frac{A_3^2}{2\pi v}\frac{\Gamma(1-\Delta_\pm)}{\Gamma(\Delta_\pm)}\left|\Gamma\left(\frac{\Delta_\pm}{2}+ir\right)\right|^4 \times(\cosh[2\pi r]-\cos[\pi\Delta_\pm]). \tag{D23}$$

The cone ordering temperature T_{cone} is plotted in Fig. 17. We observe that the interlayer coupling enhances T_{cone} dramatically and even leads to a substantial T_c when $J'=0$. The reason for this is simply that the nonfrustrated nature of the interlayer exchange leads to an appreciable interchain coupling of transverse spin components even when $q_0 \ll 1$, as Eq. (D22) shows. Indeed, in the AF and IC phases, we also have transverse ordering, but J' does not actually contribute to T_c, and the plot with of $T_c(J'=0)$ is relevant in those cases.

The effect of interlayer exchange J'' on the two orders can now be compared. Notably, despite its smallness—$J''=0.045J$—interlayer coupling completely eliminates SDW order in a system of weakly coupled layers, $T_{\text{SDW}}<T_{\text{cone}}$ for all magnetizations from 0 to 1/2, see Fig. 18.

4. Field along the *a* axis

Here we describe how to calculate T_c in CMFT in the presence of the DM interaction D for a field along the a axis, which is the arrangement considered in Sec. IV of the main text. Here J'' is unimportant, as we will see. Bosonization of the DM term in Eq. (57) gives

$$H'_{2,\text{dm}}=\sum_{y,z}\int dx(-1)^z 2DA_3^2\cos[\beta(\theta_{y,z}-\theta_{y+1,z})], \tag{D24}$$

while the cone term is given by Eq. (D9), with $\tilde{\gamma}_{\text{cone}}=J'A_3^2\beta/2$. We observe (cf. Sec. IV B where the corresponding $T=0$ state is discussed) that the two interactions can enhance each other if the sign of the ordering vector is correlated with the sign of the DM vector. We therefore make the

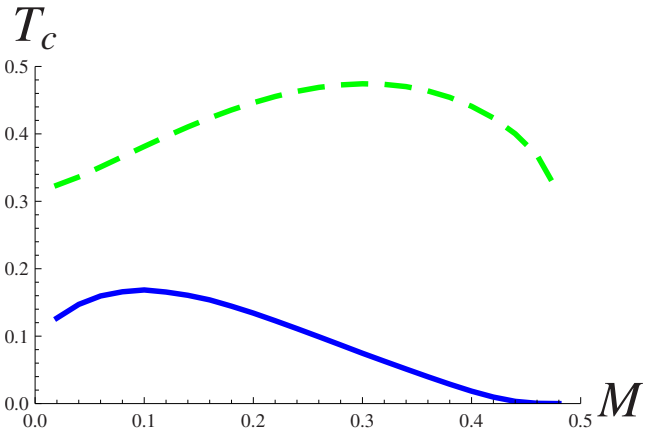

FIG. 18. (Color online) T_{SDW} (solid (blue) line) and T_{cone} [dashed (green) line] for $J''=0.045J$. Compare this with ideal 2D situation in Fig, 7 where the two orders compete strongly at intermediate values of M.

layer-dependent shift, which corresponds to Eq. (65),

$$\theta_{y,z}(x)=(-1)^z q_0 x/\beta+\tilde{\theta}_{y,z}(x). \tag{D25}$$

This should be contrasted with Eq. (D10), which describes the situation without any DM vector. The transformation in Eq. (D25) makes the competition between the staggered DM and interlayer interactions (discussed in Sec. IV) obvious since the argument of the interlayer cosine term, $\tilde{\gamma}'_\pm$ in Eq. (72), acquires a position-dependent phase,

$$\theta_{y,z}-\theta_{y,z+1}=(-1)^z 2q_0 x/\beta+\tilde{\theta}_{y,z}-\tilde{\theta}_{y,z+1}. \tag{D26}$$

The resulting oscillations eliminates the contribution of J'' to the energy within CMFT. Proceeding as described in Appendix D 2, we again obtain an equation for the critical temperature in the same form as Eq. (D15), but with $\hat{\gamma}_{\text{cone}}$ replaced by $\hat{\Gamma}^a_{\text{cone}}$,

$$\hat{\gamma}_{\text{cone}}\to\hat{\Gamma}^a_{\text{cone}}=A_3^2(J'q_0+2D). \tag{D27}$$

Note the great similarity of the above coupling with that in Eq. (D22): the two situations are related by exchanging $J''\leftrightarrow 2D$. Hence the critical temperature, T_D, for transverse (cone) type ordering follows from solving Eq. (D23) with J'' replaced by $2D$. The result is plotted in Fig. 19, which compares the case of DM interaction only $T_D(J'=0)$ with that of general $D\neq 0$, $J'\neq 0$ situation. One observes that J' leads to only a modest enhancement of T_D relative to the case with DM interaction present only. Note that Fig. 8 in the main text shows the solution with $D\neq 0$, $J'=0$.

5. CMFT at $T=0$

Here we outline calculation leading to Eq. (76). We start by changing the sign of Eq. (72) via a shift: $\theta_{y,z}\to\theta_{y,z}+(-1)^z\pi/(2\beta)$. Within CMFT, H'_2 is replaced by a single-chain sine-Gordon Hamiltonian,

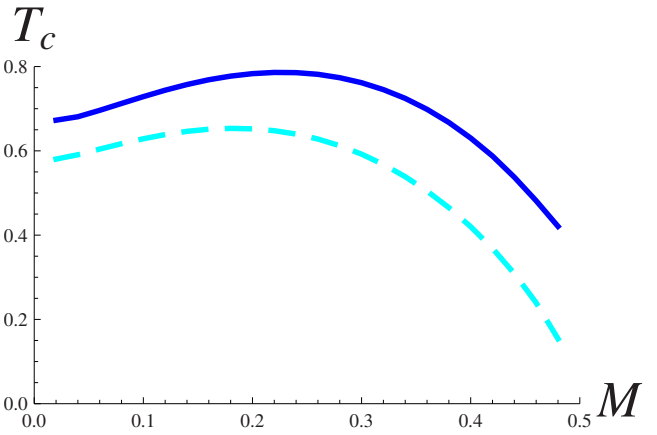

FIG. 19. (Color online) Ordering temperature with the field along the DM (a axis) axis. Dashed (cyan) curve: $T_D(J'=0)$ due to DM interaction only [$J'=0$ in Eq. (D27)]. Solid (blue) curve: T_D obtained with both D and J' interactions present.

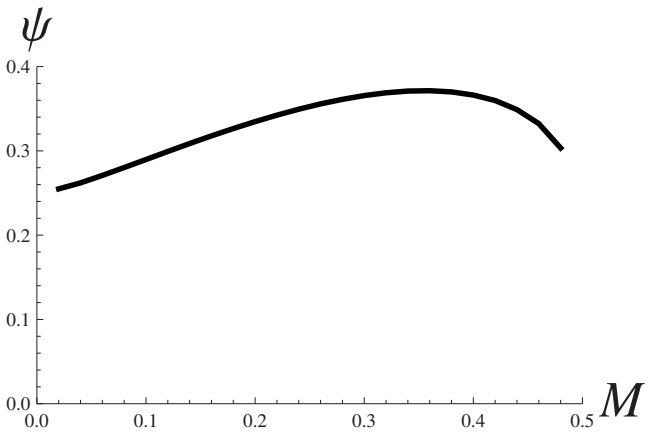

FIG. 20. The $T=0$ order parameter ψ versus M, calculated within CMFT.

$$H'_{2,\mathrm{sG}} = -2\tilde{\psi}J''A_3^2\int dx\cos\beta\theta(x). \tag{D28}$$

Here $\tilde{\psi}=\langle\cos\beta\theta\rangle$ is to be determined self-consistently. The brackets stand for averaging with the sine-Gordon action which, upon rescaling of the temporal coordinate $\tau=y/v$, reads

$$S_{\mathrm{sG}} = \int dxdy\left(\frac{1}{2}(\partial_x\theta)^2+\frac{1}{2}(\partial_y\theta)^2-2\mu\cos\beta\theta\right). \tag{D29}$$

Here $\mu=\tilde{\psi}J''A_3^2/v$. The exact solution of Eq. (D29) from Ref. 79, gives the ground-state energy density

$$F(\mu) = -\frac{1}{4}M^2\tan\left(\frac{\pi\xi}{2}\right), \tag{D30}$$

which is expressed in terms of the parameter ξ and mass gap M. These are determined by

$$\xi = \frac{\beta'^2}{1-\beta'^2} = \frac{\beta^2}{8\pi-\beta^2},$$

$$\mu = \frac{\Gamma(\beta'^2)}{\pi\Gamma(1-\beta'^2)}\left[M\frac{\sqrt{\pi}\Gamma((1+\xi)/2)}{2\Gamma(\xi/2)}\right]^{2-2\beta'^2}, \tag{D31}$$

with $\beta'=\beta/\sqrt{8\pi}$. Using the obvious relation

$$\langle\cos\beta\theta\rangle = -\frac{1}{2}\frac{dF(\mu)}{d\mu}, \tag{D32}$$

we obtain, after some algebra,

$$\tilde{\psi} = \sigma'(M)\left(\frac{J''A_3^2}{v}\right)^{\pi R^2/(2-2\pi R^2)},$$

$$\sigma'(M) = \frac{\tan[\pi\xi/2]}{2\pi(1-\beta'^2)}\left[\frac{\Gamma\left(\frac{\xi}{2}\right)}{\Gamma\left(\frac{1+\xi}{2}\right)}\right]^2\left[\frac{\pi\Gamma(1-\beta'^2)}{\Gamma(\beta'^2)}\right]^{1/(1-\beta'^2)}. \tag{D33}$$

The order parameter ψ in Eq. (76) is related to the self-consistently calculated $\tilde{\psi}$ very simply, $\psi=A_3\tilde{\psi}$. Hence the prefactor in Eq. (76) follows as

$$\sigma(M) = A_3^{1/(1-\Delta_\pm)}\sigma'(M). \tag{D34}$$

The resulting order parameter, $\psi(M)$, is plotted in Fig. 20 as a function of magnetization. Because the exponent $\pi R^2/(2-2\pi R^2)$ in Eq. (D33) is always small (it varies from $1/2$ at $M=0$ to $1/6$ at $M=1/2$), one observes that $\psi(M)$ is a slow-varying function of magnetization M. The overall nonmonotonic shape of $\psi(M)$ is in excellent agreement with the experimental data reported in Fig. 3(b) of Ref. 16: the order parameter first rises with increasing magnetization, reflecting the increasing relevance of transverse spin correlations, and then falls down rapidly as $M\to 1/2$ as a result of diminishing density of magnons. However, the CMFT result shown in the figure does suffer one problem, discussed in the next section, leading it to break down close to saturation (where it incorrectly predicts that ψ remains finite as $M\to 1/2$).

6. Limitations of CMFT

The results of CMFT for the critical temperature and order parameter, discussed in the previous sections, exhibit unphysical behavior on approaching the saturation magnetization: in these calculations, the T_c for the cone state remains finite in this limit, as does the zero temperature order parameter ψ. These features are both clearly incorrect, as both T_c and ψ must decrease to zero as the spins become fully polarized. We will investigate the breakdown of CMFT in this subsection in more detail, and determine the proper scaling theory for the vicinity of magnetization saturation.

First, let us observe the failure of CMFT more directly. Consider the solution of Eqs. (D18) in the $\Delta_\pm\to 1/4$ limit in

more detail. First, note that the first equation there is readily solved by $r=O(1)$ which is not particularly sensitive to the value of M. This immediately tells us that $s\sim(A_3^2J'/v)^2$ for $\Delta_\pm=1/4$. Near the saturation[31] $A_3^2\sim(\frac{1}{2}-M)^{1/2}$ while $v\sim(\frac{1}{2}-M)J$, which implies $s\sim(J'/J)^2/(\frac{1}{2}-M)$. Hence $T_c\sim vs=(J')^2/J$ approaches a constant value while the ordering momentum $q_0=2rs\sim(J'/J)^2/(\frac{1}{2}-M)$ diverges as $M\to\frac{1}{2}$. The latter divergence is a clear indication of the failure of CMFT. It can be traced the fact that CMFT is by construction an expansion about the 1D chain limit. The natural parameter of this expansion is J'/v which is supposed to be small everywhere. This assumption clearly breaks down near saturation, where the spin velocity v vanishes and the expansion is not justified anymore.

Physically, near saturation, one has a dilute gas of spin flips, which can be thought of as hard-core bosons or, in one dimension, equivalently, as spinless fermions. Their density $n=\frac{1}{2}-M$ determines Fermi-momentum $k_F=\pi n$, which in turn determines the (Fermi) velocity as $v=k_F/m$. Since the mass m is of the order of inverse chain exchange constant J, we obtain the scaling quoted above, $v\sim(\frac{1}{2}-M)J$. The velocity vanishes because precisely at saturation, the hard-core magnons possess a *quadratic* dispersion relation, which is beyond the Luttinger liquid paradigm of *linearly* dispersing collective excitations. (The scaling of $A_3\sim n^{1/4}$ follows from the fact that the scaling dimension of the spin-flip operator $\mathcal{S}^+_\pi$ is $\pi R^2=1/4$.)

To solve the problem correctly we need to start with a 2D description, which is actually simple near the saturation. We define the "order parameter" field $\Psi_y(x)\sim S^+_{y;\pi}(x)$, which is just the annihilation operator for a spin flip. Because the flips are dilute, we expand their kinetic energy near the bottom of their 1d band, and the Hamiltonian of the layer is given by

$$H_{\rm sat}=\sum_y\int dx\Psi_y^\dagger(x)\left(-\frac{\partial_x^2}{2m}-\mu\right)\Psi_y(x)$$
$$-J'(\Psi_y^\dagger(x)i\partial_x\Psi_{y+1}(x)+\text{H.c.})+\cdots, \qquad \text{(D35)}$$

where the chemical potential $\mu\sim h_{\rm sat}-h$ describes the deviation from the saturating magnetic field $h_{\rm sat}$ and dots stand for the interaction terms (which are irrelevant at the 2D critical point). The scaling behavior for small J'/J and small deviations from saturation, can already be read off from Eq. (D35), which should be considered for this purpose as a (1+1)-dimensional quantum field theory. The magnetization density, relative to saturation is $\frac{1}{2}-M\sim\Psi^\dagger\Psi$ which scales like an inverse length. Furthermore, the J' term above scales in the same way, since it is missing one x derivative. Thus physical quantities should be scaling functions of $\Xi=(J'/J)/(\frac{1}{2}-M)$, as claimed in Eq. (30). The overall scaling behavior of T_c is determined by the dynamical critical exponent, which is $z=2$ due to the quadratically dispersing magnons. Since T_c therefore scales as the square of an inverse length, the result in Eq. (31) follows.

We may understand the result more physically, and in particular the behavior of the scaling function $\mathcal{F}(\Xi)$ by considering Eq. (D35) and its consequences in more detail. First, the behavior for small Ξ corresponds just to the CMFT result in the limit of $M\to1/2$. The limit of large Ξ is more interesting, and represents 2+1-dimensional physics. Transforming to momentum space, we find that the magnons have the following dispersion:

$$\epsilon_k=\frac{k_x^2}{2m}-\mu-J'k_x\cos k_y$$
$$=\frac{(k_x-mJ'\cos k_y)^2}{2m}-\frac{m(J')^2}{2}\cos^2k_y-\mu. \qquad \text{(D36)}$$

We expand around the minimum, writing $k_x=mJ'+q_x$, $k_y=q_y$, which gives the continuum dispersion relation,

$$\epsilon_k\approx-\left(\mu+\frac{m(J')^2}{2}\right)+\frac{q_x^2}{2m}+\frac{m(J')^2q_y^2}{2}. \qquad \text{(D37)}$$

The continuum theory describes a free Bose gas with anisotropic effective mass. It of course forms a Bose condensate at low temperature, which is described in the usual way by taking the continuum limit $\Psi_y(x)\to e^{imJ'x}\Psi(x,y)$, with

$$\Psi(x,y)=\sqrt{n_s}e^{i\theta(x,y)}. \qquad \text{(D38)}$$

Here θ is the 2D superfluid phase, and $n_s\sim\frac{1}{2}-M$. For the above anisotropic Bose condensate, standard manipulations give the phase-only effective Hamiltonian (superfluid kinetic energy),

$$H_{\rm sat}=\frac{1}{2}\int dxdy(\rho_x(\partial_x\theta)^2+\rho_y(\partial_y\theta)^2). \qquad \text{(D39)}$$

Equation (D39) describes an anisotropic 2D XY model with stiffnesses $\rho_x=n_s/m\sim n_sJ$ and $\rho_y\sim m(J')^2n_s=n_s(J')^2/J$. Its critical temperature is determined by the geometric mean of the two stiffnesses: $T_c=\pi\sqrt{\rho_x\rho_y}/2\sim n_sJ'$. This argument describes the *large* Ξ limit of the scaling function $\mathcal{F}(\Xi)$. Note also that this argument implies that the ordering momentum $q_0\sim T_{\rm cone}/v$ remains small even near the saturation. This we saw already in spin-wave theory in Appendix G, where we observed $q_0\sim J'/J$.

Away from saturation, so that $M-\frac{1}{2}\gg J'/J$, the CMFT is applicable, and Eq. (D18) predicts small q_0 again. For this reason we expect that q_0 is uniformly small for all magnetizations, and lattice effects, of the kind mentioned in the end of Appendix D 2, remain unimportant in all the regimes considered. For this reason we chose to keep only the leading terms of the small wave-vector expansion (that is, approximate lattice differences by spatial derivatives) throughout the main text.

7. Calculation of susceptibilities

Here we present some technical details of the evaluation of susceptibilities used in this appendix. We define for convenience the susceptibility in space and time,

$$\chi_\Delta(x,\tau,T)=\langle\mathcal{O}_\Delta(x,\tau)\mathcal{O}_\Delta(0,0)\rangle_{0;T}, \qquad \text{(D40)}$$

evaluated at temperature T. It is straightforward to perform the average in Eq. (D40) with the free boson Hamiltonian Eq. (7), see, for example, Ref. 80,

$$\chi_\Delta(x,\tau;T) = \frac{1}{2}\exp\{-4\pi\Delta I(y,\tau)\},$$

$$I(y,\tau) = T\sum_{\omega_n}\int_{-\infty}^{\infty}\frac{dq}{2\pi}e^{-\alpha|q|}\frac{1-\cos[qy]\cos[\omega_n\tau]}{q^2+\omega_n^2}. \tag{D41}$$

Here $y=x/v$, $\alpha=a_0/v$ is the short-distance cutoff needed to regularize the integral, $\omega_n=2\pi Tn$ is the standard bosonic Matsubara frequency, and $0\leqslant\tau\leqslant 1/T$ is the Matsubara time. The frequency summation is standard (we use GR 1.445.2 in Ref. 81) and leads to

$$I(y,\tau) = \frac{1}{4\pi}\int_0^\infty\frac{dq}{q}\frac{e^{-\alpha q}}{1-e^{-q/T}}(2-e^{iqy-q\tau}-e^{-iqy-q\tau} + e^{-q/T}[2-e^{iqy+q\tau}-e^{-iqy+q\tau}]). \tag{D42}$$

Next we expand the denominator in series which is evaluated term by term with the help of the identity

$$\int_0^\infty\frac{dq}{q}(e^{-Aq}-e^{-Bq}) = \ln\left(\frac{B}{A}\right). \tag{D43}$$

In this way we arrive at

$$4\pi I = \ln\frac{(\alpha+\tau)^2+y^2}{\alpha^2} + \sum_{m=1}^{\infty}\left(\ln\frac{(m+\alpha T)^2-T^2(\tau-iy)^2}{(m+\alpha T)^2} + \ln\frac{(m+\alpha T)^2-T^2(\tau+iy)^2}{(m+\alpha T)^2}\right). \tag{D44}$$

For later use we note here that small $(\tau,y)\sim 0$ behavior is described by the first term on the right-hand side of the above equation. It is easy to check that small (t,y) behavior, where $t=1/T-\tau$, is described by a similar $\ln[(\alpha+t)^2+y^2]$ term (which is contained in $m=1$ contributions).

Focusing for the moment on the regime where $|t|\gg\alpha$ (i.e., including the small τ limit but not the limit near $\tau=1/T$), we next observe that $m\neq 0$ contain no singular dependence on α, which allows us to set $\alpha=0$ there. The well-known identity $\ln[\sin(x)/x]=\Sigma_{k=1}^{\infty}\ln[1-x^2/(\pi^2k^2)]$ leads us to

$$4\pi I = \ln\left[\frac{(\alpha+\tau)^2+y^2}{\alpha^2}\frac{\sin[\pi T(\tau-iy)]\sin[\pi T(\tau+iy)]}{\pi^2T^2(\tau^2+y^2)}\right]. \tag{D45}$$

Hence we obtain, when $|t|\gg\alpha$,

$$2\chi_\Delta(x,\tau;T) = \left\{\frac{\tau^2+y^2}{(\alpha+\tau)^2+y^2}\times\frac{\pi^2T^2\alpha^2}{\sin[\pi T(\tau-iy)]\sin[\pi T(\tau+iy)]}\right\}^\Delta, \tag{D46}$$

which is imaginary time version of the expression obtained in Ref. 82. The appearance of the cutoff α in the temporal τ direction is a generic feature of the bosonization technique (see Ref. 83 for more examples). The first factor in Eq. (D46) clearly carries the information on the small τ limit. To account for *both* $\tau\approx 0$ and $\tau\approx 1/T$ properly, we must include another similar factor,

$$2\chi_\Delta(x,\tau;T) = \left\{\frac{\tau^2+y^2}{(\alpha+\tau)^2+y^2}\frac{t^2+y^2}{(\alpha+t)^2+y^2}\times\frac{\pi^2T^2\alpha^2}{\sin[\pi T(\tau-iy)]\sin[\pi T(\tau+iy)]}\right\}^\Delta. \tag{D47}$$

Equation (D47) then is correct for the full imaginary time interval. To separate the short and long time behaviors of $\chi_\Delta(x,\tau;T)$ we approximate it as

$$\chi_\Delta(x,\tau;T) = \chi_\Delta^{>}(x,\tau;T)+\chi_\Delta^{<}(x,\tau;T). \tag{D48}$$

Here the first term describes long-distance behavior,

$$\chi_\Delta^{>}(x,\tau;T) = \left\{\frac{\pi^2T^2\alpha^2}{\sin[\pi T(\tau-iy)]\sin[\pi T(\tau+iy)]}\right\}^\Delta, \tag{D49}$$

which gives the naïve limit of Eq. (D47) when $\alpha\to 0$, valid away from the endpoints. The second,

$$\chi_\Delta^{<}(x,\tau;T) = \left\{\frac{\alpha^2}{(\alpha+\tau)^2+y^2}\right\}^\Delta-\left\{\frac{\alpha^2}{\tau^2+y^2}\right\}^\Delta+\left\{\frac{\alpha^2}{(\alpha+t)^2+y^2}\right\}^\Delta-\left\{\frac{\alpha^2}{t^2+y^2}\right\}^\Delta, \tag{D50}$$

accounts for an important difference in the short-distance behavior of the full Eq. (D47) and the approximate Eq. (D49) expressions for $\chi_\Delta(x,\tau;T)$. Observe that the short-distance behavior is not sensitive to temperature as it takes place on the scale determined by α while the long-distance one describes correlations on a much-longer thermal scale $1/T$.

For CMFT, we require certain limits of the Fourier transform of the susceptibility, Eq. (D6), or

$$\chi_\Delta(q,\omega_n;T) = \int_{-\infty}^{\infty}dx\int_0^{1/T}d\tau e^{iqx+i\omega_n\tau}\chi_\Delta(x,\tau;T). \tag{D51}$$

a. SDW case

For the SDW case, we need the static ($\omega_n=0$), zero momentum ($q=0$) limit of Eq. (D51) in the range $1/2<\Delta<1$. Here we must take some care to keep the short and long time contributions separate. We split $\chi_\Delta(0,0;T)=\chi_\Delta^{>}(0,0;T)+\chi_\Delta^{<}(0,0;T)$, Fourier transforming separately Eq. (D49) and Eq. (D50). The first contribution is rather standard and given by

$$\chi_\Delta^{>}(0,0;T) = \frac{\pi v\alpha^2}{2}(2\pi T\alpha)^{2\Delta-2}\frac{\Gamma(1-\Delta)\Gamma^2(\Delta/2)}{\Gamma(\Delta)\Gamma^2(1-\Delta/2)}. \tag{D52}$$

Observe that Eq. (D52) diverges as $1/(1-\Delta)$ when $\Delta\to 1$. In the case of the SDW order this limit corresponds to the be-

havior near saturation where Δ approaches 1 at the full magnetization, $M=1/2$ [see Table I and Eq. (A1)]. The divergence is not physical and stems from the incorrect short-distance behavior of Eq. (D49). It is compensated by $\chi^{<}_{\Delta}(0,0;T)$, which yields two identical contributions from the two terms in Eq. (D50). Substituting $\tau=\alpha t$, $y=\alpha z$ and using $\int_0^\infty dz/(1+z^2)^{\Delta}=\sqrt{\pi}\Gamma(\Delta-1/2)/[2\Gamma(\Delta)]$ we arrive at

$$\chi^{<}_{\Delta}(0,0;T)=\frac{v\alpha^2\sqrt{\pi}\Gamma(\Delta-1/2)}{(2-2\Delta)\Gamma(\Delta)}((1+L)^{2-2\Delta}-L^{2-2\Delta}-1), \tag{D53}$$

where $L=1/(\alpha T)\gg 1$. Simple calculation shows that this expression diverges logarithmically near $\Delta=1/2$, $\chi^{<}_{\Delta\approx 1/2}(0,0;T)\sim\ln(Le)$, which however represents a small subleading correction to Eq. (D52), which diverges linearly, $\chi^{>}_{\Delta\approx 1/2}(0,0;T)\sim L$, in this region. Thus $\chi^{<}_{\Delta\approx 1/2}(0,0;T)$ can be safely neglected. Near $\Delta=1$ limit things are different: here $\chi^{<}_{\Delta\approx 1}(0,0;T)$ results in a large T-independent contribution

$$\chi^{<}_{\Delta\approx 1}(0,0;T)=-\frac{v\alpha^2\sqrt{\pi}\Gamma(\Delta-1/2)}{(2-2\Delta)\Gamma(\Delta)}\approx-\frac{v\alpha^2\pi}{2(1-\Delta)}. \tag{D54}$$

Similar short-distance correction can be found in Refs. 82 and 84. Collecting both contributions we finally obtain, for $1/2<\Delta<1$,

$$\chi_{\Delta}(0,0;T)=\frac{\pi v\alpha^2}{2}\left\{(2\pi T\alpha)^{2\Delta-2}\frac{\Gamma(1-\Delta)\Gamma^2(\Delta/2)}{\Gamma(\Delta)\Gamma^2(1-\Delta/2)}-\frac{\Gamma(\Delta-1/2)}{\sqrt{\pi}(1-\Delta)\Gamma(\Delta)}\right\}. \tag{D55}$$

At $\Delta=1$ this expression reduces to

$$\chi_{\Delta=1}(0,0;T)=-\pi v\alpha^2\ln[2\pi T\alpha], \tag{D56}$$

which is free of unphysical $(1-\Delta)^{-1}$ divergence. The resulting $T_c(\Delta=1)$ is exponentially small in $v/\tilde{\gamma}_{\mathrm{SDW}}$ ratio.[84]

b. Cone order

For the CMFT treatment of the cone state, one requires the static susceptibility at nonzero wave vector, with $\Delta=\Delta_{\pm}=\pi R^2$. This is always less than or equal to $1/2$, making the short-time corrections in Eq. (D50) negligible. Therefore we may directly Fourier transform only the long time term, Eq. (D49). The result is well known (see, e.g., Ref. 18),

$$\chi_{\Delta}(q,0;0)=\frac{\pi\alpha^2}{2}(2\pi T\alpha)^{2\Delta-2}\frac{\Gamma(1-\Delta)}{\Gamma(\Delta)}\times\left|\frac{\Gamma(\Delta/2+ivq/(4\pi T))}{\Gamma(1-\Delta/2+ivq/(4\pi T))}\right|^2. \tag{D57}$$

APPENDIX E: GENERATION OF BIQUADRATIC INTERACTION

In this appendix, we detail the generation of the biquadratic interaction, Eq. (83). We use a standard Wilsonian RG, in which one derives the low-energy theory by integrating out high-energy modes.

We begin by passing from the Hamiltonian formulation to the (Euclidean) Lagrangian one, integrating out the conjugate field ϕ in the path integral. Furthermore, we rescale the temporal direction, introducing $x_0=v\tau$, $x_1=x$, in order to render the free action rotationally invariant in the $\boldsymbol{x}=(x_0,x_1)$ plane. The free action of the θ fields, corresponding to Eq. (7), is

$$S_0=\frac{1}{2}\int d^2\boldsymbol{x}|\boldsymbol{\nabla}\theta_y|^2=\frac{1}{2}\int_0^{\Lambda}\frac{d^2\boldsymbol{k}}{(2\pi)^2}k^2\theta_y(k)\theta_y(-k). \tag{E1}$$

Here we have introduced a momentum space cutoff Λ, which is actually of $O(1)$ (the lattice spacing). Furthermore, throughout this appendix, we have suppressed the z index of the chains to simplify the formulae. Note that, due to the change from τ to x_0, the interaction terms become perturbations with dimensionless couplings, given by original ones divided by v.

The RG proceeds in the standard way, by progressively integrating out modes within a shell of width $d\Lambda=\Lambda d\ell$ near the cutoff, thereby reducing the latter to a "running" cutoff $\Lambda_\ell=\Lambda e^{-\ell}$, which defines the logarithmic scaling variable $\ell\in\{0,\infty\}$. Following the convention used in the main text, we do not perform any iterative rescaling of length and time scales, thereby allowing the cutoff to "run" to increasingly smaller value as the RG proceeds.

Formally, the integration of modes is accomplished, in each iteration, by writing

$$\theta_y=\theta_y^{<}+\theta_y^{>}, \tag{E2}$$

where the "slow" field $\theta_y^{<}$ contains nonzero Fourier components with $k<\Lambda_{\ell+d\ell}=\Lambda_\ell e^{-d\ell}$, and the "fast" field $\theta_y^{>}$ contains the remaining ones with $\Lambda_{\ell+d\ell}<k<\Lambda_\ell$. We integrate out the fast field at each iteration, perturbatively in the interactions. After this, we relabel $\theta_y^{<}\to\theta_y$, which then defines the theory at the reduced cutoff $\Lambda_{\ell+d\ell}$.

At zeroth order in the interactions, the free action renormalizes trivially, since the slow and fast modes are decoupled. It remains in the form of Eq. (E1), with Λ replaced by Λ_ℓ. To first order, the perturbations $H'_{1,2,3}$ renormalize very simply, according to their scaling dimensions. We illustrate this explicitly for the cone/twist interaction under consideration here. Ignoring the SDW term, we have the action corresponding to H'_1 in Eq. (27),

$$S'_1=-\tilde{\gamma}_{\mathrm{cone}}\sum_y\int dxd\tau(\partial_x\theta_y+\partial_x\theta_{y+1})\cos\beta(\theta_y-\theta_{y+1})=\frac{i\tilde{\gamma}_{\mathrm{cone}}}{\beta v}\sum_y\int d^2\boldsymbol{x}(n^-_{y+1}\partial_x n^+_y-n^+_{y+1}\partial_x n^-_y). \tag{E3}$$

Here we introduced the shorthand $n^{\pm}_y=e^{\pm i\beta\theta_y}$. To first order in the RG, we use Eq. (E2) and average Eq. (E3) over the fast fields using the free action. Since the fields are decoupled at each y, the two $n^{\pm}$ factors average independently. One has

$$\langle n_y^{\pm}\rangle_> = e^{\pm i\beta\theta_y^<}\langle e^{\pm i\beta\theta_y^>}\rangle_> = e^{\pm i\beta\theta_y^<} \times \exp\left[-\frac{\beta^2}{2}\int_{\Lambda_{\ell+d\ell}}^{\Lambda_\ell}\frac{d^2\boldsymbol{k}}{(2\pi)^2}\frac{1}{k^2}\right] = e^{\pm i\beta\theta_y^<}e^{-\Delta_\pm d\ell}, \tag{E4}$$

where $\Delta_\pm=\beta^2/(4\pi)=\pi R^2$ is just the scaling dimension of the $n_y^\pm$ field. Letting $\theta^<\to\theta$, we see that Eq. (E4) applied to Eq. (E3) simply multiplies $\tilde{\gamma}_{\rm cone}$ by the constant $e^{-2\Delta_\pm d\ell}$. Hence, we have $\tilde{\gamma}_{\rm cone}(\ell+d\ell)=(1-2\Delta_\pm d\ell)\tilde{\gamma}_{\rm cone}(\ell)$, or

$$\partial_\ell\tilde{\gamma}_{\rm cone} = -2\Delta_\pm\tilde{\gamma}_{\rm cone}. \tag{E5}$$

This of course integrates to

$$\tilde{\gamma}_{\rm cone}(\ell) = \tilde{\gamma}_{\rm cone}(0)e^{-2\Delta_\pm\ell} = \tilde{\gamma}_{\rm cone}(0)\left(\frac{\Lambda_\ell}{\Lambda}\right)^{2\Delta_\pm}. \tag{E6}$$

The same treatment holds for the interlayer coupling $\tilde{\gamma}'_\pm$ (see Eq. (72),

$$\tilde{\gamma}'_\pm(\ell) = \tilde{\gamma}'_\pm\left(\frac{\Lambda_\ell}{\Lambda}\right)^{2\Delta_\pm}. \tag{E7}$$

As we have discussed, this is the most strongly relevant interaction for fields in the *b*-*c* plane, which we consider here. The RG can be considered perturbative provided the dimensionless rescaled coupling, $\tilde{\gamma}'_\pm(\ell)/v$, remains small compared with the typical value of the bare action at the corresponding scale, Λ_ℓ^2. This fixes the value of the cutoff, Λ'', at which the coupled chains form correlated *a*-*b* planes,

$$\frac{\tilde{\gamma}''_\pm}{v}(\Lambda''/\Lambda)^{2\Delta_\pm} = (\Lambda'')^2. \tag{E8}$$

Solving for Λ'' and using $\tilde{\gamma}''_\pm=A_3^2J''$,

$$\Lambda'' \sim \left(\frac{J''A_3^2}{v}\right)^{1/(2-2\Delta_\pm)}, \tag{E9}$$

where we have used that the bare cutoff Λ is $O(1)$. Thus the corresponding spatial scale which determines the renormalization of all interactions is given by $\xi''=1/\Lambda'' \sim (v/J'')^{1/(2-2\Delta_\pm)}$, in agreement with Eq. (74).

Let us now, finally, generate the biquadratic term. This occurs as a *second* order contribution of $\tilde{\gamma}_{\rm cone}$ to the effective action. Expanding the action in powers of this term, we get in second order ($Z=\int e^{-S_0}[1+S_{(1)}+S_{(2)}+\cdots]$)

$$S_{(2)} = \frac{1}{2}\left(\frac{\tilde{\gamma}_{\rm cone}}{\beta v}\right)^2\sum_y\int d^2\boldsymbol{x}d^2\boldsymbol{x}'\{\partial_{x'}(n_y^+(\boldsymbol{x})n_y^+(\boldsymbol{x}')) \times \partial_x(n_{y+1}^-(\boldsymbol{x})n_{y+1}^-(\boldsymbol{x}'))+\text{H.c.}\}. \tag{E10}$$

Terms which do not have the necessary $e^{i2\beta\theta_y}$ structure are omitted here. Now we integrate out the fast fields in each chain. Then, in chain y we obtain the combination like this

$$\partial_{x'}\left\{e^{i\beta[\theta_y^<(x)+\theta_y^<(x')]} \times\exp\left(-\beta^2\int^>\frac{d^2\boldsymbol{k}}{(2\pi)^2}\frac{1+\cos[\boldsymbol{k}\cdot(\boldsymbol{x}-\boldsymbol{x}')]}{k^2}\right)\right\} \approx e^{i2\beta\theta_y^<(X)}(-\beta^2)\int^>\frac{d^2\boldsymbol{k}}{(2\pi)^2}\frac{k_x\sin[\boldsymbol{k}\cdot\boldsymbol{\rho}]}{k^2}, \tag{E11}$$

where $\boldsymbol{X}=(\boldsymbol{x}+\boldsymbol{x}')/2$ and $\boldsymbol{\rho}=\boldsymbol{x}-\boldsymbol{x}'$ are the center of mass and relative coordinates. The most relevant term that emerges has the spatial derivative acting on the c function which is produced by fast modes (the superscript on the integral indicates that it is over the support of the fast modes only). In the second line above, the derivative has been carried out, bringing down the integral factor shown from the derivative of the exponential. After doing so, we have approximated the exponential itself by 1. This approximation is exact to first order in $d\ell$, which is infinitesimally small. Then

$$S_{(2)} = -\frac{1}{2}\left(\frac{\tilde{\gamma}_{\rm cone}}{\beta v}\right)^2\beta^4\int d^2\boldsymbol{\rho}\int^>\frac{d^2\boldsymbol{k}_1}{(2\pi)^2}\int^>\frac{d^2\boldsymbol{k}_2}{(2\pi)^2} \times\frac{k_{1x}\sin[\boldsymbol{k}_1\cdot\boldsymbol{\rho}]}{k_1^2}\frac{k_{2x}\sin[\boldsymbol{k}_2\cdot\boldsymbol{\rho}]}{k_2^2} \times\int d^2\boldsymbol{X}2\cos[2\beta(\theta_y^<-\theta_{y+1}^<)]. \tag{E12}$$

The integral over the relative distance $\boldsymbol{\rho}$ produces difference of two deltafunctions, $\delta(\boldsymbol{k}_1+\boldsymbol{k}_2)-\delta(\boldsymbol{k}_1-\boldsymbol{k}_2)$, which, thanks to the $k_{1x}k_{2x}$ factor in the numerator, only doubles the final result. The whole of the momentum-shell integration reduces to

$$\int^>\frac{d^2\boldsymbol{k}_1}{(2\pi)^2}\frac{k_{1x}^2}{k_1^4} = \frac{1}{4\pi}\int_{\Lambda_{\ell+d\ell}}^{\Lambda_\ell}\frac{dk}{k} = \frac{d\ell}{4\pi}. \tag{E13}$$

The generated biquadratic correction to the action is $-S_{(2)}$. Taking $\theta^<\to\theta$, we see that we indeed generate a biquadratic interaction of the form

$$H_{\rm bq} = \tilde{\gamma}_{\rm bq}\sum_y\int dx\cos[2\beta(\theta_y(x)-\theta_{y+1}(x))], \tag{E14}$$

with

$$d\tilde{\gamma}_{\rm bq} = v\frac{\beta^2 d\ell\,\tilde{\gamma}_{\rm cone}^2}{4\pi v^2}. \tag{E15}$$

Here we have added a factor v to the generated interaction, accounting for the transformation back to imaginary time τ from x_0. The scaling dimension of this term is $2\times(2\beta)^2/(4\pi)=8\Delta_\pm$. Hence, the RG flow equation for $\tilde{\gamma}_{\rm bq}$ is

$$\partial_\ell\tilde{\gamma}_{\rm bq} = -8\Delta_\pm\tilde{\gamma}_{\rm bq}+\frac{\beta^2\tilde{\gamma}_{\rm cone}^2}{4\pi v}. \tag{E16}$$

Note that $\tilde{\gamma}_{\rm cone}$ here is itself a function of running RG scale ℓ, as specified in Eq. (E6). Solving Eq. (E16) is easy and leads to

$$\tilde{\gamma}_{\rm bq}(\ell) = \frac{\beta^2 \tilde{\gamma}_{\rm cone}(0)^2}{16\pi\Delta v}(e^{-4\Delta\ell} - e^{-8\Delta\ell}), \qquad \text{(E17)}$$

which shows that $\ell \gg 1$ behavior is controlled by the driving term $\tilde{\gamma}^2_{\rm cone}/v$ on the right-hand-side of Eq. (E16).

As discussed above, the chains enter the strongly coupled limit at $\xi'' = \exp[\ell''] \sim (v/J'')^{1/(2-2\Delta_\pm)}$, where Eq. (E17) must be stopped. At this point, the phases θ_y may be regarded as no longer fluctuating, and hence reduce to the classical phases ϑ_y of the main text. Thus $\tilde{\gamma}_{\rm bq}(\ell'')$ corresponds directly to $g_{\rm bq}$ defined in Eq. (83). Combining therefore Eq. (E17) with Eq. (E4), which tells us that spontaneous moment of the a-b planes $|\psi| \sim (\xi'')^{-\Delta}$, we arrive at the estimate Eq. (84), $g_{\rm bq} \sim (J')^2 |\psi|^4 / v$.

APPENDIX F: NEGLIGIBLE DM COUPLINGS

In Sec. II C, it was stated that three of the five allowed DM couplings, D_a, D'_b, and D'_c, can be safely neglected. In this appendix, we explain why this is the case.

1. D_a

First consider the D_a term. As with all the DM couplings, this is only effective for fields parallel to its DM vector, in this case the a axis. For such fields, like the D_c term studied in Sec. VI, it can be "gauged away" for a single chain, by an x *dependent* spin rotation about the z axis of spin. Unlike the D_c coupling, however, the D_a interaction is constant within each triangular plane. Therefore this rotation has negligible effects upon the other in-plane couplings, most importantly $D'_a = D$, which we have argued dominates the physics in this field orientation, but also J', which plays a subsidiary but still important role. This gauge rotation *does* affect the J'' interaction, however, since the D_a term is staggered along the z axis, see Eq. (16). We have seen already in Sec. IV C that J'' itself is already (without D_a) ineffective in establishing interlayer correlations, and its only effects arise through generating the J''_2 interaction between second neighbor layers, Eq. (69). The J''_2 interaction is, happily, also unaffected by the gauge rotation, as the second neighbor layers involved rotate identically. Thus even if some D_a is present, the analysis of Sec. IV remains unchanged.

2. D'_b

Next consider the D'_b interaction. Unlike the $D = D'_a$ interaction, this coupling has the same sign on both diagonal bonds between chains [$\boldsymbol{D}^+_{y,z} = \boldsymbol{D}^-_{y,z}$ in Eq. (17)]. This means that, like the J' coupling, this interaction is highly frustrated. As a consequence, the leading order contributions arising from this term involve a gradient, analogous to the twist/cone term in, e.g., Eq. (26). Thus the effects of this term are generally strongly suppressed, both by this gradient (and associated increased scaling dimension) *and* by its small magnitude, which is of at most a few percent. In other words, it carries the same scaling dimension as the twist/cone coupling, but is probably at least a factor of 10 smaller in magnitude. Thus it is always negligible.

3. D'_c

Finally, we turn to the D'_c term. This interaction is similar in some ways to the $D = D'_a$ interaction, which dominates for fields along a. Both are unfrustrated, as they have opposite signs on the two diagonals, and both are staggered along the a (z) direction. However, D'_c is also staggered along c (y), while D was constant within the triangular planes.

The fate of D'_c is less clear than that of the prior two terms under consideration. It is neither trivially gauged away nor obviously negligible. However, it is easy to establish that it does compete with many of the key interactions that have already been identified as driving forces in the system. As such, provided D'_c is not too large, it loses this competition and has minimal effects.

First, we see that D'_c has the same scaling dimension and hence relevance as the J'' term. Moreover, like the D term, it competes with the J'' interaction because of the staggering along z. Hence, if D'_c is not comparable to J'', it will lose this competition. Indeed, if one assumes the form, Eq. (75), which satisfies the $\gamma''_\pm$ coupling ($\propto J''$), the D'_c term identically vanishes.

Second, the D'_c term also competes with the D_c term, since the latter favors opposite rotations on neighboring chains, which the D'_c term attempts to couple. Transforming to the rotating frame favored by D_c, Eq. (88), will make the D'_c term oscillate, and hence average out over long distances.

Thus to have any significant effect, the D'_c term would need to be large enough to overcome at least two competing interactions. At least for small D'_c, we conclude that the phase diagrams established in the main text are unchanged. Evidently, this is the case in Cs_2CuCl_4.

APPENDIX G: SPIN-WAVE ANALYSIS IN A HIGH FIELD

In this appendix, we study the effect of the DM interaction and the interlayer interaction J'' on the high field magnons, and particularly on the ordering wave vector infinitesimally below the saturation field. In a strong magnetic field, the ground state is a fully polarized ferromagnetic state and one can easily solve the single-magnon problem exactly. By comparing measurements of the high field magnons with such calculations, the microscopic parameters of the standard Hamiltonian Eq. (3) were determined.[16,32,37] However, in the standard model, all the possible DM vectors are not included. We present here a complete analysis based on Eq. (15), which was derived in Appendix B.

Let us first show that the components of the DM vector perpendicular to an applied field can be negligible in the spin-wave analysis. To show this, we decompose $\boldsymbol{S}_i$ into $\langle \boldsymbol{S} \rangle + \delta \boldsymbol{S}_i$, where $\langle \boldsymbol{S} \rangle$ is the ordered moment parallel to the applied field $\boldsymbol{h}$. In the linear spin wave theory we neglect $\delta \boldsymbol{S}_i$ parallel to $\boldsymbol{h}$, which means $\delta \boldsymbol{S}_i \times \delta \boldsymbol{S}_j$ is always parallel to $\boldsymbol{h}$ and does not couple to the component of the DM vector perpendicular to $\boldsymbol{h}$. One can also show that the DM interaction does not produce single magnon terms which is proportional to $\delta \boldsymbol{S}_i$ using the symmetry argument in Appendix B. In what follows, we only retain $D_\zeta = \boldsymbol{D} \cdot \hat{\zeta}$ where $\zeta \equiv \boldsymbol{h}/h$. We now take the direction of the field ($\hat{\zeta}$) as a quantization axis

of spins. Introducing $S_i^\nu = \boldsymbol{S}_i \cdot \hat{\nu}$ and $S^\pm \equiv S_i^\xi \pm iS_i^\eta$ such that $\hat{\nu} = \hat{\xi}, \hat{\eta}, \hat{\zeta}$ form an orthonormal basis, the local Hamiltonian for the bond ij is written as

$$H_{ij} = J_{ij}\boldsymbol{S}_i \cdot \boldsymbol{S}_j + D_{ij,\zeta}(S_i^\xi S_j^\eta - S_i^\eta S_j^\xi) = \frac{\tilde{J}_{ij}}{2}(e^{i\phi_{ij}}S_i^+ S_j^- + \text{H.c.}) + J_{ij}S_i^\zeta S_j^\zeta, \quad \text{(G1)}$$

where $\tilde{J}_{ij} = \sqrt{J_{ij}^2 + D_{ij,\zeta}^2}$ and $\tan\phi_{ij} = D_{ij,\zeta}/J_{ij}$. In the following, we focus on $\hat{\zeta} = \hat{a}$, $\hat{b}$, and $\hat{c}$ cases and introduce

$$\tilde{J}_\zeta = \sqrt{J^2 + (D_\zeta)^2}, \quad \tan\phi_\zeta = D_\zeta/J, \quad \text{(G2)}$$

$$\tilde{J}'_\zeta = \sqrt{(J')^2 + (D'_\zeta)^2}, \quad \tan\phi'_\zeta = D'_\zeta/J' \quad \text{(G3)}$$

for on-chain and diagonal bonds, respectively. We now apply the Holstein-Primakoff transformation,

$$S_i^\zeta = S - n_i, \quad S_i^+ = (2S - n_i)^{1/2}b_i, \quad S_i^- = b_i^\dagger(2S - n_i)^{1/2}, \quad \text{(G4)}$$

with $n_i = b_i^\dagger b_i$ and $S = 1/2$, and obtain

$$H_{ij} \sim \tilde{J}_{ij}S(e^{i\phi_{ij}}b_i^\dagger b_j + \text{H.c.}) - J_{ij}S(n_i + n_j) + JS^2. \quad \text{(G5)}$$

Denoting by $b_{\alpha,\boldsymbol{k}}$ the Fourier transform of the boson at the position $\boldsymbol{R} + \boldsymbol{\delta}_\alpha$, the spin wave Hamiltonian is written as

$$H_{\text{SW}} = \sum_{\boldsymbol{k}} \Psi_{\boldsymbol{k}}^\dagger[\mathcal{H}(\boldsymbol{k}) + h - (2J + 4J' + 2J'')S]\Psi_{\boldsymbol{k}}, \quad \text{(G6)}$$

where $\Psi_{\boldsymbol{k}} = (b_{1,\boldsymbol{k}}, b_{2,\boldsymbol{k}}, b_{3,\boldsymbol{k}}, b_{4,\boldsymbol{k}})^T$ and the 4×4 matrix $\mathcal{H}(\boldsymbol{k})$ depend on the field direction.

1. Field along the *a* axis

Let us first consider the case of field along the a axis. In this case, $\mathcal{H}(\boldsymbol{k})$ in Eq. (G6) is given by

$$\mathcal{H}(\boldsymbol{k}) = \frac{1}{2}\begin{pmatrix} \mathsf{A}_{a,\boldsymbol{k}}(\phi_a, \phi'_a) & \mathsf{B}_{\boldsymbol{k}} \\ \mathsf{B}_{\boldsymbol{k}}^\dagger & \mathsf{A}_{a,\boldsymbol{k}}(-\phi_a, -\phi'_a) \end{pmatrix}. \quad \text{(G7)}$$

Here, the matrices $\mathsf{A}_{a,\boldsymbol{k}}(\phi_a, \phi'_a)$ and $\mathsf{B}_{\boldsymbol{k}}$ are

$$\mathsf{A}_{a,\boldsymbol{k}}(\phi_a, \phi'_a) = \begin{pmatrix} 2\tilde{J}_a\cos(k_b - \phi_a) & \tilde{J}'_a f_a(\phi'_a; \boldsymbol{k}) \\ \tilde{J}'_a f_a(-\phi'_a; -\boldsymbol{k}) & 2\tilde{J}_a\cos(k_b - \phi_a) \end{pmatrix},$$

and $\mathsf{B}_{\boldsymbol{k}} = J''(1 + e^{ik_a})I$, where I is the 2×2 identity matrix and $f_a(\phi'_a; \boldsymbol{k}) = (e^{-i\phi'_a}e^{ik_b} + e^{i\phi'_a})(1 + e^{ik_c})$. We also note that k_μ is defined by $\boldsymbol{k}\cdot\hat{\mu}$ for $\mu = a, b$, and c. We now try to find the location of the minimum of the spectrum of 1-magnon excitations, which is given in the form of $\boldsymbol{k}^* = (0, 2\pi(1/2 + \epsilon), 0)$. Using the relations such as $\cos\phi_a = J/\tilde{J}_a$, the eigenvalues of $\mathcal{H}(0, k_b, 0)$ are explicitly obtained as

$$\omega_{1,\pm} = J\cos k_b + 2J'\cos(k_b/2) \pm \sqrt{(J'')^2 + [D_a \sin k_b + 2D'_a \sin(k_b/2)]^2}, \quad \text{(G8)}$$

$$\omega_{2,\pm} = J\cos k_b - 2J'\cos(k_b/2) \pm \sqrt{(J'')^2 + [D_a \sin k_b - 2D'_a \sin(k_b/2)]^2}. \quad \text{(G9)}$$

Putting $D_a = 0$, one finds the results consistent with Ref. 16. Among the four solutions, $\omega_{1,\pm}$ and $\omega_{2,\pm}$, $\omega_{1,-}$ has the lowest energy around $k_b = 2\pi(1/2 + \epsilon_0)$, where $\epsilon_0 = J'/(2\pi J)$ which is the incommensuration in the absence of D_a and D'_a. It is convenient to introduce a variable $X = \cos(k_b/2)$. Then we rewrite $\omega_{1,-}$ as

$$\frac{\omega_{1,-}}{J} = 2X^2 - 1 + 2\frac{J'}{J}X - \sqrt{\frac{(J'')^2}{J^2} + 4(1 - X^2)\left(\frac{D_a}{J}X + \frac{D'_a}{J}\right)^2}. \quad \text{(G10)}$$

Assuming X is small, we expand the above equation and have the following approximate expression for the incommensuration,

$$\sin(\pi\epsilon) = \frac{J'}{2J}\left(1 - \frac{2D_aD'_a}{J'\sqrt{(J'')^2 + 4(D'_a)^2}} + \frac{(D_a)^2 - (D'_a)^2}{J\sqrt{(J'')^2 + 4(D'_a)^2}} - \frac{4(D_aD'_a)^2}{J[(J'')^2 + 4(D'_a)^2]^{3/2}}\right). \quad \text{(G11)}$$

Whether the incommensuration is enhanced or not depends on the signs of D_a and D'_a and the subtle balance of them. We note that, if D_a is present, and not too small, the incommensuration can be substantially modified from the DM-free value since the second term in the brackets in the first line of Eq. (G11) is small only in the ratio D_a/J'. Since D_a was neglected in the experimental fits in Ref. 16, this might lead to small errors in the magnetic parameters, at perhaps a level of ten percent of their estimated values, i.e., an uncertainty in J of $\pm 0.1J'_{\text{estimated}}$, and similarly for $D = D'_a$. Errors of the order of 10% of the largest interaction, J, are clearly ruled out by the fits.[74]

2. Field along *b* axis

Next we consider the case of field along the b axis. In this case, we have

$$\mathcal{H}(\boldsymbol{k}) = \frac{1}{2}\begin{pmatrix} \mathsf{A}_{b,\boldsymbol{k}}(\phi'_b) & \mathsf{B}_{\boldsymbol{k}} \\ \mathsf{B}_{\boldsymbol{k}}^\dagger & \mathsf{A}_{b,\boldsymbol{k}}(-\phi'_b) \end{pmatrix}, \quad \text{(G12)}$$

where

$$\mathsf{A}_{b,\boldsymbol{k}}(\phi'_b) = \begin{pmatrix} 2J\cos k_b & \tilde{J}'_b f_b(\phi'_b; \boldsymbol{k}) \\ \tilde{J}'_b f_b(-\phi'_b; -\boldsymbol{k}) & 2J\cos k_b \end{pmatrix}, \quad \text{(G13)}$$

with $f_b(\phi'_b; \boldsymbol{k}) = e^{i\phi'_b}(1 + e^{ik_b})(1 + e^{ik_c})$. We minimize the excitation energy to find the ordering wave vector of the form $\boldsymbol{k}^* = (0, 2\pi(1/2 + \epsilon), 0)$. The lowest eigenvalue of $\mathcal{H}(0, k_b, 0)$ is

$$\omega = J\cos k_b - \sqrt{(J'')^2 - 4J'J''\cos(k_b/2) + 4(\tilde{J}'_b)^2\cos^2(k_b/2)}. \quad \text{(G14)}$$

Similar to the previous subsection, we rewrite the above as

$$\frac{\omega}{J} = 2X^2 - 1 - \sqrt{\frac{(J'')^2}{J^2} - 4\frac{J'J''}{J^2}X + 4\frac{(\tilde{J}_b')^2}{J^2}X^2}, \quad \text{(G15)}$$

where $(\tilde{J}_b')^2=(J')^2+(D_b')^2$. One can find the incommensuration $\sin(\pi\epsilon)=-X$ from the minimum of the above equation and observe that DM interaction, D_b', always enhances the incommensuration from its $D_b'=0$ value $J'/(2J)$.

3. Field along the c axis

Finally, we consider the case of field along the c axis. In this case, $\mathcal{H}(\boldsymbol{k})$ in Eq. (G6) is given by

$$\mathcal{H}(\boldsymbol{k}) = \frac{1}{2}\begin{pmatrix} \mathsf{A}_{c,\boldsymbol{k}}(\phi_c,\phi_c') & \mathsf{B}_{\boldsymbol{k}} \\ \mathsf{B}_{\boldsymbol{k}}^{\dagger} & \mathsf{A}_{c,\boldsymbol{k}}(\phi_c,-\phi_c') \end{pmatrix}, \quad \text{(G16)}$$

where

$$\mathsf{A}_{c,\boldsymbol{k}}(\phi_c,\phi_c') = \begin{pmatrix} 2\tilde{J}_c\cos(k_b-\phi_c) & \tilde{J}_c' f_c(\phi_c';\boldsymbol{k}) \\ \tilde{J}_c' f_c(-\phi_c';-\boldsymbol{k}) & 2\tilde{J}_c\cos(k_b+\phi_c) \end{pmatrix}, \quad \text{(G17)}$$

with $f_c(\phi_c';\boldsymbol{k})=e^{i\phi_c'}(1+e^{ik_b+ik_c})+e^{-i\phi_c'}(e^{ik_b}+e^{ik_c})$. The minimum of the spectrum of one-magnon excitation is also of the form $\boldsymbol{k}^*=(0,2\pi(1/2+\epsilon),0)$. The lowest eigenvalue of $\mathcal{H}(0,k_b,0)$ is explicitly obtained as

$$\omega_1 = -J'' + J\cos k_b - \sqrt{(D_c)^2\sin^2 k_b + 4(J')^2\cos^2(k_b/2)}. \quad \text{(G18)}$$

Here we have used the relations such as $\cos\phi_c=J/\tilde{J}_c$. The remarkable point here is that the minimum and hence the incommensuration ϵ is independent of D_c' and J''. So once we know ϵ and J, J', it uniquely determine the strength of D_c. Let us now assume that ϵ is of the order J'/J, which is true if $D_c=0$, and obtain approximate eigenenergy as

$$\frac{\omega_1}{J} = 2\sin^2(\pi\epsilon) - 2\frac{\sqrt{(J')^2+(D_c)^2}}{J}\sin(\pi\epsilon) - \frac{J''}{J} - 1, \quad \text{(G19)}$$

where we have neglected a term proportional to $\sin^4(\pi\epsilon)$. From the above equation, we can obtain the incommensuration ϵ as a function of J, J', and D_c as

$$\sin(\pi\epsilon) = \frac{\sqrt{(J')^2+(D_c)^2}}{2J}. \quad \text{(G20)}$$

From this relation, we see that the D_c on the J bonds enhances the incommensuration ϵ. This is in contrast to the measured incommensurability,[32] which is reduced compared to the expected one from the ideal standard model.

[1] P. Anderson, Mater. Res. Bull. **8**, 153 (1973).
[2] D. A. Huse and V. Elser, Phys. Rev. Lett. **60**, 2531 (1988).
[3] B. Bernu, C. Lhuillier, and L. Pierre, Phys. Rev. Lett. **69**, 2590 (1992).
[4] L. Capriotti, A. E. Trumper, and S. Sorella, Phys. Rev. Lett. **82**, 3899 (1999).
[5] R. Coldea, D. A. Tennant, A. M. Tsvelik, and Z. Tylczynski, Phys. Rev. Lett. **86**, 1335 (2001).
[6] R. Coldea, D. A. Tennant, and Z. Tylczynski, Phys. Rev. B **68**, 134424 (2003).
[7] T. Radu, H. Wilhelm, V. Yushankhai, D. Kovrizhin, R. Coldea, Z. Tylczynski, T. Lühmann, and F. Steglich, Phys. Rev. Lett. **95**, 127202 (2005).
[8] Y. Tokiwa, T. Radu, R. Coldea, H. Wilhelm, Z. Tylczynski, and F. Steglich, Phys. Rev. B **73**, 134414 (2006).
[9] C. H. Chung, K. Voelker, and Y. B. Kim, Phys. Rev. B **68**, 094412 (2003).
[10] S. V. Isakov, T. Senthil, and Y. B. Kim, Phys. Rev. B **72**, 174417 (2005).
[11] J. Alicea, O. I. Motrunich, and M. P. A. Fisher, Phys. Rev. Lett. **95**, 247203 (2005).
[12] M. Kohno, L. Balents, and O. Starykh, J. Phys.: Conf. Ser. **145**, 012062 (2009).
[13] M. Kohno, O. A. Starykh, and L. Balents, Nat. Phys. **3**, 790 (2007).
[14] O. A. Starykh and L. Balents, Phys. Rev. Lett. **98**, 077205 (2007).
[15] M. Kohno, Phys. Rev. Lett. **103**, 197203 (2009).
[16] R. Coldea, D. A. Tennant, K. Habicht, Habicht, P. Smeibidl, C. Wolters, and Z. Tylczynski, Phys. Rev. Lett. **88**, 137203 (2002).
[17] A. A. Nersesyan, A. O. Gogolin, and F. H. L. Essler, Phys. Rev. Lett. **81**, 910 (1998).
[18] M. Bocquet, F. H. L. Essler, A. M. Tsvelik, and A. O. Gogolin, Phys. Rev. B **64**, 094425 (2001).
[19] M. Q. Weng, D. N. Sheng, Z. Y. Weng, and R. J. Bursill, Phys. Rev. B **74**, 012407 (2006).
[20] S. Yunoki and S. Sorella, Phys. Rev. B **74**, 014408 (2006).
[21] Y. Hayashi and M. Ogata, J. Phys. Soc. Jpn. **76**, 053705 (2007).
[22] T. Pardini and R. R. P. Singh, Phys. Rev. B **77**, 214433 (2008).
[23] H. C. Jiang, M. Q. Weng, Z. Y. Weng, D. N. Sheng, and L. Balents, Phys. Rev. B **79**, 020409(R) (2009).
[24] D. Heidarian, S. Sorella, and F. Becca, Phys. Rev. B **80**, 012404 (2009).
[25] T. Tay and O. Motrunich, Phys. Rev. B **81**, 165116 (2010).
[26] R. B. Griffiths, Phys. Rev. **133**, A768 (1964).
[27] I. Affleck and M. Oshikawa, Phys. Rev. B **60**, 1038 (1999).
[28] N. M. Bogoliubov, A. G. Izergin, and V. E. Korepin, Nucl. Phys. B **275**, 687 (1986).
[29] S. Qin, M. Fabrizio, L. Yu, M. Oshikawa, and I. Affleck, Phys. Rev. B **56**, 9766 (1997).
[30] D. C. Cabra, A. Honecker, and P. Pujol, Phys. Rev. B **58**, 6241 (1998).
[31] T. Hikihara and A. Furusaki, Phys. Rev. B **69**, 064427 (2004).
[32] M. Y. Veillette, J. T. Chalker, and R. Coldea, Phys. Rev. B **71**, 214426 (2005).
[33] H. J. Schulz, Phys. Rev. Lett. **77**, 2790 (1996).
[34] A. W. Sandvik, Phys. Rev. Lett. **83**, 3069 (1999).
[35] A. Kolezhuk and T. Vekua, Phys. Rev. B **72**, 094424 (2005).

[36] T. Nikuni and H. Shiba, J. Phys. Soc. Jpn. **64**, 3471 (1995).
[37] M. Y. Veillette and J. T. Chalker, Phys. Rev. B **74**, 052402 (2006).
[38] E. M. Stoudenmire and L. Balents, Phys. Rev. B **77**, 174414 (2008).
[39] M. Oshikawa, M. Yamanaka, and I. Affleck, Phys. Rev. Lett. **78**, 1984 (1997).
[40] A. V. Chubukov and D. I. Golosov, J. Phys.: Condens. Matter **3**, 69 (1991).
[41] K. Hida and I. Affleck, J. Phys. Soc. Jpn. **74**, 1849 (2005).
[42] P. M. Chaikin and T. C. Lubensky, *Principles of Condensed Matter Physics* (Cambridge University Press, Cambridge, 1995).
[43] K. Okunishi and T. Tonegawa, J. Phys. Soc. Jpn. **72**, 479 (2003).
[44] T. Hikihara, T. Momoi, A. Furusaki, and H. Kawamura, Phys. Rev. B **81**, 224433 (2010).
[45] S. Lee, R. K. Kaul, and L. Balents, arXiv:0911.0038 (unpublished).
[46] E. F. Shender, Sov. Phys. JETP **56**, 178 (1982).
[47] C. L. Henley, J. Appl. Phys. **61**, 3962 (1987).
[48] M. Yoshida, T. Suzuki, T. Waki, and M. Takigawa, Poster Presentation at Highly Frustrated Magnetism 2008 Conference, 2008 (unpublished).
[49] M. Takigawa (private communication).
[50] M.-A. Vachon, G. Koutroulakis, V. F. Mitrović, A. Reyes, P. Kuhns, R. Coldea, and Z. Tylczynski, J. Phys.: Condens. Matter **20**, 295255 (2008).
[51] T. Ono *et al.*, J. Phys. Soc. Jpn. **74** (Suppl.), 135 (2005).
[52] Zheng Weihong, R. H. McKenzie, and R. P. Singh, Phys. Rev. B **59**, 14367 (1999).
[53] K. Foyevtsova, Y. Zhang, H. O. Jeschke, and R. Valenti, J. Phys.: Conf. Ser. **145**, 012038 (2009).
[54] T. Ono *et al.*, J. Phys.: Condens. Matter **16**, S773 (2004).
[55] Y. Fujii, H. Hashimoto, Y. Yasuda, H. Kikuchi, M. Chiba, S. Matsubara, and M. Takigawa, J. Phys.: Condens. Matter **19**, 145237 (2007).
[56] H. Tsujii, C. R. Rotundu, T. Ono, H. Tanaka, B. Andraka, K. Ingersent, and Y. Takano, Phys. Rev. B **76**, 060406 (2007).
[57] N. A. Fortune, S. T. Hannahs, Y. Yoshida, T. E. Sherline, T. Ono, H. Tanaka, and Y. Takano, Phys. Rev. Lett. **102**, 257201 (2009).
[58] J. Alicea, A. V. Chubukov, and O. A. Starykh, Phys. Rev. Lett. **102**, 137201 (2009).
[59] M. Bocquet, Phys. Rev. B **65**, 184415 (2002).
[60] M. Y. Veillette, A. J. A. James, and F. H. L. Essler, Phys. Rev. B **72**, 134429 (2005).
[61] D. Dalidovich, R. Sknepnek, A. J. Berlinsky, J. Zhang, and C. Kallin, Phys. Rev. B **73**, 184403 (2006).
[62] J. Merino, R. McKenzie, J. Marston, and C. Chung, J. Phys.: Condens. Matter **11**, 2965 (1999).
[63] A. E. Trumper, Phys. Rev. B **60**, 2987 (1999).
[64] J. O. Fjærestad, W. Zheng, R. R. P. Singh, R. H. McKenzie, and R. Coldea, Phys. Rev. B **75**, 174447 (2007).
[65] W. Zheng, J. O. Fjærestad, R. R. P. Singh, R. H. McKenzie, and R. Coldea, Phys. Rev. B **74**, 224420 (2006).
[66] W. Zheng, J. O. Fjærestad, R. R. P. Singh, R. H. McKenzie, and R. Coldea, Phys. Rev. Lett. **96**, 057201 (2006).
[67] W. Zheng, R. R. P. Singh, R. H. McKenzie, and R. Coldea, Phys. Rev. B **71**, 134422 (2005).
[68] A. L. Chernyshev and M. E. Zhitomirsky, Phys. Rev. B **79**, 144416 (2009).
[69] J. Alicea, O. I. Motrunich, and M. P. A. Fisher, Phys. Rev. B **73**, 174430 (2006).
[70] J. Alicea, O. I. Motrunich, M. Hermele, and M. P. A. Fisher, Phys. Rev. B **72**, 064407 (2005).
[71] S. Yunoki and S. Sorella, Phys. Rev. Lett. **92**, 157003 (2004).
[72] C. Chung, J. Marston, and R. McKenzie, J. Phys.: Condens. Matter **13**, 5159 (2001).
[73] R. F. Bishop, P. H. Y. Li, D. J. J. Farnell, and C. E. Campbell, Phys. Rev. B **79**, 174405 (2009).
[74] We would like to thank R. Coldea for pointing this experimental finding to us.
[75] M. Kenzelmann, R. Coldea, D. A. Tennant, D. Visser, M. Hofmann, P. Smeibidl, and Z. Tylczynski, Phys. Rev. B **65**, 144432 (2002).
[76] F. H. L. Essler, A. Furusaki, and T. Hikihara, Phys. Rev. B **68**, 064410 (2003).
[77] S. Bailleul, D. Svoronos, P. Porcher, and A. Tomas, C. R. Seances Acad. Sci., Ser. 2 **313**, 1149 (1991).
[78] T. Moriya, Phys. Rev. **120**, 91 (1960).
[79] S. Lukyanov and A. Zamolodchikov, Nucl. Phys. B **493**, 571 (1997).
[80] T. Giamarchi, *Quantum Physics in One Dimension* (Oxford University Press, Oxford, 2004).
[81] I. S. Gradshteyn and I. M. Ryzhik, *Tables of Integrals, Series, and Products*, 6th ed. (Academic, New York, 2000).
[82] H. J. Schulz, Phys. Rev. B **34**, 6372 (1986).
[83] O. A. Starykh, A. Furusaki, and L. Balents, Phys. Rev. B **72**, 094416 (2005).
[84] H. J. Schulz and C. Bourbonnais, Phys. Rev. B **27**, 5856 (1983).